RELATIVE ORBIT CONTROL OF COLLOCATED GEOSTATIONARY SPACECRAFT

A Dissertation

Submitted to the Faculty

of

Purdue University

by

Raoul R. Rausch

In Partial Fulfillment of the

Requirements for the Degree

of

Doctor of Philosophy

December 2012

Purdue University

West Lafayette, Indiana

This dissertation is dedicated to my parents Roger and Mathilde. Without their continuous support and patience, I would have never been able to complete this work.

ACKNOWLEDGMENTS

This research topic has been a very interesting and challenging experience. My time at Purdue and research has also been very rewarding and fulfulling. I want to thank my advisor Professor Howell for her continuous support and guidance and the seemingly infinite patience. The patience, she has shown with me completing this project and the advice and recommendations, she provided on reviews of this thesis, certainly surpassed anything that could have been expected.

I also wish to thank the other members of my graduate committee, Professors James M. Longuski, Martin Corless and Inseok Hwang for their advice, questions and reviews of this dissertation.

I am grateful to all the past and present members of my research group. They have provided much support and guidance and without their feedback, this work would have been difficult to complete. In particular, I would like to thank Masaki Kakoi, Chris Patterson, Lucia Capdevila, Tash Bosnac and Geoffrey Wawrzyniak. Through their friendship and technical discussions they have made this work possible. Former research group members German Porras and Christoph Wagner and my colleaque and friends Navin Davendralingam and Phoi-Tack Lew have provided much advice and motivation to complete this work. A very special appreciation goes to my friends Michael Skoby, Daniel Mendoza and Tia Pedigo, who provided much support and advice through times of personal hardship.

Throughout my graduate career, I enjoyed the support and mentorship of many people at SES and at the Space Vehicles Directorate of the Air Force Research Laboratory. A very special appreciation goes to Mr. Pascal Wauthier and Dr. Muriel Hooghe and all the other people, I have worked with at SES. Without their support and the technical expertise and allowing me the use of their high fidelity inertial progation routines, this project would have been very difficult to complete. I would also

like to thank Mr. Joseph Gonner and Mr. Richard Starkovs and for all the insightful discussions I had with them during my employment with SES. I would like to thank the Space Scholar's Program of the United States Air Force Research Laboratory Space Vehicles Directorate for providing me the opportunity to spend two amazing summers at Kirtland AFB and for allowing me to work on fascinating projects.

Finally, I wish to thank those who have provided the funding for my graduate studies. The German section of Purdue School of Languagues and Cultures has supported me by offering me the opportunity to teach German. Teaching German has been an enlightening and educational experience for me. Support was also provided by the Fond National de Recherche of Luxembourg under the contract AFR/BFR 06/057 and SES.

TABLE OF CONTENTS

LIST OF TABLES

LIST OF FIGURES

ABSTRACT

Rausch, Raoul R. Ph.D., Purdue University, December 2012. Relative Orbit Control of Collocated Geostationary Spacecraft. Major Professor: Kathleen C. Howell.

A relative orbit control concept for collocated geostationary spacecraft is presented. One chief spacecraft, controlled from the ground, is responsible for the orbit determination and control of the remaining vehicles. Any orbit relative to the chief is described in terms of equinoctial orbit element differences and a linear mapping is employed for quick transformation from relative orbit measurements to orbit element differences. It is demonstrated that the concept is well-suited for spacecraft that are collocated using eccentricity-inclination vector separation and this formulation still allows for the continued use of well established and currently employed stationkeeping schemes, such as the Sun-pointing-perigee strategy. The relative approach allows to take determinisitic thruster cross-coupling effects in the computation of stationkeeping corrections into account. The control cost for the proposed concept is comparable to ground-based stationkeeping. A relative line-of-sight constraint between spacecraft separated in longitude is also considered and an algorithm is developed to provide enforcement options. The proposed on-board control approach maintains the deputy spacecraft relative orbit, is competitive in terms of propellant consumption, allows enforcement of a relative line-of-sight constraint and offers increased autonomy and flexibility for future missions.

1. INTRODUCTION

Since the first spacecraft was launched into Earth Geostationary Orbit (GEO) in 1963, the number of geostationary spacecraft has risen steadily over the last four decades and currently exceeds 430 vehicles. Most telecommunication satellites and a number of weather satellites are located in geostationary orbit. With ever-growing communication demands, the number of satellites is only expected to increase in the coming decades. By international agreements regulating the frequency spectrum, geostationary spacecraft are constrained to longitudinal boxes centered on a nominal longitude [1]. Additionally, the spacecraft latitude is generally constrained to afford easy access to GEO with inexpensive fixed (non-tracking) ground antennas, such as those employed by millions of satellite television users. To avoid violations of the assigned control box, regular stationkeeping maneuvers are required to counteract the perturbations due to the gravity of the Sun, Earth, and Moon. These gravitational perturbations otherwise drive the spacecraft outside of its assigned "box". In the early 1990s, to maximize the effective use of desirable longitudinal positions and to accommodate the growing number of spacecraft, satellite operators started to collocate multiple spacecraft within one longitudinal control box [2–4]. Collocation of multiple vehicles provides a number of benefits over using a single spacecraft. For example, the cost of registering and leasing frequencies in orbital slots can be decreased, mutual on-orbit backup options are ensured in the event of spacecraft or transponder failure, and multiple vehicles afford satellite operators the ability to tailor capacities to changing customer needs by moving spacecraft to different orbital locations as the demand arises.

Currently, the orbital tracking and control of geostationary spacecraft remains the sole responsibility of satellite controllers on the ground. With the increasing number of spacecraft, satellite operators are seeking new strategies that allow increased au-

tonomy. Recent proposals suggest a fleet of smaller, more specialized spacecraft that will form future communications platforms [5,6]. Such concepts demonstrate the need for more autonomous operation and control concepts that allow for the incorporation of relative constraints between spacecraft. Of particular interest, the enforcement of a line-of-sight constraint to allow the use of high-bandwidth inter-satellite links (ISL) between spacecraft can enable increased communication.

Spacecraft formation flying has been proposed for various applications, ranging from optical interferometry for imaging extra-terrestrial planets to Earth observations. NASA considers spacecraft formation flying an enabling technology for its Earth science missions and the US Air Force relies on autonomous relative control for some future applications. Engineers at both the European Space Agency (ESA) and the German Aerospace Center (DLR) are interested in testing critical technologies. The recent PRISMA mission demonstrates autonomous formation flying in Low-Earth Orbit (LEO) [7]. For collocated geostationary communications satellites, formation flying potentially offers increased autonomy as well as positioning and control for inter-satellite links in satellite communications platforms.

1.1 Problem Definition

The overarching goal of this investigation is increased autonomy in the orbital maintenance of constellations of collocated geostationary spacecraft. A relative orbit control concept has been developed that might offer an alternative to traditional ground-based stationkeeping. Ground-operations are limited to the orbit determination and orbit control (stationkeeping) of one spacecraft, identified as the "chief". For the remaining spacecraft, denoted "deputies", the relative orbit determination and the necessary relative orbital correction maneuvers are generated as a result of autonomous algorithms on-board the chief vehicle. The constellation is designed to meet all "absolute" constraints while simultaneously maintaining safe separations through an eccentricity and inclination vector (e-i) separation strategy. With the

chief controlled via proven fuel-efficient stationkeeping strategies, the deputies are only required to loosely maintain their pre-determined relative orbit to ensure safe vehicle separation. Correction burns are further limited to tangential (East-West (E-W)) and normal (North-South (N-S)) burns since many geostationary spacecraft are not equipped with radial thrusters as traditional optimal stationkeeping strategies do not require radial corrections. The relative orbit control concept should i) provide increased autonomy over ground-based stationkeeping approaches, (ii) allow for operational constraints, and (iii) be competitive in terms of propellant consumption. Much progress has been accomplished in the last decade in terms of the relative orbit control of constellations of spacecraft. The proposed framework combines traditional geostationary stationkeeping strategies with these advancements in the proposed relative orbit control formulation.

1.2 Previous Work

Broad interest in the geosynchronous (GEO) orbit originated with the science fiction author Arthur C. Clarke who proposed the use of geosynchronous orbits for long-range and global communications in a Wireless World paper in 1945 [8]. Clark envisioned a trio of large, manned space stations arranged in a triangle around the Earth. Since this first vision of the future, orbital perturbations and stationkeeping of GEO satellites have been developed and discussed by numerous researchers. In a 1978 journal article, Shrivastava cited more than 200 relevant papers [9]. Contributions mentioned here are, therefore, limited to the most fundamental developments or directly relevant to the present study. Stationkeeping requirements for geosynchronous orbits are decomposed into E-W (planar) and N-S (out-of-plane) correction maneuvers. Generally, only tangential thrust accelerations are used for E-W stationkeeping since these maneuvers are twice as effective as radial burns. A comprehensive discussion of the basic E-W stationkeeping requirements was first offered by Kamel et al. [10]. These requirements were then later generalized and refined

by Kechichian [11, 12]. Gartrell first developed a method for combined eccentricity and longitude control [13]. To minimize propellant consumption, Kamel and Wagner analyzed the detailed effects of Solar Radiation Pressure (SRP) on the behavior of a geostationary satellite; from the investigation, two efficient variants of the use of the Sun-Pointing Perigee Strategy (SPPS) [14] were proposed. Chao and Baker then derived closed-form expressions for the evolution of the eccentricity vector in the phase space as a result of the solar radiation pressure perturbation [15]. In modern operational implementations, the SPPS is typically augmented by maintaining the tip of the eccentricity vector on an eccentricity control circle, whose size is determined by a collocation strategy [2, 16]. More recently, Romero and Gambi [17] proposed the use of nonlinear programming for further optimization of the SPPS; Emma and Pernicka [18] offered an algorithm for the autonomous control of longitude and eccentricity using differential corrections. Slavinskas and Dabbaghi determined and tabulated impulse requirements for various methods of inclination drift compensation [19]. A model to describe the evolution of the orbital pole under the effects of the Sun, the Moon and the Earth precession was then employed by Soop, and allowed for the computation of the desired inclination vector correction [20]. The basic principles of ground-based stationkeeping planning for GEO satellites under high-thrust propulsion, using independent normal and tangential burns, are available in Soop, Campan, Sidi and Chao [20–23].

With ever growing communications demands, a desire to increase capacity at a particular longitudinal location and a plan to create on-orbit backup capacity, satellite operators began to collocate multiple satellites in a single longitudinal control box [23]. As demonstrated by Harting et al. [22], the risk of collisions cannot be ignored for collocated spacecraft and a coordinated separation strategy is required for the safe collocation of multiple spacecraft in one longitudinal control box. The original separation strategy, as described by Slabinski, involved simple longitude separation [24], but it became quickly apparent that safer strategies were available by separating the spacecraft using the eccentricity vector. In 1984, a method comprised

of separation in both the relative eccentricity (e) and the inclination (i) vectors, was first suggested [25]. Operational implementations of the e-i collocation strategy were discussed by Wauthier and Francken for the SES ASTRA spacecraft and by Pattinson for the EUTELSAT spacecraft [2,3]. Park presented an algorithm for the collocation design using e-i vector separation as applied to the KoreaSat constellation [26]. Even today, e-i vector separation is employed by nearly all of the major satellite operators worldwide [2, 3, 26]. An excellent comparison of the different separation techniques for geostationary satellites is detailed in Soop [20].

Concepts for automating the stationkeeping of geostationary spacecraft have been proposed since the 1980s. Three studies, by Chao and Peterson, Kluever and Tanck, and Park et al., do not incorporate the general assumption of open-loop ground-based control. In contrast, these authors formulate the stationkeeping problem as a closed-loop regulation problem with the goal of autonomous onboard execution [27–29]. Their proposed autonomous concepts, however, rely on long-term histories of satellite operations and on ground-based tracking and are not well-suited for constellations of multiple spacecraft within a single longitudinal box. Utilization of the Global Positioning System (GPS) for onboard orbit determination and to automate the stationkeeping of GEO satellites was proposed by Chao and Bernstein [30]. However, the use of GPS is complicated by the fact that the GPS satellites are located below the geostationary altitude.

The first relative motion analysis dates back to Hill's lunar motion theory [31]. In the 1960s, Clohessy and Whiltshire (CW) rediscovered Hill's linearized equations while studying spacecraft rendezvous [32]. Interest in the US Air Force TechSAT 21 constellation [33] and numerous proposed Earth observation missions have inspired most of the contemporary literature related to spacecraft formation flying and most analysis is focused on constellations in inclined Low-Earth Orbits (LEO). Extensive effort has been devoted to extending relative Cartesian equations (CW-type dynamics) to incorporate first-order effects from the Earth equatorial bulge (the J_2 term of the Earth gravitational potential), eccentricity, and higher order nonlinearity [34]. Lovell

and Tragesser introduced a set of relative orbit elements derived from the Clohessy-Wiltshire equations that supplies an instantaneous snapshot of the relative orbit and the authors then developed a series of relative reconfiguration algorithms [35]. Lovell and Tragesser's relative orbit elements (roe) intuitively describe the size, location, and orientation of the deputy trajectory relative to the chief, as well as the location of the deputy along its relative path. Alfriend et al. proposed modeling the relative orbit in terms of orbit element differences, between the orbit elements of the deputy and the chief spacecraft, rather than Cartesian states, and developed a linear mapping to relate orbit element differences to chief-centered Cartesian coordinates, or curvi-linear coordinates, and vice versa [36]. Alfriend and Gim extended their work by developing the Gim-Alfriend State Transition Matrix (STM), that employs a linear mapping incorporating the first-order J_2 perturbation [37, 38]. Schaub evaluated impulsive control options to establish mean orbit element differences and proposed the application of a linear mapping to offer hybrid control options [39, 40]. Breger and How proposed a linear model predictive control option including the effects of J_2 [41,42]. Comparing many of the proposed relative dynamics formulations, Alfriend and Yan concluded that the reference orbit eccentricity and differential gravitational perturbations produce the greatest effect on the accuracy of the relative model, with nonlinear effects the smallest, and models using orbit element differences to be most accurate [43]. More recently, the DLR has successfully employed eccentricity and inclination vector separation for low Earth orbit proximity operations for GRACE and TanDEM-X/TerraSAR-X [44, 45] and for autonomous formation flying in support of the PRISMA mission [7].

Formation flying, defined as relative orbit control, with application to geostationary communications spacecraft has received little attention. Vassar and Sherwood first proposed relative orbit control for two geostationary spacecraft separated in longitude using an LQR controller [46]. Similar analysis was later completed by Sparks and Kapila [47, 48]. The first comprehensive investigation applicable to collocated geostationary communications spacecraft was performed in the mid-1990s at

the DLR [49, 50]. Blumer proposed a concept assuming identical simultaneous stationkeeping burns for all collocated spacecraft followed by relative orbit corrections to reestablish the desired relative orbits based on Clohessy-Wiltshire dynamics. Besides the non-optimal assumptions of identical simultaneous SK burns for all spacecraft, the relative orbit control concept, as conceived by Blumer, was complicated by insufficient insight into the necessary relative corrections due to the relative Cartesian formulation. He and Han proposed closed-loop relative orbit control using a set of relative orbit elements that were not well-suited for e-i vector separated constellations [51]. Gurfil and Beigelman proposed a design algorithm for collocated GEO spacecraft using orbit element differences. Their algorithm determined the optimal constellation/collocation design minimizing a given performance index, while ensuring safe separation [53]. Applications of their algorithm are limited since the relevant perturbations from the Sun, the Moon, as well as the tesseral terms in the Earth gravitational potential are not incorporated. Future concepts, such as the ESA SKIKIT and SkiLAN proposals, suggest the use of a fleet of smaller, more specialized spacecraft to form future communications platforms requiring increased autonomous operation and control concepts allowing for relative constraints between spacecraft.

1.3 Scope of Present Work

The overarching goal is increased autonomy in the orbit maintenance of constellations of collocated geostationary spacecraft. A relative orbit control concept is developed that might offer an alternative to traditional ground-based stationkeeping. Ground-operations are limited to the orbit control (stationkeeping) of the chief spacecraft, and necessary orbit control of the deputies is performed completely autonomously on-board the chief vehicle. The deputy spacecraft must be maintained within their longitudinal control box and safe separation must be ensured at all times. Correction burns are further limited to tangential, East-West (E-W), and normal, North-South (N-S), burns since many geostationary spacecraft are not equipped with

radial thrusters because traditional optimal stationkeeping strategies do not require radial corrections. The autonomous stationkeeping of the deputy spacecraft is demonstrated and a framework is presented allowing the enforcement of a relative line-of-sight or coning constraint for constellations of spacecraft separated in longitude. To verify the effectiveness of the proposed relative orbit control concept, numerical simulations in a high-fidelity model are implemented that include an accurate gravity model of the Earth and all relevant perturbing forces from the Sun, the Moon and solar radiation pressure. This work is arranged as follows:

- Chapter 2: The discussion in this chapter summarizes the background material that underlies the foundations of this investigation. The geostationary environment is described and the different reference frames and coordinate sets are introduced. The dynamic model and the main perturbing accelerations affecting geostationary spacecraft are discussed and the basic underlying principles of geostationary stationkeeping are presented.

- Chapter 3: A relative orbit determination and control concept is developed in terms of equinoctial orbit elements. Measurements of the deputies' relative orbit are available on-board the chief spacecraft and mapped into orbit element differences. Equinoctial orbit element differences are well-suited for relative orbit determination because they only slowly vary with time, subject to perturbations or disturbances. Relative orbit control is achieved using a modified form of the Gauss Variational Equations (GVE). Differential perturbations and thruster alignment are considered for accurate orbit propagation as well as efficient propellant consumption.

- Chapter 4: Autonomous stationkeeping of the deputy spacecraft is achieved by loosely maintaining the nominal relative orbit from on-board the chief. Current stationkeeping strategies typically employ a "repeating" nominal stationkeeping cycle for operational reasons. A similar stationkeeping cycle is employed for the relative stationkeeping. The semi-autonomous stationkeeping concept

is demonstrated for a number of different constellations of spacecraft under a separation strategy based on the eccentricity-inclination vector. The performance is gauged by the fuel efficiency compared to conventional ground-based stationkeeping.

- Chapter 5: A relative line-of-sight "coning" constraint between a chief separated in longitude from a deputy spacecraft is introduced. While the line-of-sight constraint is maintained by the nominal constellation design, a relative control concept is presented to efficiently reestablish the line-of-sight if it is violated. The proposed approach utilizes insight gained from the orbit element difference formulation and the relative orbit control concept to provide burn sequences for reconfiguration.

- Chapter 6: Concluding remarks are presented along with recommendations for future research.

2. BACKGROUND

Constellations of spacecraft in geostationary orbit are the focus of this investigation. The geostationary orbit is defined and orbit elements are employed to characterize spacecraft motion. The three dominant perturbations affecting the orbit of a geostationary spacecraft are i) Luni-Solar gravitation that causes a secular variation of the inclination vector; ii) tri-axiality of the Earth's gravitational potential that produces accelerations in longitude; and iii) solar radiation pressure that shifts the eccentricity vector along a natural eccentricity circle as the Sun moves in near-circular motion around the Earth. To counteract the effects of these perturbations, stationkeeping maneuvers are necessary and current stationkeeping strategies are examined.

2.1 The Geostationary Orbit

The ideal Earth geostationary orbit is a circular, equatorial orbit, with an orbital period that precisely matches that of the Earth. To an observer at the equator on the surface of the Earth, a spacecraft in geostationary orbit remains fixed since the spacecraft orbital rate equals the Earth's rotation rate. The Earth's rotation has a sideral period of 23 hours 56 minutes and 4.09 seconds, and the geosynchronous spacecraft moves in an orbit with the same period. A perfectly geostationary orbit is a mathematical abstraction, only achieved if the gravitationally attracting body is centrobaric or spherically symmetric with no additional perturbing forces acting on the vehicle. This abstraction is useful, however, as an approximation, since all perturbations including the non-spherical Earth potential, gravity fields due to the Moon and Sun as well as solar radiation pressure, are small compared to the Earth point mass potential.

As a first approximation, assume that the Earth is perfectly spherically symmetric and point mass gravity is the only force acting on the spacecraft. Then, assuming that the vehicle is also a point mass, Newton's inverse square law of gravity describes the acceleration acting on the spacecraft. Of course, the gravity force is then a function of the mass of the Earth and the inverse of the square of the distance between the center of the Earth and the spacecraft. The resulting relative acceleration on the vehicle, as viewed by an inertial observer, is written as follows

$$\ddot{\bar{r}} = \frac{-GM_{\oplus}m}{r^2}\frac{\bar{r}}{r}, \tag{2.1}$$

where $\bar{r}$ is the vector extending from the center of the Earth to the spacecraft, $\bar{r}/r$ is the unit vector directed from the Earth toward the spacecraft and $\mu_{\oplus} = GM_{\oplus}$ is the gravitational parameter of the Earth. As is standard notation, G is the universal gravitational constant and $M_{\oplus}$ reflects the mass of the Earth. Dots indicate derivatives with respect to dimensional time. From kinematics, the relative component of acceleration in the radial direction is $m\omega^2 r$, where ω is the orbit angular velocity. In a circular orbit, angular velocity is constant. Thus, by adjusting the orbital radius of the circular orbit to match the angular velocity of the Earth's rotation, it follows that

$$\frac{-GM_{\oplus}m}{r^2} = m\Psi^2 r, \tag{2.2}$$

where Ψ is the rotational rate of the Earth. Dividing both sides by m, the spacecraft mass, equation (2.2) is balanced only for one possible orbital radius r given by

$$r = \sqrt[3]{\frac{\mu_{\oplus}}{\Psi^2}}. \tag{2.3}$$

The values adopted by the 1989 International Rotation Service are $\Psi = 360.985647$ deg/day$= 0.729211585 \times 10^{-4}$ rad/s and $\mu_{\oplus} = 398600.440$ km^3/s^2, respectively [20]. Inserting these values into equation (2.3) yields an ideal geostationary radius $r_{GEO} =$ 42164.17 km. Incorporating all other forces, the instantaneous geostationary orbit, in fact, varies due to the perturbations and 42,164.5 km is actually a mean value. Note that for a perfectly circular orbit, the radius is also equivalent to the semi-major axis

a_{GEO}. For an ideal geostationary orbit, the only free parameter is the longitude. The location of a spacecraft in geostationary orbit is usually specified by the longitude of the subsatellite point, the point where the line connecting the spaceraft with the center of the Earth intersects the Earth's surface.

2.2 Earth Centered Inertial Frame ECI

Newton's laws, as stated in their most original form, are valid relative to an inertial observer. An inertial reference frame is defined such that the origin is located at the center of the Earth (geocentric). The Earth Centered Inertial (ECI) frame is assumed to be inertially fixed in space but, in practice, it is slowly shifting over time. Since a truly inertial system is impossible to realize, the standard J2000 system [52] is adopted as the best representation of an ideal, inertial frame at a fixed epoch. The shift of this frame is so slow relative to the motion of interest, it can reasonably be neglected. For the assumed inertial ECI frame, the unit vector $\widehat{X}$ is directed toward the vernal equinox and the unit vector $\widehat{Z}$ is parallel to the geographic north pole. (Note that a caret indicates a vector of unit magnitude.) The unit vector $\widehat{Y}$ completes the right-handed triad. The fundamental plane associated with the ECI frame is the Earth equatorial plane, which is oriented at an angle relative to the ecliptic plane as indicated in Figure 2.1. The position of a point in the ECI frame can be specified by either Cartesian coordinates or inertial spherical coordinates. The Cartesian coordinates x, y, z are defined

$$\bar{r} = x\hat{X} + y\hat{Y} + z\hat{Z}. \tag{2.4}$$

The geocentric scalar distance r is the distance between the center of the Earth and the spacecraft. The right ascension α is the angle between the inertial $\hat{X}$-axis and the projection of $\bar{r}$ onto the inertial, equatorial, plane and the geocentric declination δ is the out-of-plane angle between the intertial, equatorial plane and the line extending

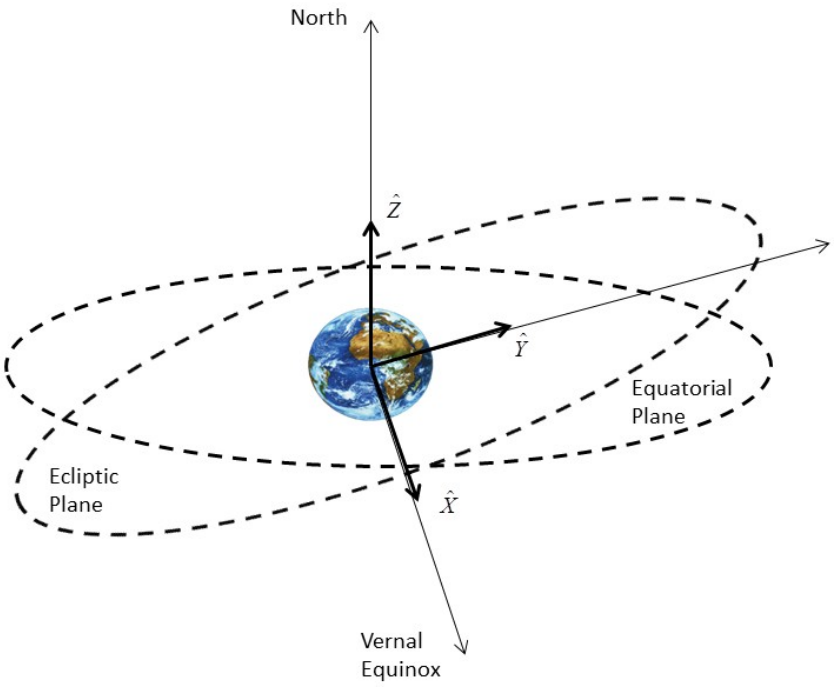

Figure 2.1. Earth Centered Inertial (ECI) Frame

between the Earth and the spacecraft as illustrated in Figure 2.2. The conversion from inertial spherical to Cartesian coordinates and vice versa is accomplised by

$$\begin{bmatrix} x \\ y \\ z \end{bmatrix} = \begin{bmatrix} r\cos\alpha\cos\delta \\ r\cos\delta\sin\alpha \\ r\sin\delta \end{bmatrix} \tag{2.5}$$

and

$$\alpha = \arctan\frac{y}{x}, \delta = \arctan\frac{z}{\sqrt{x^2+y^2}}, r = \sqrt{x^2+y^2+z^2}, \tag{2.6}$$

where the quadrant for α is selected such that the sign of the denominator x is equal to the sign of $\cos\alpha$, i.e. $-90^o < \alpha, 90^o$ for $x > 0$ and $90^o < \alpha < 0$. In the inertial frame, an ideal spacecraft is moving and it is not apparent whether it remains fixed with respect to an observer on the surface of the Earth.

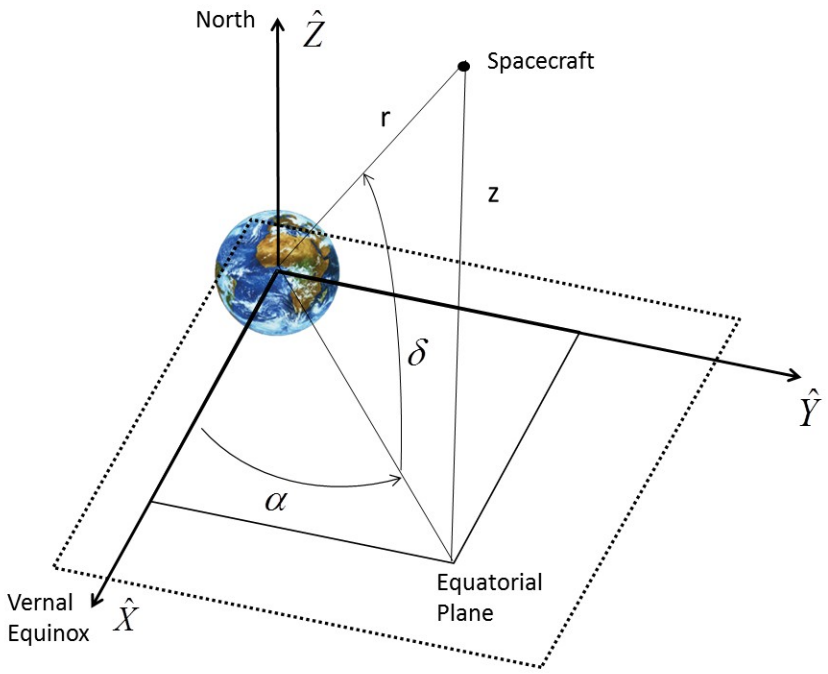

Figure 2.2. Cartesian and Spherical Inertial Coordinates

2.2.1 Earth Centered "Fixed" Frame

The Earth Centered Fixed Frame (ECF) is actually a rotating frame that is fixed in the Earth as it rotates on its own axis. The ECF frame is useful for modeling spacecraft motion with respect to a fixed location on the surface of the Earth. The ECF origin is concurrent with the Earth's center and, thus, this geocentric coordinate system rotates with the Earth relative to the inertial frame. For the assumed ECF frame, the unit vector $\widehat{X}_{ECF}$ is aligned with the Greenwich meridian. The unit vector $\widehat{Z}_{ECF}$ is aligned with the inertial unit vector, $\widehat{Z}$, and parallel to the geographic North Pole. The unit vector $\widehat{Y}_{ECF}$ then completes the right-handed triad. The location of a spacecraft in the geostationary orbit is usually specified by the geographical longitude λ and the geographical latitude ϕ. The longitude λ is the angle between the $\widehat{X}_{ECF}$ axis and the projection of $\bar{r}$ onto the equatorial plane and the latitude ϕ is the out-of-plane angle between the equatorial plane and the line extending between

the Earth and the spacecraft as illustrated in Figure 2.3. For a perfectly symmetric and spherical Earth, the latitude ϕ is equal to the declination δ. The coordinate set r, λ and ϕ form the spherical coordinates in the ECF frame. Longitude λ is measured positively towards the East and differs from the right ascension α by the right ascension of the Greenwich meridian Θ as expressed in

$$\lambda = \alpha - \Theta. \tag{2.7}$$

The right ascension of the Greenwich meridian Θ is also commonly denoted the Greenwich Hour Angle (GHA) and is the angle between the inertial $\widehat{X}$ and the Greenwich meridian as is shown in Figure 2.3. The Greenwich hour angle is the local sideral time associated with the Greenwich meridian and is calculated as a function of the Universal Coordinated Time (UTC) time through the uniform angular velocity, denoted ψ; the resulting relationship is

$$\Theta = \Theta_0 + \psi(t - t_0), \tag{2.8}$$

where Θ_0 is the value of Θ at a time t_0. The Greenwich sidereal angle Θ_0 is the value of the Greenwich sidereal angle Θ at an epoch t_0, which is available from tables [20]. A spacecraft placed in an ideal geostationary orbit will remain invariant in the ECF frame.

2.3 Satellite State Representations

The state vector of a body or spacecraft in space can be defined by six independent quantities. Many different representations are possible and this work employs three different sets to express the state vector: i) the instantaneous position and velocity of the spacecraft, ii) a set of elements commonly labeled Keplerian or classical orbit elements and iii) a set of elements denoted as non-singular or equinoctial orbit elements. Any of these sets completely specifies the two-body conic orbit from a complete set of initial conditions that defines the initial value problem.

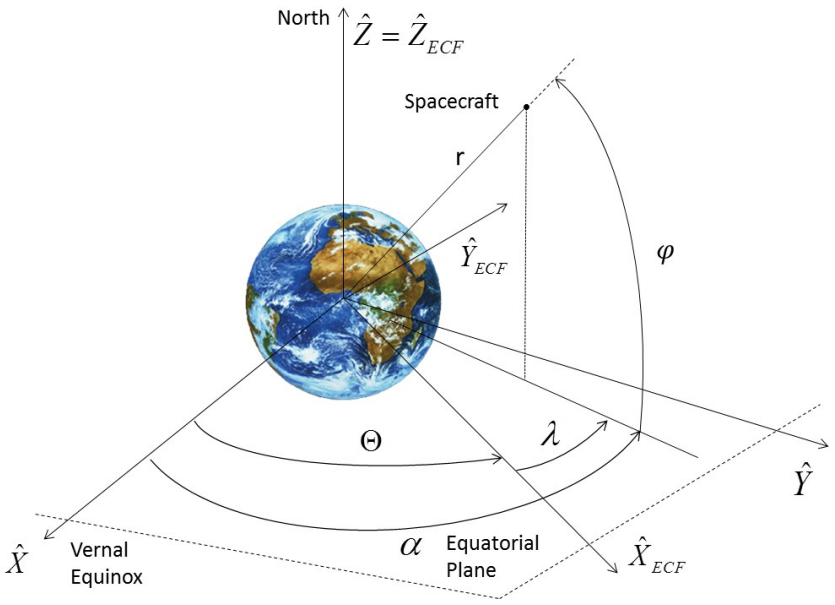

Figure 2.3. Greenwich Hour Angle, Geographical Latitude and Longitude

2.3.1 Position and Velocity Coordinates

A common way to parametrize the orbital motion of a spacecraft about a central body is to adopt a state vector comprised of the Cartesian coordinates. The Cartesian state vector includes the position and velocity vectors of the spacecraft measured in terms of the ECI reference frame and are denoted as follows

$$\bar{r} = \begin{bmatrix} x & y & z \end{bmatrix}^T, \tag{2.9}$$

$$\bar{v} = \dot{\bar{r}} = \begin{bmatrix} \dot{x} & \dot{y} & \dot{z} \end{bmatrix}^T. \tag{2.10}$$

The six-dimensional state vector representation is then given by

$$\bar{x}_{In} = \begin{bmatrix} x & y & z & \dot{x} & \dot{y} & \dot{z} \end{bmatrix}^T \tag{2.11}$$

at a particular epoch. The epoch associated with a state vector is often considered the seventh component of the state vector.

2.3.2 Keplerian Orbit Elements

An alternative and, perhaps, the most common parameter set to describe fundamentally conic orbital motion are the Keplerian Orbital Elements (KOE). The classical Keplerian orbital elements consist of six parameters: semi-major axis a, eccentricity e, inclination i, right ascension of the ascending node Ω, argument of perigee ω and true anomaly ν. The definitions of the KOE are referenced in the ECI frame as indicated in Figure 2.4. The first two parameters describe the size and shape of the orbit, the next three describe the orientation of the orbit in space and the final parameter describes the position of the body in the orbit. Additional parameters used to describe the body's position in the orbit are the eccentric anomaly E and the mean anomaly M and are represented in Figure 2.5.

- The *semi-major axis* a specifies the size of the orbit and is half the distance between perigee (the location in the orbit closest to the Earth) r_p and apogee (the location in the orbit farthest from the Earth) r_a.

- The *eccentricity* e characterizes the shape of the orbit and is the magnitude of a vector $\bar{e}$ that is directed along the line of apses towards perigee. A perfect circular orbit possesses an eccentricity of zero and, for elliptical orbits, the eccentricity is between zero and one.

- The *inclination* i is an angle between the orbital plane and the equatorial plane with a value between zero and 180 degrees. It is defined as the angle between the angular momentum vector $\bar{h} = \bar{r} \times \bar{v}$ of the orbit and the inertial unit vector $\hat{Z}$

$$\cos i = \frac{\hat{Z} \cdot \bar{h}}{h} \tag{2.12}$$

- The *Right Ascension of the Ascending Node (RAAN)* Ω is the angle between the direction defined as the point of Ares the intersection of the equatorial plane and the ecliptic plane and the direction defined by the ascending node. The nodal line reflects the intersection of the orbital plane and the equatoral plane.

- The *argument of perigee* ω is the angle measured, in the orbital plane, from the ascending node direction to the line of apsides, i.e., to the eccentricity vector $\bar{e}$, which is always directed toward perigee

$$\omega = arccos\left(\frac{\bar{n}\cdot\bar{e}}{ne}\right) \tag{2.13}$$

- The *true anomaly* ν is the angle from the perigee direction $\bar{e}$ to the radial position vector $\bar{r}$ of the body in the orbit.

- The *eccentric anomaly* E is an angle measured only in elliptical orbits. It is evaluated as the angle between two lines. First is the eccentricity vector. Then, a line from the center of the ellipse to the auxiliary circle; the point on the auxiliary circle corresponds to the projection of the body's location orthogonal to the line of apsides.

- The *mean anomaly* M is the angle swept out from the center of the ellipse, increasing uniformly with time, and effectively represents the mean motion. The mean anomaly is related to the time since passage through periapsis as

$$M = n(t - t_p), \tag{2.14}$$

  where n is the mean motion defined by

$$n = \sqrt{\frac{GM_{\oplus}}{a^3}}. \tag{2.15}$$

Eccentric and true anomaly are related, consistent with the following equations

$$\sin E = \frac{\sin \upsilon\sqrt{1-e^2}}{1+e\cos\upsilon}, \tag{2.16}$$

$$\cos E = \frac{e+\cos\upsilon}{1+e\cos\upsilon}. \tag{2.17}$$

The eccentric anomaly and mean anomaly are also related through Kepler's equation

$$E - e\sin E = M, \tag{2.18}$$

that is, the position of a body in the orbit as a function of time in terms of the eccentric anomaly. The computation of the eccentric anomaly E involves a transcedental operation and an interative scheme must be employed. In this work, the state using Keplerian orbit elements is denoted

$$\bar{x}_{KOE} = \begin{bmatrix} a & e & i & \Omega & \omega & anomaly \end{bmatrix}^T \tag{2.19}$$

with the *anomaly* component equal to either true anomaly ν or mean anomaly M. Keplerian orbit elements offer a general description of the orbit shape and orientation in space.

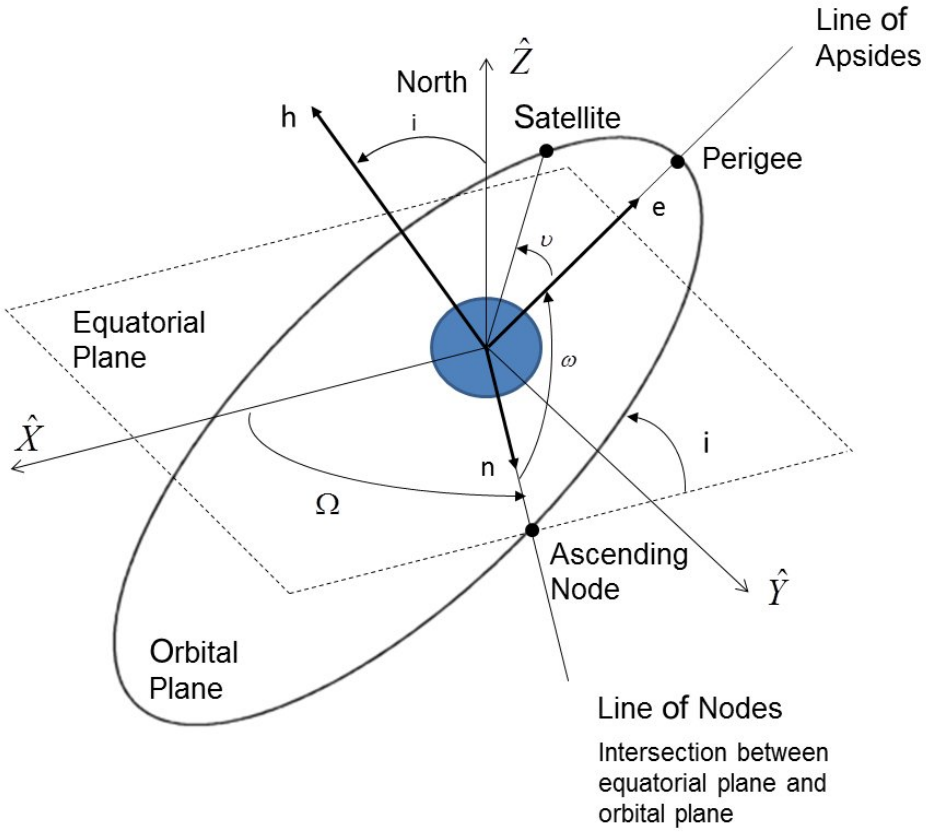

Figure 2.4. Keplerian Orbit Elements

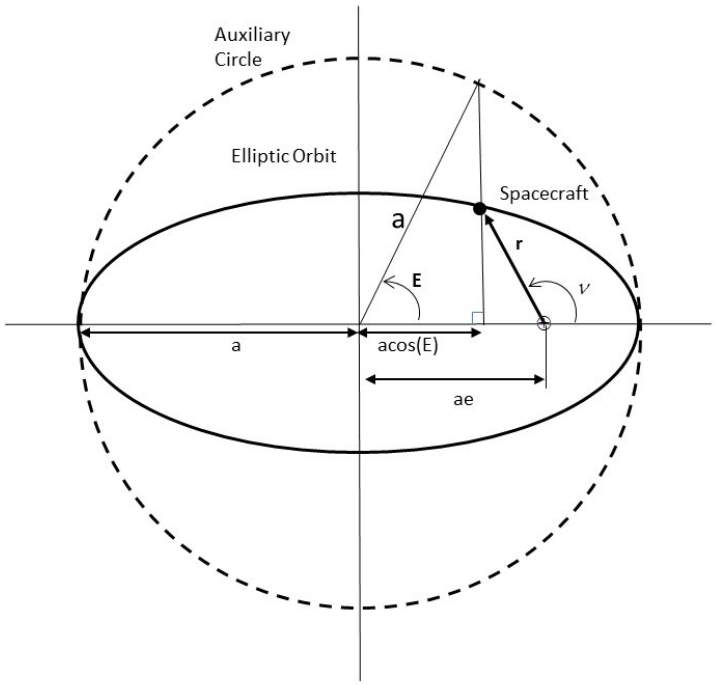

Figure 2.5. True and Eccentric Anomalies for Elliptic Orbits

2.3.3 Equinoctial Orbit Elements

Keplerian orbit elements suffer from two singularities and are, hence, poorly suited for geostationary orbits. For near-circular orbits, the line of apsides and the argument of perigee are poorly defined. For near-equatorial orbits, the ascending node is not well defined and, hence, the second singularity occurs in the compuation of the right ascension of the ascending node. Thus, geostationary orbits are most commonly represented in terms of equinoctial orbit elements. A quantity useful for elliptic, near-equatorial orbits, is the sum of the argument of perigee ω and the RAAN Ω, i.e., the longitude of perigee, ϖ,

$$\varpi = \omega + \Omega. \tag{2.20}$$

Note that this quantity only has physical meaning for near-equatorial orbits since Ω is measured in the Earth's equatorial plane, whereas ω is measured in the orbit plane. A useful quantity for an inclined circular orbit, is the argument of latitude, the angle

measured eastwards from the ascending node to the spacecraft position vector given by

$$w = \omega + \nu. \tag{2.21}$$

Note that both the argument of periapsis and the true anomaly are measured in the orbit plane. For a perfectly circular orbit, both the longitude of perigee and the argument of perigee remain undefined. However, the true longitude L can be computed as

$$L = \omega + \Omega + \nu, \tag{2.22}$$

and the mean longitude is denoted by

$$\lambda = \Omega + \omega + M. \tag{2.23}$$

For a near-circular, near-equatorial orbit, such as the geostationary orbit, the true longitude is approximated by the right ascension α.

Geostationary orbits are most commonly represented in terms of equinoctial orbit elements and a slightly modified set is employed. In the present investigation, the absolute orbit is characterized by the longitude offset (relative to the nominal longitude), the drift rate with respect to the nominal geostationary mean motion as in

$$n_{Geo} = \sqrt{\frac{\mu}{{a_{Geo}}^3}}, \tag{2.24}$$

as well as the eccentricity and inclination vectors. Thus, the orbital elements are defined as follows:

- *Drift Rate*

$$D = \sqrt{\frac{\mu}{a^3}} - n_{Geo} \tag{2.25}$$

- *Eccentricity vector* $\bar{e} = (e_x, e_y)$ with

$$e_x = e \cdot \cos(\Omega + \omega), \tag{2.26}$$

$$e_y = e \cdot \sin(\Omega + \omega). \tag{2.27}$$

The eccentricity vector is in the orbital plane and directed from Earth to the orbit perigee with magnitude equal to eccentricity, e. The eccentricity vector components, e_x and e_y, are projections of the eccentricity vector onto the $\hat{X}$ and $\hat{Y}$ axes of the ECI equatorial plane for small inclination.

- *Inclination vector* $\bar{i} = (i_x, i_y)$ with

$$i_x = \sin i/2 \cdot \cos \Omega, \tag{2.28}$$

$$i_y = \sin i/2 \cdot \sin \Omega. \tag{2.29}$$

The inclination vector components, i_x and i_y, are the projections of the angular momentum vector onto the $\hat{X}$ and $\hat{Y}$ axes of the ECI equatorial plane and for small inclination, the two-dimensional inclination vector $\bar{i}$ is offset by 90^o from the line of nodes in the ECI equatorial plane.

- *Longitude offset or deviation* $\Delta\lambda$

$$\Delta\lambda = \Omega + \omega + M - \Theta - \lambda_{nominal}, \tag{2.30}$$

where $\lambda_{nominal}$ is the nominal station longitude.

In this work, the state using equinoctial orbit elements is denoted as

$$\bar{x}_{equin} = \begin{bmatrix} D & e_x & e_y & i_x & i_y & \Delta longitude \end{bmatrix}^T. \tag{2.31}$$

with the longitude component equal to either true longitude L or mean longitude λ. The equinoctial orbit elements are primarily used to represent the orbital motion of geostationary spacecraft.

2.4 Force Models

The different forces acting on a geostationary spacecraft and their effects on the motion are critical to the model. In the absence of any perturbations, the shape and orientation of the orbit as well as the orbital elements remain constant. In reality,

however, an ideal geostationary orbit is not possible due to the gravitational perturbative forces from the Sun, the Moon, as well as differential gravity from the Earth, which all contribute to changing the orbit elements. Since all these perturbing forces are small compared to the spherical nature of the Earth gravity potential, the ideal geostationary orbit remains a good approximation but, in reality, the instantaneous orbit is allowed to deviate slightly from the ideal geosynchronous orbit. Any force acting on the spacecraft other than the spherical symmetric attraction of the Earth produces an perturbing acceleration that modifies the orbital elements. In Table 2.4, the magnitudes of the most dominant accelerations at the geostationary altitude are summarized. The perturbing accelerations listed in the top portion of Table 2.4 are included in the high-fidelity ephemeris model, developed by DLR and the commercial satellite operator SES, that is employed for all inertial propagations. The perturbing accelerations listed in the bottom portion of Table 2.4 are generally not modeled for geostationary applications [53]. The perturbations that are the most dominant in influencing the behavior of effecting geostaionary spacecraft are:

- Nonspherical Earth gravitation (J_2, J_{22})
- Gravitational attraction of Sun and Moon
- Solar Radiation Pressure (SRP)

For the dominant perturbing forces, the spacecraft mass is negligable in the calculation of the perturbing acceleration with the exception of SRP. Solar radiation pressure is dependent on the spacecraft surface area to mass ratio, A/M. The effects of each perturbation on the geostationary orbit are noticeable. A distinction is used for classification, that is, between short-term effects, with a period of one day or less, and long-term effects.

Table 2.1 Sizes of the different perturbing accelerations affecting a geostationary spacecraft [53]

Earth (point mass)	2.3×10^{-4} km/s^2
Moon (point mass)	1.1×10^{-8} km/s^2
J_2 (radial)	7.7×10^{-9} km/s^2
Sun (point mass)	5.0×10^{-9} km/s^2
J_{22},J_{31},J_{33} (tangential)	1.7×10^{-10} km/s^2
SRP (A/M =0.05 m^2/kg)	2.3×10^{-10} km/s^2
J_{40} (radial)	3.7×10^{-13} km/s^2
J_{60} (radial)	3.2×10^{-15} km/s^2
Indirect SRP of the Earth	2.0×10^{-12} km/s^2
Venus	4.3×10^{-12} km/s^2
Relativity	2.3×10^{-14} km/s^2
Tidal Bulge	2.7×10^{-14} km/s^2

2.4.1 Non-Sperical Terms in the Earth Gravitational Potential

In reality, the Earth is not a perfect homogenous sphere exerting only a radial inverse square attractive force. The Earth's gravitational potential must be corrected to include additional terms. Specifically, the perturbing forces from the Earth tesseral terms, J_{22}, J_{31} and J_{33}, are significant for geostationary spacecraft since these particular terms include a secular effect. In other orbits, the directions of these perturbations vary throughout the orbit and the cumulative net effect is close to zero. In a geostationary orbit, however, as the relative position of the satellite with respect to the Earth remains fixed, the direction of the acceleration from these tesseral terms remains constant and produces a significant cumulative effect on the evolution of the longitude. Using a spherical harmonic expansion of the Earth's potential, as described by Kaula [54], the potential can be expressed in the general form

$$\begin{aligned} U = &-\frac{\mu}{r} + \frac{\mu}{r}\sum_{n=2}^{\infty} J_n \left(\frac{R_e}{r}\right)^n P_n\left(\sin\delta\right) \\ &- \frac{\mu}{r}\sum_{n=2}^{\infty}\sum_{m=1}^{n}\left(\frac{R_e}{r}\right)^n P_{n,m}\left(\sin\delta\right)\cos\left(m\left(\lambda-\lambda_{n,m}\right)\right), \end{aligned} \tag{2.32}$$

where

$$P_{n,m}(x) = \left(1 - x^2\right)^{m/2} \frac{d^m P_n(x)}{dx^m} \tag{2.33}$$

and

$$P_n(x) = \frac{1}{(-2)^n n!} \frac{d^n}{dx^n} \left(1 - x^2\right)^n. \tag{2.34}$$

In equation (2.32), the position of the spacecraft is represented in the spherical coordinates, r (radius), δ (latitude) and λ (longitude), R_e is the mean equatorial radius of the Earth and $P_{n,m}$ are the associated Legendre polynominals. The terms $J_{n,m}$ are scaling factors and $\lambda_{n,m}$ are orientation parameters. According to Soop [20], for the geostationary orbit the zonal terms, primarily J_2, produce an acceleration in the radial and out-of-plane directions. The radial component adds to the central potential and results in an increase of the geostationary orbit altitude by 0.5 km. The out-of-plane component influences the direction of the inclination vector drift, resulting in a drift in the RAAN angle Ω of approximately

$$\frac{d\Omega}{dt} = 4.9^o/\text{year}. \tag{2.35}$$

The tesseral terms yield a constant acceleration in either the East or West directions depending on the longitude. This acceleration is evaluated as

$$a^{Drift} = -\frac{1}{r \cos\delta} \frac{\delta U}{\delta \lambda} \tag{2.36}$$

and, with equation (2.32) substituted, results in

$$a_{2,2}^{Drift} = -5.589 \times 10^{-8} \sin(2(\lambda + 14.9))\text{m/s}^2 \tag{2.37}$$

due to the J_{22} tesseral. Using this simplified analysis for only the J_{22} tesseral, clearly four equilibrium points exist in longitude where the acceleration is zero. Further analysis demonstrates that two are stable and two are unstable. Incorporating all appropriate terms from the Earth's potential, the true stable and unstable longitudes are determined as

- Stable points at 75.1^o E and 105.3^o W

- Unstable points at 11.5^o W and 161.9^o E

A spacecraft accelerates towards the nearest stable point. In Figure 2.6, the natural evolution of the longitude appears, along with the longitudinal drift, as well as the evolution of the semi-major axis from the Earth's gravity for a spacecraft at 23.5^{o}E over the course of one year.

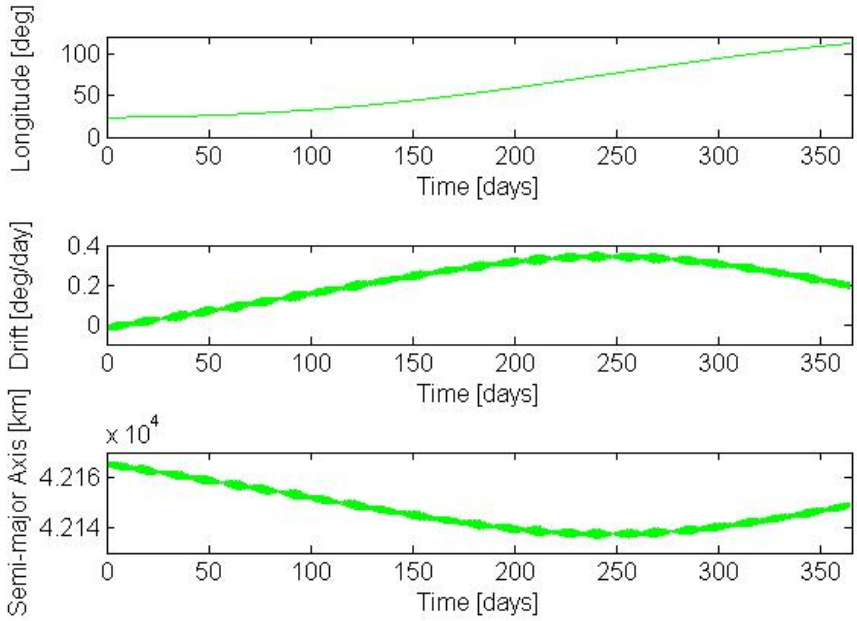

Figure 2.6. Natural longitude, longitudinal drift and semi-major axis evolution over one year for a spacecraft starting at λ=23.5^o

2.4.2 Third Body (Luni-Solar) Perturbations

All the planets exert a gravitational attraction on a geostationary spacecraft. These forces are proportional to the mass of the body and inversely proportional to the square of the distance of the celestial body to the spacecraft. Since geostationary spacecraft are much closer to the Earth, the effects of these forces are typically modeled as perturbations. The two largest perturbations are produced by the grav-

itational attraction of the Sun and the Moon. The total acceleration on a satellite in an inertial reference system including only the dominant point mass Earth gravity plus additional point masses is written

$$\ddot{\bar{r}} = -\frac{\mu}{r^3}\bar{r} + \sum_{k=1}^{2} \frac{\mu_k}{|\bar{r}_k - \bar{r}\,|^3}\left(\bar{r}_k - \bar{r}\right), \tag{2.38}$$

where the subscript $k = 1$ represents the Sun and $k = 2$ identifies the Moon. However, the Earth itself is also attracted by the Sun and the Moon and since an Earth-centered reference frame is used, the acceleration of the satellite in this reference system is due to the difference of the gravitational attraction of the Sun and the Moon with respect to their attraction to the Earth. Subtracting the acceleration of the Earth due to the gravity of the Sun and Moon results in

$$\ddot{\bar{r}} = -\frac{\mu}{r^3}\bar{r} + \sum_{k=1}^{2} \mu_k \left[\frac{\bar{r}_k - \bar{r}}{|\bar{r}_k - \bar{r}\,|^3} - \frac{\bar{r}_k}{r_k^3}\right]. \tag{2.39}$$

Since r_k is much larger than r, the terms inside the summation almost cancel. To better visualize the remaining effect, the equation is expanded linearly in r/r_k and truncated yielding

$$\ddot{\bar{r}} \approx -\frac{\mu}{r^3}\bar{r} + \sum_{k=1}^{2} \frac{\mu_k}{r_k^3}\left[\frac{3}{r_k^2}\left(\bar{r}_k\bar{r}\right)\bar{r}_k - \bar{r}\right]. \tag{2.40}$$

The last term in equation (2.40) is a negative, almost constant, radial acceleration which raises the geostationary orbit. The precession of the reference frame yields another almost constant radial acceleration on the order of 4×10^{-8} m/s^2, lowering the mean geostationary orbit. When all the constant contributions of the gravitational potentials due to the Earth, the Sun and the Moon, as well as the Coriolis acceleration due to the reference system are incorporated, the mean geostationary radius becomes 42164.5 km. The second term in equation (2.40) is the oscillating acceleration in the direction of the perturbing body, which consists of an in-plane and a out-of-plane acceleration for both the Sun and the Moon. A detailed analytic treatment of the effects of the luni-solar perturbations and the evolution of the inclination vector is presented in [21, 23]. The acceleration components due to the perturbations are analyzed in terms of their components:

- *In-plane acceleration component* The in-plane component of the perturbations, due to the Sun, reaches its maximum twice a day when the satellite is located on the same or opposite side of the Earth relative to the Sun. The result is a libration in the radius r and the longitude λ twice per orbit, where r is largest in the direction of the Sun and opposite to it. The libration in λ is shifted ahead of that in r by 45^o. A similar result applies to the in-plane component due to the Moon. Both contributions are added, resulting in the largest contribution when the Sun and Moon are both in line with the Earth, which occurs twice per month, known as the spring tide. The smallest contribution occurs when the Sun and Moon are at right angles relative to the Earth, known as neap tide. The eccentricity vector $\bar{e}$ rotates in the negative direction, once per sidereal day. However, this daily rotation is a result of fitting the orbital elements to the shape of the perturbed orbit. At spring tide, the perturbed orbit is an ellipse with the minor axis oriented in the direction of the Sun and the Moon with the Earth lying at the center of the ellipse and not at the focal point. The mean eccentricity vector, averaged over one orbit, rotates in the positive direction with the same period as the Moon's orbit around the Earth, with a radius of 3.5×10^{-5} km. The effect of the Sun on the mean eccentricity vector is dominated by the effect of the Solar radiation pressure.

- *Out-of-plane acceleration component* The inclination vector phase space is best used to visualize the out-of-plane component of the Luni-Solar perturbations. In the Earth-centered reference frame, the Sun's orbital plane is at an angle of approximately 23.442^o with respect to the Earth's equatorial plane. This results in a maximum northward acceleration during half of the day and a maximum southward acceleration during the other half of the day, both solstices. During the autumn and spring equinoxes, the Sun's out-of-plane component cancels. The result is a torque on the orbital angular momentum vector, shifting it to a direction close to the inertial $\hat{X}$-axis. The inclination vector will grow in the direction close to the inertial $\hat{Y}$-axis. The result is a semi-annual periodic

motion of the inclination vector together with a drift. The mean drift of the inclination vector, per year due to the Sun, starting from zero inclination is given by

$$\frac{di^{Sun}}{dt} = 0.27^{\circ}/\text{year}. \tag{2.41}$$

Similarly for the Moon, the acceleration and corresponding torque on the spacecraft angular momentum vector have a maximum twice per lunar period and zero in between. However, even though the Moon has a constant inclination of 5.14^o with respect to the ecliptic, its ascending node rotates or precesses around the pole of the ecliptic, due to the same out-of-plane acceleration of the Sun, once in 18.6 meton years. This leads to an oscillation of the Moon's inclination with respect to the Earth approximately equal to $23.44^o \pm 5.14^o$ depending on the year in the 18.6 year cycle. Because the tilt of the Earth's rotation axis is in the same direction for the Sun and the Moon, the drift of the inclination vector resulting from the Lunar influence is also in Y-direction. The values of the drift for years with maximum and minimum inclination of the Moon's orbit are:

$$\frac{di_{min}^{Moon}}{dt} = 0.478^{\circ}/\text{year}, \tag{2.42}$$

$$\frac{di_{max}^{Moon}}{dt} = 0.674^{\circ}/\text{year}. \tag{2.43}$$

In addition to the luni-solar perturbation, the Earth J_2 term also produces a drift of Ω or a rotation of the inclination vector $\bar{i}$ around the $\hat{Z}$-axis with a value of -4.9^o/year. Additionaly, the motion of the ECI frame produces an additional drift in the inclination vector of 0.005^o/year in the direction of the negative $\hat{Y}$-axis and a rotation around the $\hat{Z}$-axis of 0.01^o/year. The direction of the mean secular drift varies depending on the inclination of the Moon. In Figure 2.7, the natural evolution of the inclination vector over one year is plotted in the inclination phase space i_x, i_y.

The effects of the third-body (Luni-Solar) gravitational perturbations are most dominant in their effect on the out-of-plane motion of geostationary spacecraft. The effect of the Sun on the mean eccentricity vector is dominated by the effect of the Solar radiation pressure.

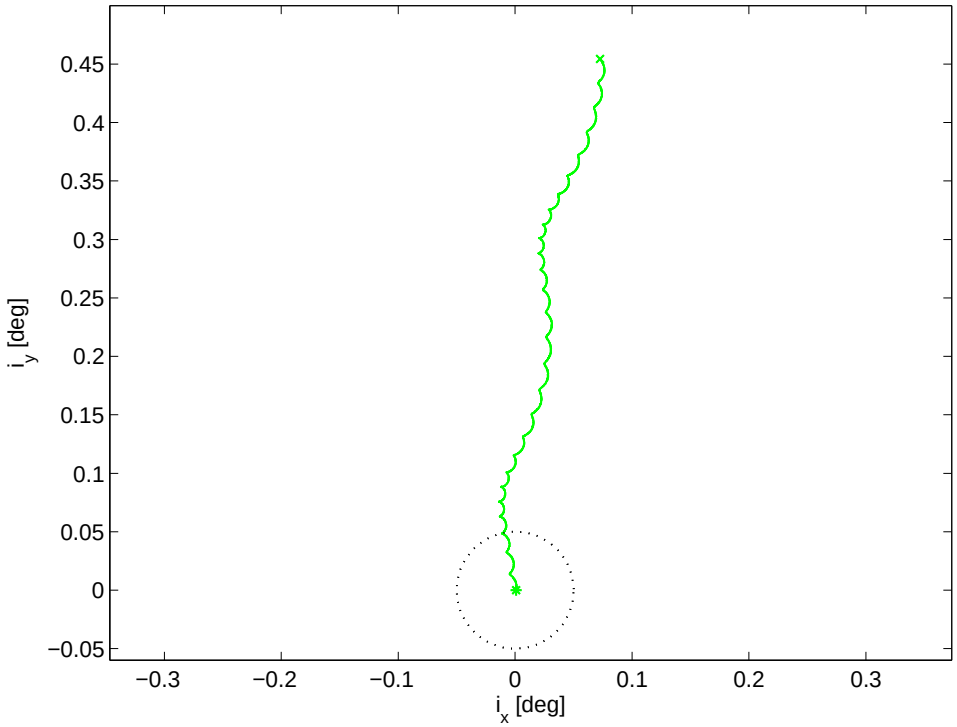

Figure 2.7. Natural Evolution of the Inclination Vector over one Year

2.4.3 Solar Radiation Pressure

Solar Radiation Pressure (SRP) is a force that results from the photons and small particles that are emitted from the Sun. In contrast to the gravitational perturbations, SRP depends on the physical characteristics of the spacecraft. The resulting acceleration is dependent on the spacecraft mass, surface area and the reflectivity coefficient. The size of the SRP force is determined by the solar flux and calculated by dividing the solar flux of the Sun by the speed of light. At one AU from the Sun, i.e., the vicinity of the Earth, the solar flux amounts to $\Phi \approx 1.367 \mathrm{Wm}^{-2}$ and the

resulting Solar radiation pressure is approximately $P_{\odot} \approx 4.56 \times 10^{-6}\mathrm{Nm}^{-2}$. Assuming that the spacecraft surface absorbs all the photons and is perpendicular to the incoming radiation, the magnitude of the resulting force becomes

$$F = -PAcos\theta_{SRP}(1+\epsilon), \tag{2.44}$$

where $Acos\theta_{SRP}$ is the surface area illuminated by the Sun and ϵ is the reflectivity coefficent, which is between 0 (complete absorption) and 1 (complete reflection). The angle θ_{SRP} is measured between the vector $\bar{n}$, that is normal to of the spacecraft surface area and the vector $\bar{r}_{Sun}$. Dividing by the spacecraft mass yields the acceleration

$$\ddot{\bar{r}}_{SRP} = P\frac{A}{m}cos\theta_{SRP}(1+\epsilon). \tag{2.45}$$

In the above equation, $(1+\epsilon)$ is commonly replaced by C_R, the radiation pressure coefficent. This acceleration is always directed away from the Sun and decreases with the square of the distance from the Sun. Since the acceleration due to SRP is proportional to the Area-to-Mass (A/M) ratio, it changes over the lifetime of a spacecraft and can vary significantly between smaller and larger vehicles. For communications satellites with large solar arrays which remain perpendicular to the Earth's equator, the acceleration will vary over the course of the year by the cosine of the Sun's declination.

Solar radiation pressure results in an increase in the semi-major axis during half the sidereal day, when the component is in-line with the velocity vector of the spacecraft and achieves its minimum during the other half of the sidereal day. Averaged over an entire orbit, the semi-major axis is not affected by SRP. In Figure 2.8, the acceleration due to SRP is decomposed into radial and tangential components; the figure illustrates the effects of SRP on the shape of the geostationary orbit in terms of eccentricity. The out-of-plane component of the acceleration is opposite to the gravity of the Sun and, thus, effectively reduces the drift of the inclination vector.

The effect of SRP is best examined in the plane of the eccentricity vector, or eccentricity phase space, that is, $e_x - e_y$ space. A detailed analytical treatment of the

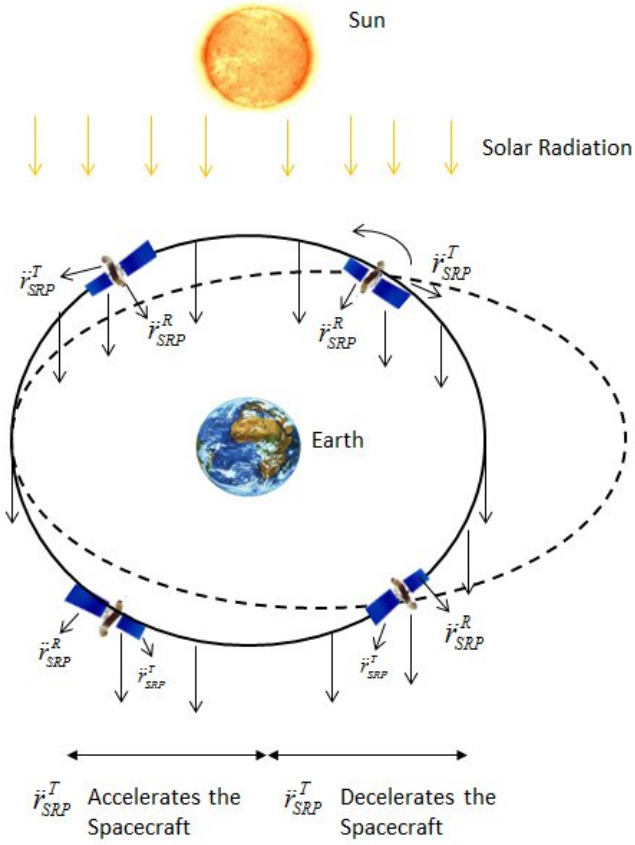

Figure 2.8. Effects Induced on the Orbit Eccentricity by Solar Radiation Pressure

evolution of the eccentricity vector is detailed in work by Sidi [21] and Carrou [23]. For the simplified scenario assuming a planar equatorial orbit for the Sun, as well as constant value for $\sigma = \frac{C_R A}{MP}$, the evolution of the eccentricity vector is descibed by

$$e_x(t) = e_x(t_0) + E_N \left(\cos \lambda_{Sun}(t) - \cos \lambda_{Sun}(t_0)\right) \tag{2.46}$$

$$e_y(t) = e_y(t_0) + E_N \left(\cos \lambda_{Sun}(t) - \cos \lambda_{Sun}(t_0)\right) \tag{2.47}$$

where λ_{Sun} is the longitude of the Sun and E_N is the radius of the natural eccentricity circle. This radius is defined as

$$E_N = \frac{3 C_R \; A \; P_o}{2 \, m \, V_{Geo} n_{Sun}}, \tag{2.48}$$

where n_{Sun} is the mean motion of the Sun's apparent orbit around the Earth. Over the course of one year, the tip of the eccentricity vector traces out a circle, whose center is located at

$$C_x = e_x(t_0) - E_N cos\lambda(t_0), \tag{2.49}$$

$$C_y = e_y(t_0) - E_N cos\lambda(t_0). \tag{2.50}$$

The natural evolution of the eccentricity vector, subject to the gravity of the Sun and Moon, as well as the solar radiation pressure, over the course of one year, is plotted in Figure 2.9. The steady-state eccentricity vector rotates about its inertial center completing one full circle every year. An fuel-efficient stationkeeping strategy,

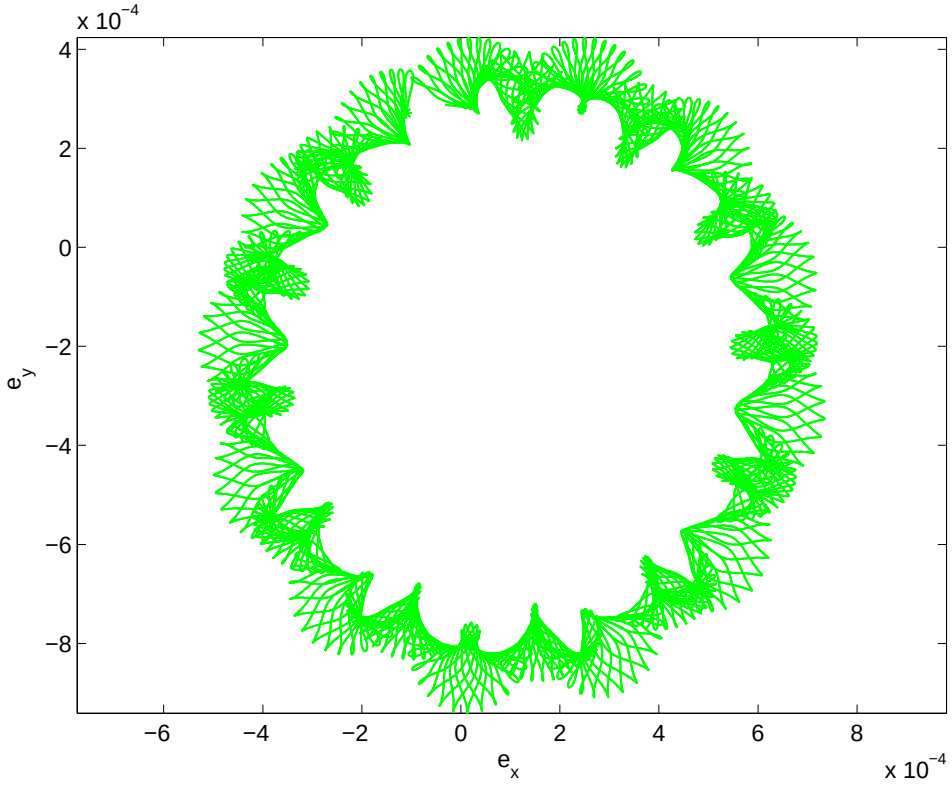

Figure 2.9. Natural Evolution of the Eccentricity Vector over one Year

in terms of propellant is the SPPS, where the spacecraft eccentricity vector is forced to move along an eccentricity control circle and move Sun-synchronously. For large

communications spacecraft, the eccentricity control circle is often smaller than the natural eccentricity circle.

2.5 Eccentricity and Inclination Separation

Without a coordinated separation strategy, the probability of close encounters and potential collisions is unacceptably large. A proven and commonly employed separation strategy is based on assigning each spacecraft in the constellation a different eccentricity and inclination vector (e-i), which is equivalent to off-setting the perigee and the line of nodes corresponding of each orbit. The use of the eccentricity and inclination vector separation strategy for safely maintaining multiple spacecraft at one longitudinal position is well documented [2, 20]. Eccentricity and inclination vector separation ensures separation in the radial, tangential, and normal directions. The eccentricity and inclination vector phases uniquely define the orbit shape and orientation in space. The difference in eccentricity vectors ensures separation in radial and tangential directions and the difference in inclination vectors creates an out-of-plane separation. A combination of eccentricity and inclination seperation ensures safe separation at all times. An advantage to this approach is that each spacecraft uses the entire longitudinal control box, while still maintaining safe separation. The eccentricity and inclination vector phase spaces are illustrated in Figure 2.10. Note that the origin of both the eccentricity and inclination phase indicates a perfect circular, equatorial orbit.

Eccentricity and inclination vector separation is generally combined with the Sun-Pointing-Perigee-Strategy (SPPS). The individual satellite target eccentricity vectors are not directed toward the Sun, although they move Sun-synchronously as viewed from the center of the dashed circles in Figure 2.10. With all the spacecraft following a coordinated stationkeeping strategy, the relative eccentricity and inclination vectors remain nominally constant in magnitude and direction as long as the size of the eccentricity control circle is the same for all the spacecraft in the constellation.

The implementation of the eccentricity and inclination vector separation strategy in the eccentricity and inclination phase space is illustrated in Figure 2.10. Selecting the relative eccentricity and inclination vectors for each deputy to be parallel, yields the maximum out-of-plane separation, when the in-plane separation vanishes. Detailed adaptations and improvements for an operational safe and practical implementation are discussed by Wauthier et al. [2].

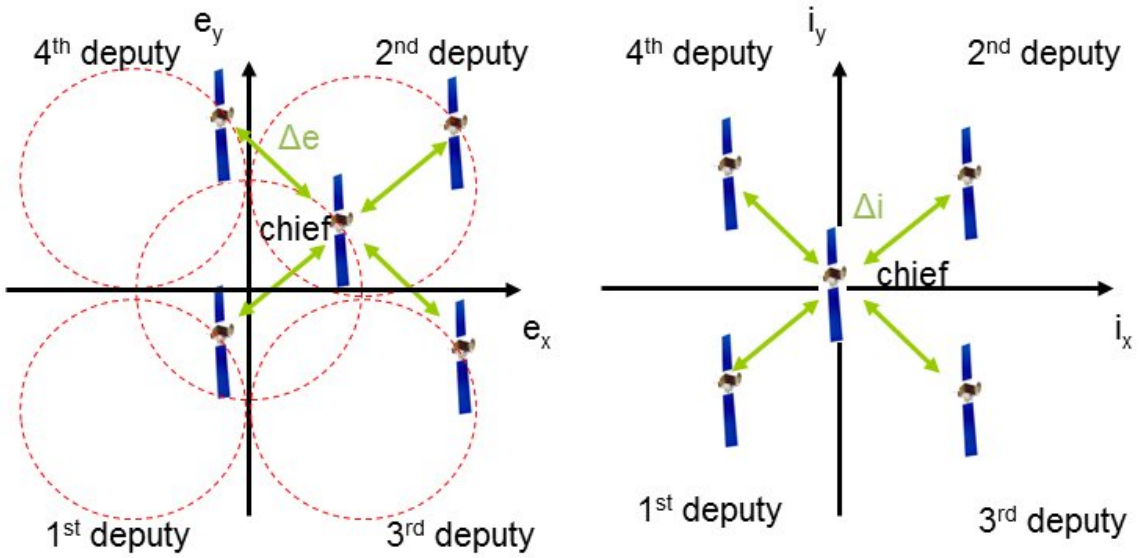

Figure 2.10. The spacecraft are separated using eccentricity and inclination vector separation. The red dashed circles in the $e_x - e_y$ phase space indicate the eccentricity control circles delivered by the spacecraft over the course of one year while following a Sun-pointing-perigee-strategy.

3. RELATIVE ORBIT GUIDANCE AND CONTROL

Two key components of any relative orbit control concept are an efficient relative orbit determination process and an effective relative orbit control formulation. For relative orbit determination, measurements that can easily be related to the parameters that are employed to describe the nominal orbit are critical and the capability to reasonably approximate the relative orbit at a future time must be available. Since N-S (out-of-plane) correction maneuvers are usually significantly larger than E-W (planar) delta-V's, minute thruster misalignments result in cross-coupling between normal and radial/tangential directions. Hence, the proposed orbit control framework must allow for deterministic thruster cross-coupling to be modeled in the computation of the tangential correction burns that are applied to the deputies.

3.1 Relative Coordinates

To fully describe the relative orbit of each deputy vehicle with respect to the chief spacecraft, it is necessary to specify six independent parameters. From among the available options, the sets of relative coordinates that are employed in this analysis include chief-centered Cartesian coordinates, curvi-linear coordinates, and mean equinoctial orbit element differences. Measurements of the deputy's relative orbit with respect to the chief spacecraft are likely to be generated in terms of range, azimuth and elevation. These coordinates are readily translated into chief-centered relative Cartesian coordinates or curvi-linear coordinates. Mean equinoctial orbit element differences conveniently describe the deputy's nominal relative orbit and are then employed for the relative orbit control formulation.

3.1.1 Relative Coordinates for Measurements

Two sets of relative coordinates are investigated that are related straightforwardly to any relative orbit measurements generated on-board the chief spacecraft. First, chief-centered Cartesian coordinates are examined, followed by curvi-linear coordinates. The notation $\bar{x}^{Meas}$ is adopted to identify these measurement coordinates and either set can be employed. The performance of both sets is evaluated in this investigation.

Chief-Centered Cartesian Coordinates

The Chief-Centered Cartesian coordinates (CCC) are generally consistent with the more familiar Local-Vertical-Local-Horizon reference frame, also denoted the Hill-Clohessy-Wiltshire reference frame [32]. Consider the planar orbit about the Earth in Figure 3.1. The unit vector $\hat{x}_{CCC}$ extends radially outward from the chief and is parallel to the orbital radial direction. Then, the unit vector vector $\hat{z}_{CCC}$ is normal to the orbital plane of the chief and parallel to the inertial $\hat{Z}$-axis. The unit vector $\hat{y}_{CCC}$ completes the right-handed triad and is positive in the general direction of motion of the chief along its orbit. The relative state vector from the chief to the deputy is then defined as

$$\bar{x}_{CCC} = \begin{bmatrix} x_{CCC} & y_{CCC} & z_{CCC} & \dot{x}_{CCC} & \dot{y}_{CCC} & \dot{z}_{CCC} \end{bmatrix}^T \tag{3.1}$$

as illustrated in Figure 3.1. The x_{CCC} and y_{CCC} coordinates define the relative motion in the chief's orbit plane. The z_{CCC} coordinate reflects any motion out of the chief orbital plane. The chief-centered Cartesian coordinates are easily computed from both relative orbit measurements as well as inertial coordinates and, as a result, are extensively employed in relative orbital motion studies.

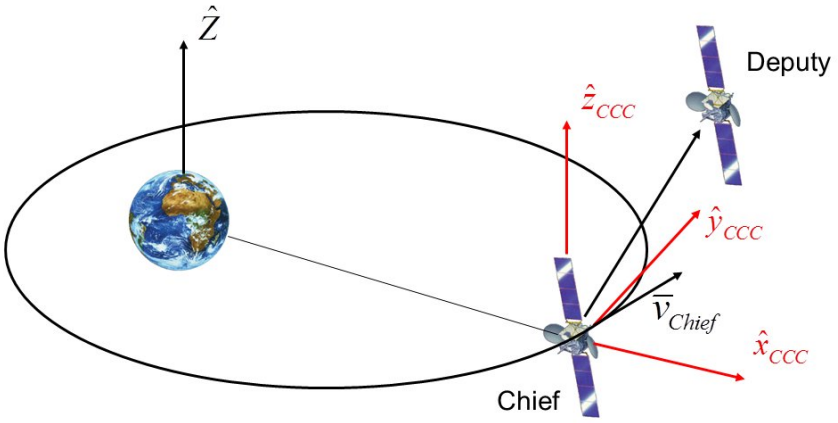

Figure 3.1. Chief Centered Cartesian Coordinate System or Hill-Clohessy-Wiltshire Coordinates

Curvilinear Coordinates

Traditionally, chief-centered Cartesian coordinates are employed in relative motion studies. However, since spacecraft actually move along curved arcs, the use of the chief-centered Cartesian reference frame results in undesirable errors due to the nonlinear terms as demonstrated by Alfriend et al. [55]. A description in terms of curvilinear coordinates may appear more natural and deliver better accuracy. The chief-centered curvilinear coordinates originate on the chief spacecraft with the x-axis along the chief's radius vector, the y-axis in the orbit plane and orthogonal to the x-axis in the direction of motion, and the z-axis is directed along the orbit normal. The corresponding unit vectors are denoted $\hat{u}_x, \hat{u}_y, \hat{u}_z$ and the corresponding sphercial coordinates are then labelled as $(\delta r, \theta_r, \phi_r)$, as illustrated in Figure 3.2. The chief spacecraft is assumed to move along a circular path of radius r_C. The vector from the origin of the Earth toward the chief spacecraft is denoted $\bar{r}_C$ and the vector from the origin of the Earth to the deputy spacecraft is denoted $\bar{r}_D$. Although $\bar{r}_D$ is clearly not parallel to $\bar{r}_C$, it can be assumed that its magnitude differs on a relatively small

scale from the distance r_C. Thus, the difference between the magnitude of the radial vectors locating the deputy and chief spacecraft is denoted by δr and computed by

$$\delta r = |\bar{r}_D| - |\bar{r}_C| \,. \tag{3.2}$$

The angle between the projection of the deputy's radius vector into the orbital plane of the chief, $\bar{r}_{DP}$, and the chief's radius vector, $\hat{u}_x = \hat{x}_{CCC}$, is θ_r, and ϕ_r is the out-of-plane angle, that is, the angle between the deputy's radius vector and the $\hat{u}_x - \hat{u}_y$ or $\hat{x}_{CCC} - \hat{y}_{CCC}$ plane. Figure 3.3 illustrates the two rotations that orient $\hat{r}_D$ relative to

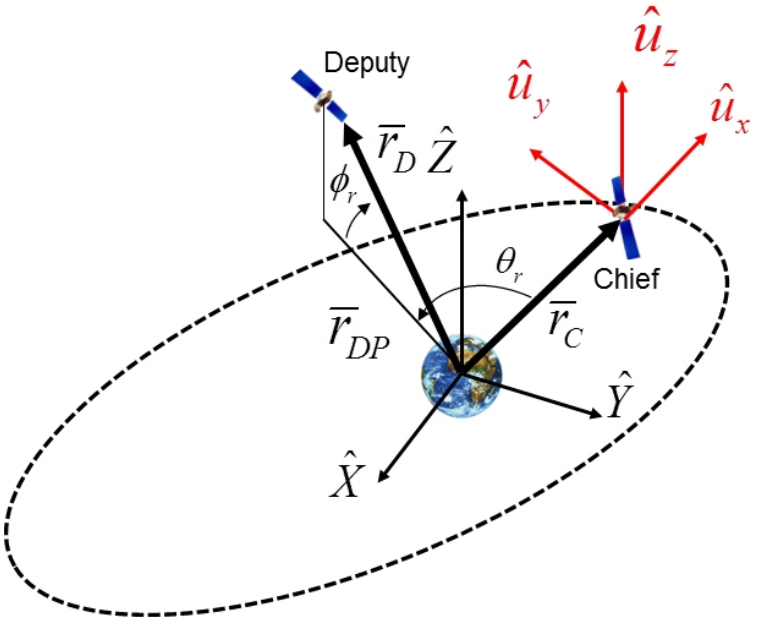

Figure 3.2. Relative Curvilinear Coordinate System

$\hat{r}_C$. A first rotation of θ_r about the $\hat{u}_z$ axis leading to the intermediate frame denoted by unit vectors $\hat{P}_D, \hat{P}_\theta, \hat{P}_Z$ with direction cosine matrix

$${}^{u}A^{P} = \begin{bmatrix} \cos\theta_r & -\sin\theta_r & 0 \\ \sin\theta_r & \cos\theta_r & 0 \\ 0 & 0 & 1 \end{bmatrix} . \tag{3.3}$$

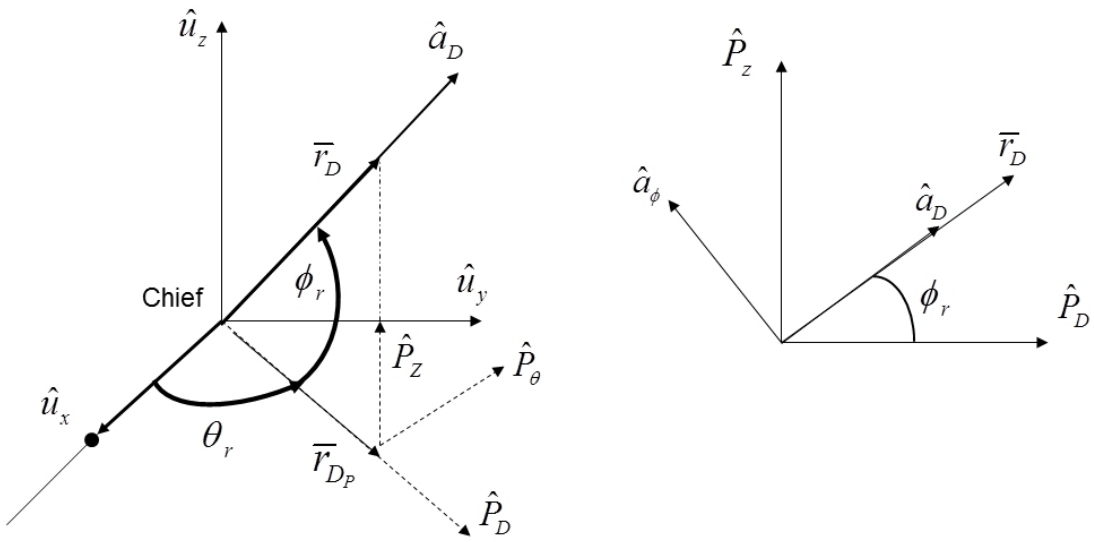

Figure 3.3. The Two Rotations Relating the Chief and Deputy Reference Frames

And a second rotation of ϕ_r about the negative $\hat{P}_\theta$ axis resulting in the deputy's rotating frame denoted by unit vectors $\hat{a}_D, \hat{a}_\theta, \hat{a}_\Phi$ with direction cosine matrix

$$^{P}A^{a} = \begin{bmatrix} \cos\phi_r & 0 & -\sin\phi_r \\ 0 & 1 & 0 \\ \sin\phi_r & 0 & \cos\phi_r \end{bmatrix}. \tag{3.4}$$

The resulting transformation matrix between $\hat{r}_C$ and $\hat{r}_D$ then is

$$\hat{r}_D = {}^{a}A^{PP}A^{u} = \begin{bmatrix} \cos\theta_r\cos\phi_r & \cos\phi_r\sin\theta_r & \sin\phi_r \\ -\sin\theta_r & \cos\theta_r & 0 \\ -\cos\theta_r\sin\phi_r & -\sin\phi_r\sin\theta_r & \cos\phi_r \end{bmatrix} \begin{bmatrix} \hat{u}_x \\ \hat{u}_y \\ \hat{u}_z \end{bmatrix}. \tag{3.5}$$

The unit vector $\hat{r}_D$ in the relative frame $(\hat{u}_x, \hat{u}_y, \hat{u}_z)$ of the chief then is

$$\hat{r}_D = \cos\phi_r\cos\theta_r\hat{u}_x + \cos\phi_r\sin\theta_r\hat{u}_y + \sin\phi_r\hat{u}_z. \tag{3.6}$$

The radius vector of the deputy is modelled as

$$\bar{r}_D = r_D\hat{r}_D = (r_C + \delta r)\,\hat{r}_D. \tag{3.7}$$

Differentiating with respect to time requires the use of the basic kinematic equation (BKE); the deputy's velocity vector then becomes

$$\bar{v}_D = \delta\dot{r}\hat{r}_D + \bar{\omega}_D \times (r_C + \delta r)\,\hat{r}_D, \tag{3.8}$$

where $\bar{\omega}_D$ is the angular velocity of the rotating frame of deputy with respect to the inertial frame. The angular velocity $\bar{\omega}_D$ is decomposed into the angular velocity of the rotating frame of the chief with respect to the inertial frame, $\bar{\omega}_C$, defined by

$$\bar{\omega}_C = n_C\hat{u}_z, \tag{3.9}$$

and the the differential angular velocity between the deputy and chief frames, as in

$$\bar{\omega}_D = \bar{\omega}_C + \bar{\omega}_{D/C}. \tag{3.10}$$

From Figure 3.3, the differential angular velocity between the deputy and chief frames, $\bar{\omega}_{D/C}$, in the chief-centered frame is

$$\bar{\omega}_{D/C} = \dot{\phi}_r \sin\theta_r\hat{u}_x - \dot{\phi}_r \cos\theta_r\hat{u}_y + \dot{\theta}_r\hat{u}_z. \tag{3.11}$$

Substituting into equation (3.8) yields

$$\bar{v}_D = \begin{bmatrix} V_R \\ V_\theta \\ V_\phi \end{bmatrix} = \begin{bmatrix} \left[\delta\dot{r}\cos\phi_r\cos\theta_r - (\delta r + a_0)\,\dot{\theta}_r\cos\phi_r\sin\theta_r - (\delta r + a_0)\,\dot{\phi}_r\sin\phi_r\cos\theta_r\right] \\ \left[\delta\dot{r}\cos\phi_r\sin\theta_r + (\delta r + a_0)\,\dot{\theta}_r\cos\phi_r\cos\theta_r - (\delta r + a_0)\,\dot{\phi}_r\sin\theta_r\sin\phi_r\right] \\ \left[\delta\dot{r}\sin\phi_r + (\delta r + a_0)\,\dot{\phi}_r\cos\phi_r\right] \end{bmatrix} \begin{bmatrix} \hat{u}_x \\ \hat{u}_y \\ \hat{u}_z \end{bmatrix}, \tag{3.12}$$

where

$$\bar{v}_D = V_R\hat{u}_x + V_\theta\hat{u}_y + V_\phi\hat{u}_z. \tag{3.13}$$

Inverting equation (3.12) to express the spherical velocity coordinates $\delta\dot{r}$, $\dot{\theta}_r$ and $\dot{\phi}_r$ in terms of velocity components yields

$$\delta\dot{r} = V_\theta\sin\theta_r\cos\phi_r + V_R\cos\phi_r\cos\theta_r + V_\phi\sin\theta_r, \tag{3.14}$$

$$\dot{\theta}_r = \frac{1}{(\delta r + a_0)\cos\phi_r}\left[-V_R\sin\theta_r + V_\theta\cos\theta_r\right], \tag{3.15}$$

and

$$\dot{\phi_r} = \frac{1}{(\delta r + a_0)} \left[\cos\phi_r V_\phi - \sin\theta_r \sin\phi_r V_\theta - \cos\theta_r \sin\phi_r V_R \right]. \tag{3.16}$$

The measurement state vector in curvi-linear coordinates is denoted by

$$\bar{x}_{Curvi} = \left[\delta r \quad r_C\theta_r \quad r_C\phi_r \quad \delta\dot{r} \quad r_C\dot{\theta_r} + \dot{r}_C\theta_r \quad r_C\dot{\phi_r} + \dot{r}_C\phi_r \right]^T, \tag{3.17}$$

where $\dot{r}_C$ reflects the change in the magnitude of the chief's position vector. Note that if the chief is in a perfect, circular, orbit, $\dot{r}_C$ is equal to zero. The chief-centered Cartesian and the curvilinear coordinates differ since the curvilinear coordinates represent the along-track and cross-track distances as measured along arc lengths rather than linear displacements.

3.1.2 Relative Coordinates for the Control Formulation

A relative orbit control formulation in terms of equinoctial orbit element differences is introduced. The chief-centered Cartesian and curvi-linear coordinates are rapidly changing throughout an orbital revolution and offer no insight into the orbital shape and the location of the spacecraft along the orbit. Hence, these coordinate sets are poorly suited for describing the nominal relative orbit and are not useful as a set of variables for formulating or implementing the control [39, 40]. The deputy spacecraft nominal relative orbit is, therefore, described in terms of mean equinoctial orbit element differences and the necessary control maneuvers are computed from mean orbit element deviations. The equinoctial orbit element differences are generated by subtracting the chief's equinoctical orbit elements from those of the deputy as in

$$\delta\overline{oe} = \overline{oe}_D - \overline{oe}_C = \left[\delta a, \delta\gamma, \delta e_x, \delta e_y, \delta i_x, \delta i_y \right]^T \tag{3.18}$$

Differential drift, D, is replaced by the difference in semi-major axis, δa, for improved numerical accuracy, since the change in differential drift is very small compared to the other control variables.

3.2 Linear Mapping between the Measurement and Control Variables

A linear mapping is employed to translate the relative state of the deputy from coordinates in the measurement state vector to the equinoctial orbit element differences that are employed in the control formulation. To avoid complex frame transformations, a linear mapping was first proposed by Alfriend et al. [36] to relate orbit element differences to chief-centered Cartesian or curvi-linear coordinates. Applications of a linear mapping that offer hybrid control options, that is, combining relative state measurements with a control implementation in orbit element differences, have since been proposed by Schaub [40]. Note that the measurement coordinates denoted by x^{Meas} can either be chief-centered Cartesian or curvi-linear coordinates as defined in in equation (3.17). To deliver a chief-centered measurement vector from equinoctial orbit elements, a mapping is derived and employed here in the form

$$\bar{x}^{Meas} = \mathbf{A}(t, \overline{oe}_C)\delta\overline{oe} \tag{3.19}$$

where $\mathbf{A}$ is 6 x 6 matrix whose rows are composed from the following relationships.

$$\begin{aligned} A_{1i} = x_{Rel} = \delta r_C = \frac{r_C}{a_C}\delta a + \frac{r_C^2}{p_C}\left[e_x \sin\gamma_C - e_y \cos\gamma_C\right]\delta\gamma \\ - \left[2r_C\left(\frac{a_C}{p_C}\right)e_x + \cos\gamma_C\frac{r_c^2}{p_C}\right]\delta e_x - \left[2r_C\left(\frac{a_C}{p_C}\right)e_y + \sin\gamma_C\frac{r_C^2}{p_C}\right]\delta e_y, \end{aligned} \tag{3.20}$$

$$A_{2i} = y_{Rel} = r_C\delta\gamma + 2\sin\gamma_C r_C\delta e_x - 2\cos\gamma_C r_C\delta e_y + \frac{2r_C}{1+i_x^2+i_y^2}\left[i_y\delta i_x - i_x\delta i_y\right], \tag{3.21}$$

$$A_{3i} = z_{Rel} = \frac{2r_C}{1+i_x^2+i_y^2}\left[\sin\gamma_C\delta i_x - \cos\gamma_C\delta i_y\right], \tag{3.22}$$

$$\begin{aligned} A_{4i} = \dot{x}_{Rel} = -\frac{V_r}{2a_C}\delta a + \left(e_x\cos\gamma_C + e_y\sin\gamma_C\right)\delta\gamma + \left(V_r a e_x + h_C\sin\gamma_C\right)\frac{\delta e_x}{p_C} \\ + \left(V_r a e_y - h_C\cos\gamma_C\right)\frac{\delta e_y}{p_C}, \end{aligned} \tag{3.23}$$

$$A_{5i} = \dot{y}_{Rel} = -\frac{3V_t}{2a_c}\delta a - V_r\delta\gamma + (3V_t a e_x + 2h\cos\gamma_C)\frac{\delta e_x}{p_C} + (3V_t a e_y + 2h\sin\gamma_C)\frac{\delta e_y}{p_C} + V_r\left[\frac{2i_y}{1+i_x^2+i_y^2}\delta i_x - \frac{2i_x}{1+i_x^2+i_y^2}\delta i_y\right], \quad (3.24)$$

$$A_{6i} = \dot{z}_{Rel} = V_r\left[\frac{2\sin\gamma_C}{1+i_x^2+i_y^2}\delta i_x - \frac{2\cos\gamma_C}{1+i_x^2+i_y^2}\delta i_y\right] + V_t\left[\frac{2\cos\gamma_C}{1+i_x^2+i_y^2}\delta i_x + \frac{2\sin\gamma_C}{1+i_x^2+i_y^2}\delta i_y\right]. \quad (3.25)$$

where r_C is the radius vector of the chief in its orbit, γ_C is the right ascension, or mean longitude, of the chief at a certain instant, h_C is the specific orbital angular momentum and p_C is the semi-latus rectum corresponding to the chief's orbit defined by

$$p_C = a_C(1+e^2). \quad (3.26)$$

Also appearing in equations (3.20) through (3.25), the inertial radial and transverse velocity components in terms of equinoctial orbit elements are written as

$$V_r = \sqrt{\frac{h}{p_C}}\left(e_x\sin\gamma_C - e_y\cos\gamma_C\right), \quad (3.27)$$

$$V_t = \sqrt{\frac{h}{p_C}}\left(1 + e_x\cos\gamma_C + e_y\sin\gamma_C\right). \quad (3.28)$$

The linear mapping, as employed, only requires knowledge of the chief mean orbit elements at an initial epoch, for example, at the beginning of a stationkeeping cycle. Generally speaking, the linear mapping offers a fairly accurate transformation from chief-centered Cartesian coordinates or curvi-linear coordinates to orbit element differences. However, small errors are introduced in the orbit element approximation due to the linear approximation.

3.3 Relative Dynamic Model

The relative dynamics are modeled in terms of mean orbit element differences and are related to the chief-centered Cartesian coordinates using the linear mapping. The resulting relationships appear as

$$\delta\overline{oe}(t) = \Phi_e(t)\delta\overline{oe}(t_0) \tag{3.29}$$

$$\bar{x}^{Meas}(t) = A(t)\Phi_e(t)A^{-1}(t)\bar{x}^{Meas}(t_0), \tag{3.30}$$

where $\bar{x}^{Meas}(t_0)$ is the measured deputy state an initial time t_0 in either chief-centered Cartesian $\bar{x}_{CCC}$ or curvi-linear coordinates $\bar{x}_{Curvi}$. Perturbations, such as solar-radiation pressure (SRP), may affect different spacecraft within the constellation independently and produce different results. But such effects are easily incorporated into the new framework. In the present investigation, the State Transition Matrix (STM) in equation (3.30) incorporates only two-body dynamics. All the orbital elements are hence assumed to remain constant, with the exception of the right ascension, which will vary with respect to time. The STM and is evaluated as

$$\Phi_e(t) = \begin{bmatrix} 1 & 0 & 0 & 0 & 0 & 0 \\ \frac{-3n_C t}{2a_C} & 1 & 0 & 0 & 0 & 0 \\ 0 & 0 & 1 & 0 & 0 & 0 \\ 0 & 0 & 0 & 1 & 0 & 0 \\ 0 & 0 & 0 & 0 & 1 & 0 \\ 0 & 0 & 0 & 0 & 0 & 1 \end{bmatrix}, \tag{3.31}$$

where n_C is the mean motion corresponding to the orbit of the chief and a_C is the chief orbit semi-major axis. The relative dynamic model allows propagating any relative state deduced from relative orbit measurements to any desired future time and, hence, is critical at determining the deputy relative orbit evolution on-board the chief.

3.4 Nominal Relative Motion

One particular constellation design is considered in this analysis. Assume that the chief spacecraft is located at the center of the constellation in both the eccentricity and inclination phase space. Such a configuration is desirable since the effects of eccentricity and inclination on the chief orbit are minimized over the course of one year. With all the spacecraft following a coordinated stationkeeping strategy, the relative eccentricity and inclination vectors remain nominally constant in magnitude and direction, assuming all spacecraft in the constellation possess identically-sized eccentricity control circles. This constellation design implies that the nominal relative motion remains invariant over time. Projections of the relative orbit onto the orbit and the meridian plane are illustrated in Figure 3.4.

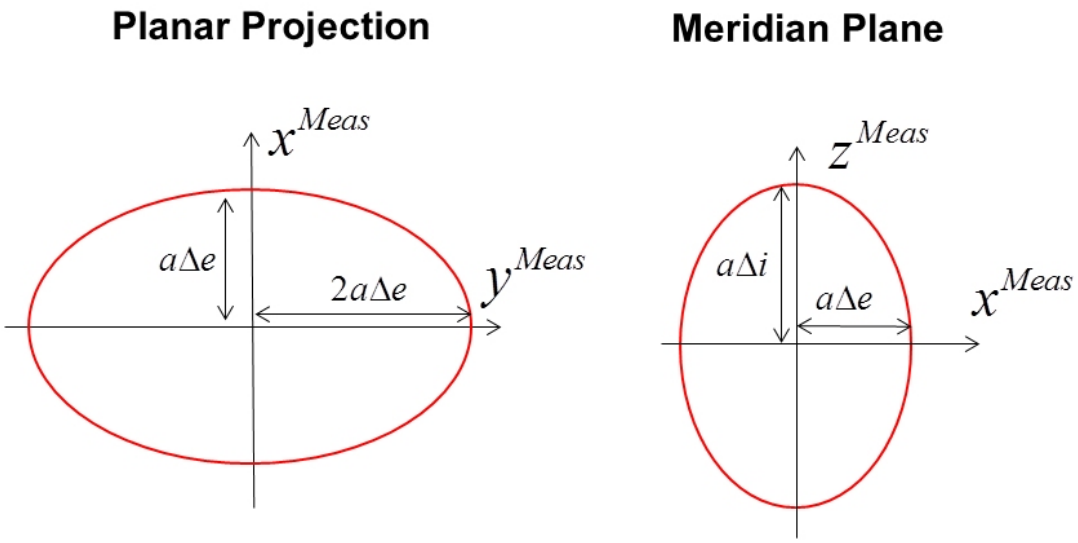

Figure 3.4. Planar and meridian plane projections of the nominal relative orbit

3.5 Relative Orbit Control

The goal of the proposed control concept is the maintenance of the deputies along their nominal relative orbits. The correction maneuvers are assumed to be implemented impulsively and the desired deviations offset the errrors in the orbit element differences and are expressed as the vector $\Delta\overline{oe}$. The corrections are then computed from a linearized variation of the Gauss Variational Equations (GVE) in equinoctial orbit elements, as developed by Eckstein [4], that incorporates terms for the deterministic thruster cross-coupling. In the stationkeeping of geostationary spacecraft, North-South (out-of-plane) correction maneuvers are generally about 60 times larger than East-West (planar) delta-V's. Combined with the North-South thrusters typically being slightly offset from the spacecraft normal axis to avoid plume impingement on the solar arrays, minute thruster misalignments result in cross-coupling between normal and radial/tangential directions. Hence it is important that the proposed orbit control framework must allow for deterministic thruster cross-coupling to be modeled in the computation of the tangential correction burns applied to the deputies. Eckstein's equations are currently in use by satellite operators for the ground-based stationkeeping maneuver computation but are equally valid for the maneuver computations incorporating the deviation in orbit element differences, $\Delta\overline{oe}$. Since outside perturbations produce little effect on the relative motion of collocated spacecraft, the difference between mean and osculating orbit element differences are negligible and Gauss' variational equations remain valid. For a realistic propulsion system, the deterministic cross-coupling terms must be considered and are represented as

$$\Delta\bar{v}_{realistic} = \begin{bmatrix} c_R & c_T & c_N \end{bmatrix}^T \Delta\bar{v}_{ideal}, \tag{3.32}$$

where the magnitude of the dominant coefficient from among the three coefficients c_R, c_T, c_N is defined as the efficiency of the particular thruster set and the ratio of the other coefficient to the dominant one as cross coupling coefficients. For example, for a N-S thruster set

$$|c_N| = \text{efficiency}, \frac{c_R}{c_N} = \kappa_R, \frac{c_T}{c_N} = \kappa_T. \tag{3.33}$$

With k impulses and the total increment Δv_k, Eckstein's equation is summarized as follows

$$\Delta oe_i = \frac{1}{V}\sum_{k=1}^{K} g_{ik}\Delta v_k \qquad i = 1, 2, 6, \tag{3.34}$$

where the coefficients are defined as

$$\begin{aligned} g_{1k} &= 2ac_{Tk} & g_{4k} &= 1/2\ c_{Nk}\sin\alpha_k \\ g_{2k} &= -c_{Rk}\cos\alpha_k + 2c_{Tk}\sin\alpha_k & g_{5k} &= 1/2\ c_{Nk}\cos\alpha_k \\ g_{3k} &= c_{Rk}\sin\alpha_k + 2c_{Tk}\cos\alpha_k & g_{6k} &= -2c_{Rk} + 2n\tau_k c_{Tk} \end{aligned} \tag{3.35}$$

and α_k is the right ascension at the time maneuver k is implemented. The relative orbit control formulation described is employed for both stationkeeping and the line-of-sight enforcement.

In the subsequent chapters, the proposed relative control concept is applied to seperate yet related problems. In chapter 4, a semi-autonomous stationkeeping approach is presented, which utilizes the relative formulation onboard the chief spacecraft to maintain the deputy spacecraft relative orbit. In chapter 5, an algorithm is presented to allow enforcement of a line-of-sight constraint between spacecraft seperated in longitude. In both applications the relative framework is key and is successfully employed.

4. SEMI-AUTONOMOUS STATIONKEEPING USING RELATIVE ORBIT CONTROL

Semi-autonomous stationkeeping of the deputy spacecraft is achieved by loosely maintaining the nominal relative orbit from on-board the chief. One spacecraft, the chief, controlled from the ground, is responsible for the orbit determination and control of the remaining vehicles. Employing the proposed relative formulation, the chief maintains the deputies relative orbit. Current stationkeeping strategies typically employ a 'repeating' nominal stationkeeping cycle for operational reasons. A similar stationkeeping cycle is employed for the relative stationkeeping. With N-S (out-of-plane) correction maneuvers generally about 60 times larger than E-W (planar) corrections, the effects of North-South thruster cross-coupling onto the relative orbit are also examined. Sample constellations are selected and the propellant expenditure is compared to the traditional ground-based approach.

4.1 Stationkeeping Cycle

Current stationkeeping strategies typically employ a 'repeating' nominal stationkeeping cycle for operational reasons. The period of these cycles depends on the available longtitude window, the number of spacecraft collocated and the location in the geostationary orbit. The duration of these cycles in operational use today is typically seven or fourteen days [2, 4]. While the specific details of stationkeeping cycles likely vary between satellite operators, the cycle chosen in this investigation is comparable to the ones employed by DLR and the commercial operator SES [2, 50]. Due to the strong cross-coupling effects of North-South correction burns, East-West burns are typically planned shortly after the North-South corrections have been performed and accurate orbit determination is available. It typically takes between one

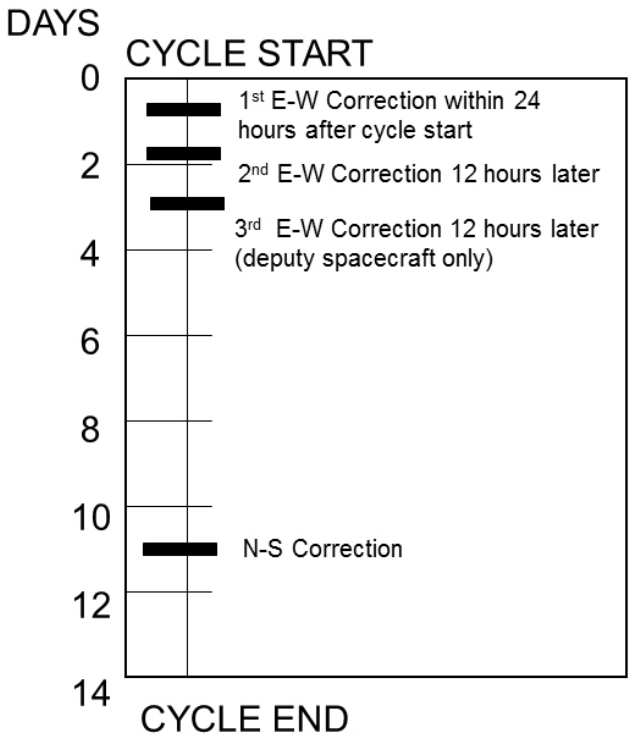

Figure 4.1. Illustration of the employed stationkeeping cycles

to two days to obtain accurate ground-based orbit determination depending on the satellite operators resources [50]. Therefore, the employed stationkeeping cycles start once accurate orbit determination is available and necessary East-West corrections are immeadiately performed at the beginning of each cycle and compensate for any North-South cross-coupling effects. The North-South correction burn is then performed towards the end of the cycle. In this investigation, a 14 day stationkeeping cycle is employed for all simulations and an outline of the cycle is illustrated in Figure 4.1.

4.2 Traditional Ground-Based Stationkeeping

To counteract the natural perturbing forces affecting a geostationary spacecraft, it is necessary to perform regular correction maneuvers to maintain the spacecraft within

the prescribed tolerance window around their nominal longitude position. This task is generally refered to as stationkeeping and needs to be performed on a periodic basis for the entire operational life of the spacecraft. A detailed discussion of traditional stationkeeping strategies is available in [20], [21] and [23]. In this investigation, the chief spacecraft is controlled using traditional stationkeeping by ground-based satellite controllers. The stationkeeping strategy employed for the chief spacecraft consists of two East-West and one North-South correction burns to control the longitude, eccentricity and inclination as follows:

- *Longitude Control* The tesseral terms of the Earth's gravity produce a constant East or West acceleration depening on the longitude resulting in a natural longitudinal drift in either East or West direction. This acceleration is computed from (2.36) or available from tables for a given longitude [20]. For the purpose of longitude control, this longitudinal acceleration $\ddot{\lambda}$ is considered constant throughout the longitude box. Since the acceleration is always in the same direction, a minimal stationkeeping cost is achieved if all the correction burns are also made in the same direction. The strategy is to minimize the longitude variation by having it librate around its nominal value. Ideally, this is achieved by correcting the drift opposite to the natural direction at the beginning of the stationkeeping cycle, such that it reaches zero half-way through and returns the longitude back to its initial position at the end. The resulting longitudinal motion is approximately a parabola starting and ending at the same value centered around the nominal longitude. In reality, however, the longitude will oscillate during the day with varying amplitudes due to the differential gravitation of Sun and Moon. The longitude control will only determine the magnitude of the necessary correction and the maneuver is typically performed during the first day of the stationkeeping cycle. The time of day however is determied by the eccentricity control strategy. In Figure 4.2, the osculating longitude is displayed with respect to time for one stationkeeping cycle. The location of the two E-W and one N-S stationkeeping correction are indicated.

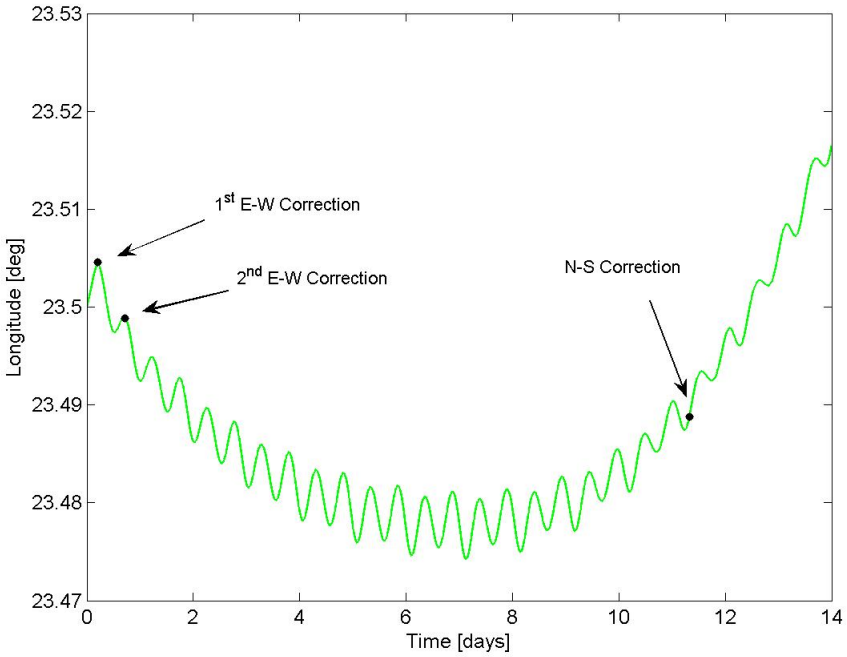

Figure 4.2. Osculating Longitude vs Time for one 14 Day Stationkeeping Cycle

- *Eccentricity Control Strategy* The employed eccentricity control strategy is the Sun Pointing Perigee Strategy (SPPS). Since the radius of the natural eccentricity circle is larger than the radius of the selected control circle, resulting in the orbit perigee to drift faster than the Sun. The resulting effect is that the eccentricity magnitude naturally increases. The required eccentricity change is to bring the orbit perigee back in line with the Sun and the eccentricity back to the control circle. The target eccentricity is chosen to align with the eccentricity of the Sun at the beginning of the stationkeeping cycle. The eccentricty is controlled by two correction burns performed in opposite directions. A linearized version of Gauss Variational equation is solved in section 4.3 for both an ideal and a realistic propulsion system. The motion of the osculating eccentricity vector in the eccentricity phase space is plotted for one stationkeeping cycle

in Figure 4.3. The dashed circle indicates the eccentricity control circle, the eccentricity vector will follow over the course of one year.

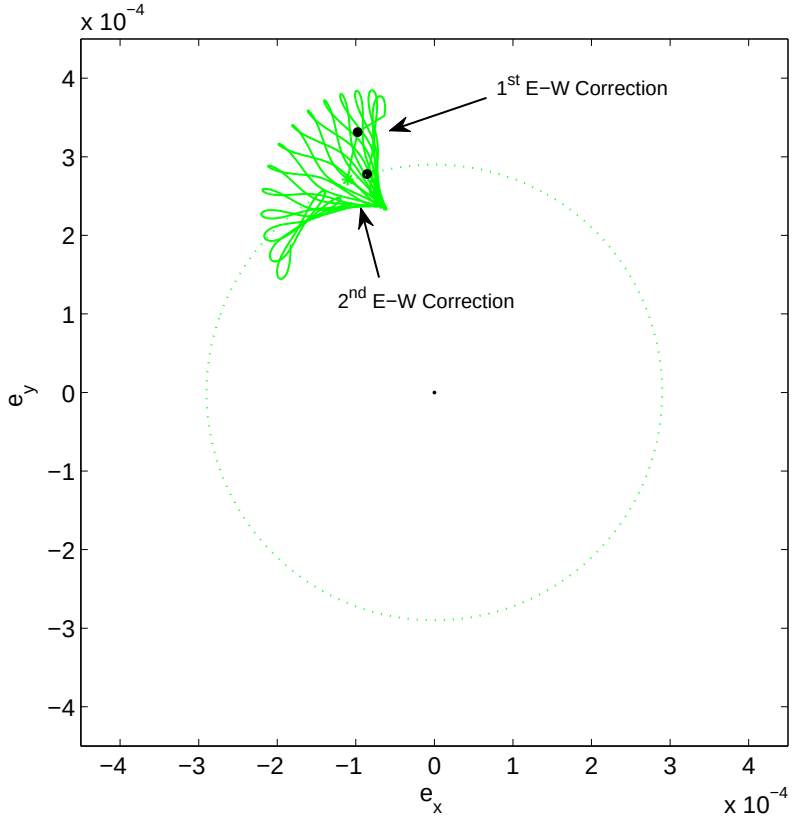

Figure 4.3. Osculating Eccentricity Vector for one 14 Day Stationkeeping Cycle

- *Inclination Control* In chapter 2, the natural inclination evolution is described to follow a mean secular drift, with a half yearly variation and a monthly variation superimposed upon it. The selected ground-based inclination control strategy for the chief spacecraft counteracts this secular mean drift, leaving the inclination to oscillate in the direction perpendicular. Such a strategy is commonly employed when the latitude window of the station keeping box is large enough in latitude to allow for the libration [20]. The motion of the osculating inclination vector in the inclination phase space for one stationkeeping cycle is plotted in Figure 4.4. The dashed circle indicates 0.5 degrees in inclination.

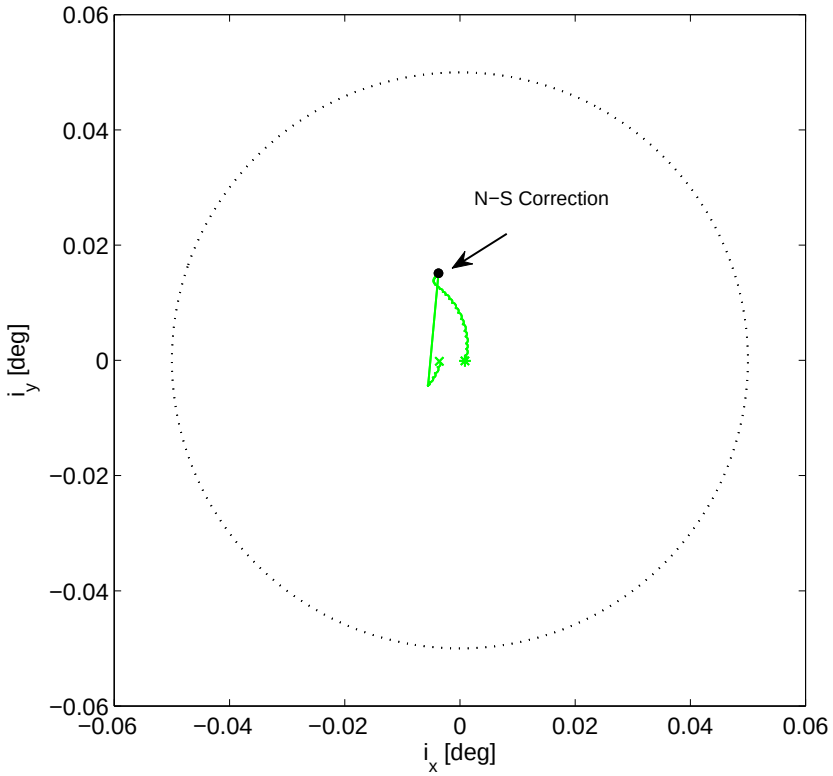

Figure 4.4. Osculating Inclination Vector for 1 14 Day Stationkeeping Cycle

4.3 Relative Stationkeeping

At the beginning of each stationkeeping cycle, the deputy orbit element differences describing the relative orbit are determined by the chief from relative orbit observations. The orbit element differences representing each deputy orbit are then propagated through the end of the cycle and adjusted for the planned stationkeeping burns of the chief. Since the deputy control strategy maintains the vehicle's prescribed nominal motion, the end-of-cycle target states are the deputy spacecraft nominal orbit element differences. At the end of each stationkeeping cycle the relative propagated orbit element differences are subtracted from the target orbit element differences as follows

$$\Delta\overline{oe} = \delta\overline{oe}_{\text{Target}} - \delta\overline{oe}_{\text{Propag}}, \tag{4.1}$$

where $\Delta\overline{oe}$ indicates the required change in orbit element differences. These deviations $\Delta\overline{oe}$ are used to compute the necessary relative correction burns for the deputy to maintain the nominal relative orbit.

The relative correction are computed similarly to the approach illustrated by Eckstein [4]. The set of equations (3.34) is solved for burn sequences involving any number of E-W and N-S maneuvers. Ground-based stationkeeping strategies for geostationary spacecraft typically only control the longitude, eccentricity and inclination, hence, only require two E-W and one N-S maneuver. Contrary to the ground-based approach, differential semi-major axis or drift must be monitored and controlled for the relative control concept to maintain the relative constellation. A burn sequence consisting of three E-W and one N-S maneuver is, therefore, employed for relative orbit control. If thruster cross-coupling effects are not considered, the in-plane and out-of-plane motion decouple in the linear case and the control maneuvers are determined separately. However, for a realistic propulsion system, the N-S correction is determined first since the cross-coupling influences the timing and magnitude of the E-W maneuvers. For out-of-plane orbit control, one properly-timed burn is generally sufficient to maintain the relative orbit and is computed for each spacecraft individually based on the difference between the target and the propagated relative inclination vectors. The magnitude and the right ascension that corresponds to the single N-S maneuver are

$$\Delta V^{NS} = 2V_{Chief}\sqrt{\Delta i_x^2 + \Delta i_y^2}, \tag{4.2}$$

$$\alpha_{inc} = a\tan\left(\frac{\delta i_y}{\delta i_x}\right), \tag{4.3}$$

where V_{Chief} is the velocity of the chief. The required out-of-plane burns for the deputy relative orbit control are nominally identical in magnitude to the N-S burn that is completed for the chief spacecraft.

4.4 Computation of Orbit Control Corrections

The chief spacecraft is controlled using traditional stationkeeping techniques, while the deputy spacecraft are maintained from on-board the chief. The chief will be maintained using two E-W and one N-S correction maneuvers, while the deputy spacecraft will perform three E-W and one N-S correction maneuver per stationkeeping cycle. Further, an ideal propulsion system is assumed for the chief spacecraft, while both ideal and realistic propulsion systems are considered for the deputy spacecraft. The orbit correction equations presented in this section are valid from both the gound-based and relative persepective, as only orbit element differences are considered in the computation.

4.4.1 Ideal Propulsion System

First, the case of an ideal propulsion system is considered. An ideal propulsion system performs North-South correction burn that have no radial or tangential component. This means that all the cross-coupling coefficients except for c_{T1}, c_{T2} and c_N will vanish, and equations (3.34) simplifiy to

$$\begin{aligned}
\Delta a &= -\tfrac{3n}{V_{Geo}} \sum_{k=1}^{K} \Delta v_k^{EW} \\
\Delta \gamma &= -\tfrac{3n}{V_{Geo}} \sum_{k=1}^{K} \tau_k \Delta v_k^{EW} \\
\Delta e_x &= \tfrac{2}{V_{Geo}} \sum_{k=1}^{K} \cos\alpha_k \Delta v_k^{EW} \\
\Delta e_y &= \tfrac{2}{V_{Geo}} \sum_{k=1}^{K} \sin\alpha_k \Delta v_k^{EW} \\
\Delta i_x &= \tfrac{1}{2V_{Geo}} \sum_{k=1}^{K} \cos\alpha_k \Delta v_k^{NS} \\
\Delta i_y &= \tfrac{1}{2V_{Geo}} \sum_{k=1}^{K} \sin\alpha_k \Delta v_k^{NS}
\end{aligned} \tag{4.4}$$

Note that the fourth and fifth equation are decoupled from the others. The top four equations describe the planar orbit control and are solved in the following sections for both two and three burn solutions.

Two East-West Burn Solution

In this section, the case of two correction maneuvers for the control of the in-plane orbital motion is examined. Traditional ground-based stationkeeping strategies, as employed for the chief spacecraft in this investigation, typically rely on two E-W burns to control the planar motion. As there is no requirement for drift control in traditional ground-based stationkeeping approaches, the equation for drift is disregarded and instead the system is augmented by the requirement for fuel minimization. A sufficient condition to minimize propellant is to require the eccentricity vector corrections to be into the same direction for both burns, as in $\Delta\bar{e} = \Delta\bar{e}_1 + \Delta\bar{e}_2$, which is achieved by offseting the maneuvers by half an orbital revolution as expressed in

$$\alpha_2 = \alpha_1 + \pi. \tag{4.5}$$

The time of the first correction burn is determined by required change in the eccentricity phase space

$$\alpha_1 = a\tan\left(\frac{\delta e_y}{\delta e_x}\right). \tag{4.6}$$

For an ideal propulsion system

$$\kappa_{R1} = \kappa_{R2} = \kappa_{N1} = 0, \quad c_{T1} \approx \pm 1, \quad c_{N2} \approx \pm 1 \tag{4.7}$$

and equations (4.4) reduce to

$$\begin{aligned} \Delta v_1^{EW} + \Delta v_2^{EW} &= -\tfrac{V_{Geo}}{3n}\Delta\gamma \\ \left(\Delta v_1^{EW} + \Delta v_2^{EW}\right)\cos\alpha_1 &= \tfrac{V_{Geo}}{2}\Delta e_x \\ \left(\tau_1\Delta v_1^{EW} + \tau_2\Delta v_2^{EW}\right)\sin\alpha_1 &= \tfrac{V_{Geo}}{2}\Delta e_y, \end{aligned} \tag{4.8}$$

where τ_1 and τ_2 is the time between the first and second correction burn to the end of the stationkeeping cycle. With

$$\Delta e = \sqrt{\Delta e_x^2 + \Delta e_y^2}, \tag{4.9}$$

and

$$\sin\alpha_1 = \frac{V\Delta e_y}{\sqrt{e_x^2 + e_y^2}} \qquad \cos\alpha_1 = \frac{V\Delta e_x}{\sqrt{e_x^2 + e_y^2}}, \tag{4.10}$$

the solution to equations (4.9) is

$$\Delta V_1^{EW} = -\frac{V}{\tau_2 + \tau_1}\left(\frac{1}{3}\frac{\Delta\lambda}{n} - \frac{\tau_2 \Delta e}{2}\right) \tag{4.11}$$

and

$$\Delta V_2^{EW} = -\frac{V}{\tau_2 + \tau_1}\left(\frac{1}{3}\frac{\Delta\lambda}{n} - \frac{\tau_1 \Delta e}{2}\right). \tag{4.12}$$

The first correction burn is performed during the first day of the stationkeeping cycle, with the subsequent burn following half a sidereal day later.

Three East-West Burn Solution

For the relative correction burns it is necessary to control differential semi-major axis, or drift, in addition to differential longitude and the eccentricity vector. Thus, it is necessary to perform a third correction maneuver. Fuel optimality is again assured by requiring the eccentricity vector corrections of all three burns to be in the same direction, as in $\Delta\bar{e} = \Delta\bar{e}_1 + \Delta\bar{e}_2 + \Delta\bar{e}_3$. The second maneuver is thus offset by half an orbital period, and the third correction maneuver by a full orbital period, from the first correction maneuver. The time of the first correction burn is again determined by required change in the eccentricity phase space

$$\alpha_1 = a\tan\left(\frac{\delta e_y}{\delta e_x}\right), \tag{4.13}$$

and the right ascension of subsequent burns is given by

$$\alpha_2 = \alpha_1 + \pi, \tag{4.14}$$

and

$$\alpha_3 = \alpha_1 + 2\pi. \tag{4.15}$$

The equations 3.34 the reduce to

$$\begin{array}{c} \Delta v_1^{EW} + \Delta v_2^{EW} + \Delta v_3^{EW} = \frac{V_{Geo}}{2a_{Geo}}\Delta a \\ \left(\Delta v_1^{EW} + \Delta v_2^{EW} + \Delta v_3^{EW}\right)\cos\alpha_1 = \frac{V_{Geo}}{2}\Delta e_x \\ \left(\Delta v_1^{EW} + \Delta v_2^{EW} + \Delta v_3^{EW}\right)\sin\alpha_1 = \frac{V_{Geo}}{2}\Delta e_y \\ \tau_1\Delta v_1^{EW} + \tau_2\Delta v_2^{EW} + \tau_3\Delta v_3^{EW} = -\frac{V_{Geo}}{3n}\Delta\gamma \end{array}. \tag{4.16}$$

Solving equations 4.16 with

$$\sin\alpha_1 = \frac{V\Delta e_y}{\sqrt{e_x^2+e_y^2}}, \qquad \cos\alpha_1 = \frac{V\Delta e_x}{\sqrt{e_x^2+e_y^2}} \tag{4.17}$$

yields,

$$\Delta v_1^{EW} = \frac{V_{Geo}}{2\left(\tau_1-\tau_3\right)}\left[-\frac{\delta a}{2a}\left(\tau_2+\tau_3\right)-\frac{\delta e}{2}\left(\tau_3-\tau_2\right)-\frac{2}{3n}\delta\gamma\right], \tag{4.18}$$

$$\Delta v_2^{EW} = \frac{V_{Geo}}{4}\left(\frac{\delta a}{a}-\delta e\right), \tag{4.19}$$

$$\Delta v_3^{EW} = \frac{V_{Geo}}{2\left(\tau_1-\tau_3\right)}\left[\frac{\delta a}{2a}\left(\tau_1+\tau_2\right)+\frac{\delta e}{2}\left(\tau_1-\tau_2\right)+\frac{2}{3n}\delta\gamma\right]. \tag{4.20}$$

The first correction burn is again performed during the first day of the stationkeeping cycle, with the second burn following half a sidereal day later and the third burn after one sidereal day.

4.5 Deterministic Thruster Cross-Coupling

In reality, thrusters are not always implemented into the normal and tangential direction. For large communication spacecraft, a thruster poininting precisely into the normal direction would introduce plume impingement onto the solar arrays, which are typically mounted into the north and south directions. N-S thrusters are therefore usually placed at a slight angle to minimize the effects of plume impingement. This offset present in most realistic propulsion systems found on geostationary spacecraft results in the North-South correction burn to also have small radial and tangential components. Additionally, over the course of a spacecraft lifetime, the fuel expenditure yields a migration of the center of mass, hence leading to small varitations in the direction of nominal thrust vector. This thruster cross-coupling is commonly assumed to be deterministic and the approach presented here follows Eckstein (3.34). For the relative correction burns, it is necessary to control the differential semi-major axis, or drift, in addition to differential longitude and the eccentricity vector. Thus, for three burns, the four in-plane components of equations (3.34) reduce to

$$-3n\left(\Delta v_1^{EW}+\Delta v_2^{EW}+\Delta v_3^{EW}\right) = V_{Geo}\Delta a^*, \tag{4.21}$$

$$\left(-\kappa_{R1}\cos\alpha_1 + 2\sin\alpha_1\right)\Delta v_1^{EW} + \left(-\kappa_{R2}\cos\alpha_2 + 2\sin\alpha_2\right)\Delta v_2^{EW} + \left(-\kappa_{R3}\cos\alpha_3 + 2\sin\alpha_3\right)\Delta v_3^{EW} = V_{Geo}\Delta e_y^*, \quad (4.22)$$

$$\left(-\kappa_{R1}\sin\alpha_1 + 2\cos\alpha_1\right)\Delta v_1^{EW} + \left(-\kappa_{R2}\sin\alpha_2 + 2\cos\alpha_2\right)\Delta v_2^{EW} + \left(-\kappa_{R3}\sin\alpha_3 + 2\cos\alpha_3\right)\Delta v_3^{EW} = V_{Geo}\Delta e_x^*, \quad (4.23)$$

$$\left(-2\kappa_{R1} - 3n\tau_1\right)\Delta v_1^{EW} + \left(-2\kappa_{R2} - 3n\tau_2\right)\Delta v_2^{EW} + \left(-2\kappa_{R3} - 3n\tau_3\right)\Delta v_3^{EW} = V_{Geo}\Delta\lambda^*, \quad (4.24)$$

where the effect of the N-S correction onto the planar orbit element variations are computed by

$$\begin{aligned}
\Delta a^* &= \delta a + 2a_{Geo}\kappa_T^{inc}\tfrac{\Delta V^{NS}}{V_{Geo}},\\
\Delta\gamma^* &= \delta\gamma - \tfrac{\Delta V^{NS}}{V_{Geo}}\left(-2\kappa_{R4}^{inc}\sin\alpha - 3n\tau_4\kappa_T^{inc}\right),\\
\Delta e_x^* &= \delta e_x - \tfrac{\Delta V^{NS}}{V_{Geo}}\left(\kappa_R^{inc}\sin\alpha + 2\kappa_T^{inc}\cos\alpha\right),\\
\Delta e_y^* &= \delta e_y - \tfrac{\Delta V^{NS}}{V_{Geo}}\left(-\kappa_R^{inc}\cos\alpha + 2\kappa_T^{inc}\sin\alpha\right),
\end{aligned} \quad (4.25)$$

and the cross-coupling coefficients in this case are defined as

$$\begin{aligned}
\kappa_{Ri} = \tfrac{c_{Ri}}{c_{Ti}} \qquad \kappa_{Ni} = \tfrac{c_{Ni}}{c_{Ti}} \qquad i = 1,2,3,\\
\kappa_R^{inc} = \tfrac{c_R^{inc}}{c_N^{inc}} \qquad \kappa_T^{inc} = \tfrac{c_T^{inc}}{c_N^{inc}}.
\end{aligned} \quad (4.26)$$

Solving for the E-W maneuvers with

$$W_i = \sqrt{1 + 1/4\kappa_{Ri}^2} \qquad i = 1,2,3, \quad (4.27)$$

$$\tau_i^* = \tau_i + 2\kappa_{Ri}/3n \qquad i = 1,2,3, \quad (4.28)$$

the time between the impulse i and the end of cycle and the optimality condition

$$\alpha^* = \alpha_i + \Delta\alpha_i + (i-1)\,\pi, \qquad \tan\Delta\alpha_i = \frac{\kappa_{Ri}}{2} \qquad i = 1,2,3, \quad (4.29)$$

the equations reduce to

$$\begin{aligned}
-3n\left(\Delta v_1^{EW} + \Delta v_2^{EW} + \Delta v_3^{EW}\right) &= V_{Geo}\Delta a^*,\\
2\left(W_1\Delta v_1^{EW} - W_2\Delta v_2^{EW} + W_3\Delta v_3^{EW}\right)\sin\alpha &= V_{Geo}\Delta e_y^*,\\
2\left(W_1\Delta v_1^{EW} - W_2\Delta v_2^{EW} + W_3\Delta v_3^{EW}\right)\cos\alpha &= V_{Geo}\Delta e_x^*,\\
-3n\left(\tau_1\Delta v_1^{EW} + \tau_2\Delta v_2^{EW} + \tau_3\Delta v_3^{EW}\right) &= V_{Geo}\Delta\lambda^*.
\end{aligned} \quad (4.30)$$

Solving for the E-W maneuvers with

$$\Delta e^* = \sqrt{\Delta e_x^{*2} + \Delta e_y^{*2}} \tag{4.31}$$

and

$$\sin\alpha^* = \frac{V\Delta e_y^*}{\Delta e^*} \qquad \cos\alpha^* = \frac{V\Delta e_x^*}{\Delta e^*}, \tag{4.32}$$

the solution to equations 4.30 is

$$\Delta V_1^{EW} = \frac{V_{Geo}}{D}\left[\frac{1}{3n}\left(W_3\tau_2^* + W_2\tau_3^*\right)\delta a^* + \frac{1}{2}s\left(\tau_2^* - \tau_3^*\right)\delta e^* - \frac{1}{3n}\left(W_2 + W_3\right)\delta\gamma^*\right], \tag{4.33}$$

$$\Delta V_2^{EW} = \frac{V_{Geo}}{D}\left[\frac{1}{3n}\left(W_1\tau_3^* + W_3\tau_1^*\right)\delta a^* + \frac{1}{2}s\left(\tau_3^* - \tau_1^*\right)\delta e^* + \frac{1}{3n}\left(W_3 + W_1\right)\delta\gamma^*\right], \tag{4.34}$$

$$\Delta V_3^{EW} = \frac{V_{Geo}}{D}\left[-\frac{1}{3n}\left(W_1\tau_2^* + W_2\tau_1^*\right)\delta a^* + \frac{1}{2}s\left(\tau_1^* - \tau_2^*\right)\delta e^* + \frac{1}{3n}\left(W_1 + W_2\right)\delta\gamma^*\right], \tag{4.35}$$

with

$$[D = \tau_1^*\left(W_2 + W_3\right) + \tau_2^*\left(W_1 - W_3\right) - \tau_3^*\left(W_1 + W_2\right). \tag{4.36}$$

The first correction burn is again performed during the first day of the stationkeeping cycle, with the second burn following approximately half a sidereal day and the third burn approximately one sidereal day later.

4.6 Numerical Results

In the following numerical simulations, a number of different constellations are examined. The constellation designs are inspired by examples presented in Wauthier [2] and Blumer [50] and are listed in table 4.1. The designs are slightly adapted to allow for the chief spacecraft to be placed at the center of the constellation in both the eccentricity and inclination phase spaces with the remaining deputies at the edges of a regular polygon to ensure maximum separation as in [2]. For all the constellations, the polygon is aligned such that the offset in eccentricity and inclination phase spaces between the chief and first deputy spacecraft is along the negative x-axis yielding

maximum separation as the resulting eccentricity and inclination vectors are parallel. In all numerical simulations, the spacecraft are assumed to be identical with ideal thruster sets and an area-to-mass ratio equal to 0.03767 m^2/kg, a value typical for large modern communications spacecraft. All numerical simulations employ a high-fidelity ephemeris model incorporating the relevant perturbations. The orbit corrections to maintain the chief spacecraft along its orbit are determined by ground-based satellite controllers, and uploaded to the chief. The relative control module on-board the chief vehicle then determines the necessary orbit corrections to maintain the deputies in their pre-described nominal orbit. The use of both chief-centered Cartesian coordinates and curvi-linear coordinates for the relative measurment vector are examined. For conciseness, Figures for only case 5 are displayed and discussed

Table 4.1 Constellations Examined for Relative On-board Stationkeeping Concept. All Constellation Designs have the Chief Spacecraft at the Center with the Deputies Offset in Regular Polygon.

	$\lambda_{nominal}$	Number of s/c	E_C	Δe	Δi
Case 1:	23.5^o East	5	2.9×10^{-4}	1.50×10^{-4}	0.015^o
Case 2:	19^o West	5	3×10^{-4}	2.72×10^{-4}	0.024^o
Case 3:	19^o West	7	3×10^{-4}	2.72×10^{-4}	0.024^o
Case 4:	19.2^o East	5	2.25×10^{-4}	2.25×10^{-4}	0.025^o
Case 5:	19.2^o East	7	2.25×10^{-4}	2.25×10^{-4}	0.025^o

in this chapter. Furthermore, since the figures for both chief-centered Cartesian and curvilinear relative coordinates look indistinguishable, only one set of figures is presented.

4.6.1 Ideal Propulsion System

The proposed relative orbit control concept using the linear mapping is modeled for fourteen day stationkeeping cycles. Two metrics are defined to evaluate the relative orbit control concept: (1) the cost to maintain the deputy spacecraft to the predefined nominal relative orbit and (2) the error in maintaining the absolute orbit within its

longitudinal control box. The Figures in this section are for numercial simulations of one year duration, comprised of 26 14-day stationkeeping cycles. In all the figures, the chief's motion is represented in bright green, the first deputy in blue, the second deputy in red, the third deputy in black, the fourth deputy in purple, the fifth deputy in cyan and the sixth deputy in turquoise. The planar projections of the deputy relative orbits in the chief-centered Cartesian frame are plotted in Figure 4.5. For this particular collocation constellation design, that is, one comprised of identical spacecraft and eccentricity control circles, and the chief is maintained at the center of the eccentricity phase space; the nominal relative orbit is identical for all six deputies. The location of the deputies at the end of the one year simulation is illustrated with the chief at the origin. As is apparent in Figure 4.5, the relative orbit remains well maintained for the duration of the year long simulation and the deputy spacecraft are offset by 60 degrees in their relative orbit. The small but noticeable drift of the relative orbit in the tangential direction is largely due to the linear assumption in the mapping transformation. The differential drift grows slightly through one cycle before a correction to offset the drift is imposed at the beginning of the next cycle.

The osculating equinoctial orbit elements are plotted in Figure 4.6 and the respective mean equinoctial orbit elements are plotted in Figure 4.7. The repetitive nature of the cycles is easily observed in the time histories corresponding to longitude and drift. In the eccentricity phase space in Figure 4.7, the eccentricity control circles are represented by the dashed circles and the eccentricity vector (reflected by the coordinates e_x,e_y) corresponding to each spacecraft are seen to follow the dashed circles. In the inclination phase space, in Figure 4.7, note that only the mean secular drift is corrected for each spacecraft; a net motion along the i_x direction is apparent. The drift of the inclination vector along the i_x direction is the result of only correcting for the mean secular drift of the inclination vector. This drift reverses every six months as seen in the year-long propagation in Figure 4.6. Osculating equinoctial orbit elements are shown in Figure 4.6. The short-term oscillations introduced from the gravitational forces of the Sun, Moon and Earth are apparent.By targeting the

relative orbit differences at the end of cycle, the orbits of the deputy spacecraft are well maintained within the imposed constraints, while still using proven fuel efficient strategies.

A comparison for the total E-W stationkeeping cost over the course of one year between traditional ground-based stationkeeping and the relative orbit control for an ideal propulsion system appears in table 4.2 for chief-centered Cartesian coordinates and in table 4.3 for curvilinear coordinates. The relative control concept is seen to supply a propellant cost that is comparable to ground-based stationkeeping approach over the course of one year. The difference in out-of-plane stationkeeping cost between the two approaches and the total annual cost is found to be negligible.

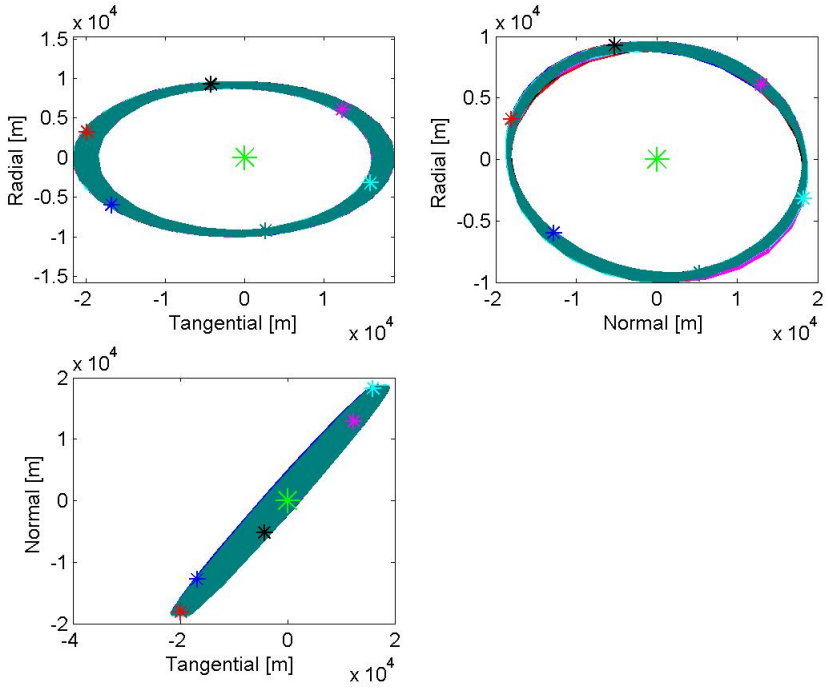

Figure 4.5. Projections of the Relative Orbit for Case 5 in the Chief Centered Cartesian Frame for a One Year Simulation for an Ideal Propulsion System - Still Need to show location of 4 deputies

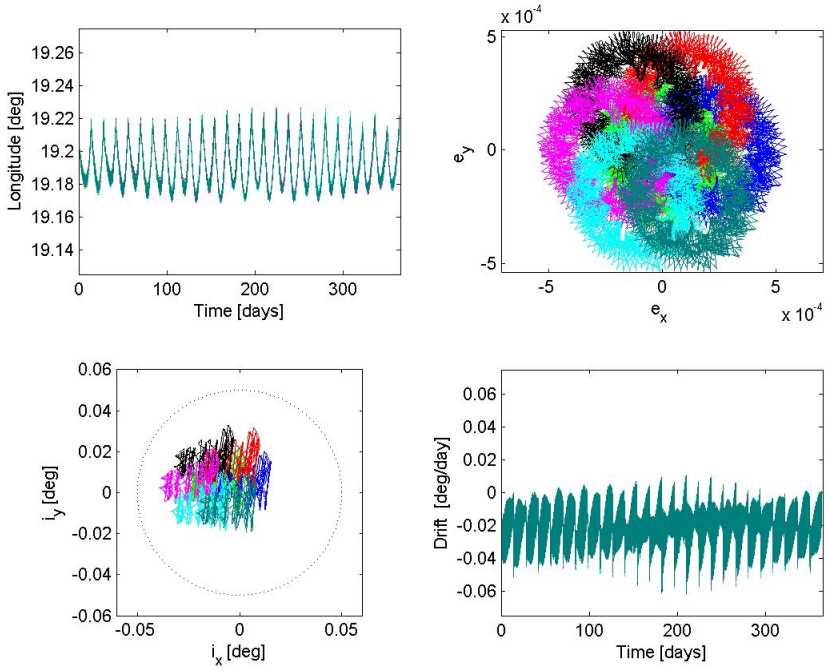

Figure 4.6. Osculating Equinoctial Orbit Elements for Case 5 for One Year for an Ideal Propulsion System

4.6.2 Realistic Propulsion System

The proposed relative orbit control concept using the linear mapping is modeled for fourteen day stationkeeping cycles using a realistic propulsion system. In this investigation, a realistic propulsion system is assumed to perform instantaneous maneuvers with the N-S thruster not perfectly aligned with the spacecraft normal axis. To avoid plume impingement onto the solar arrays this is commonly the case for large geostationary communication spacecraft. This small offset leads to the N-S maneuvers having a small radial and tangential component. In this investigation, a sample thruster cross-coupling of 2% along both the radial and tangential direction of the N-S maneuver is selected. The same thruster cross-coupling is assumed for all the deputy spacecraft in the constellation and an ideal propulsion system is modeled for the chief spacecraft.

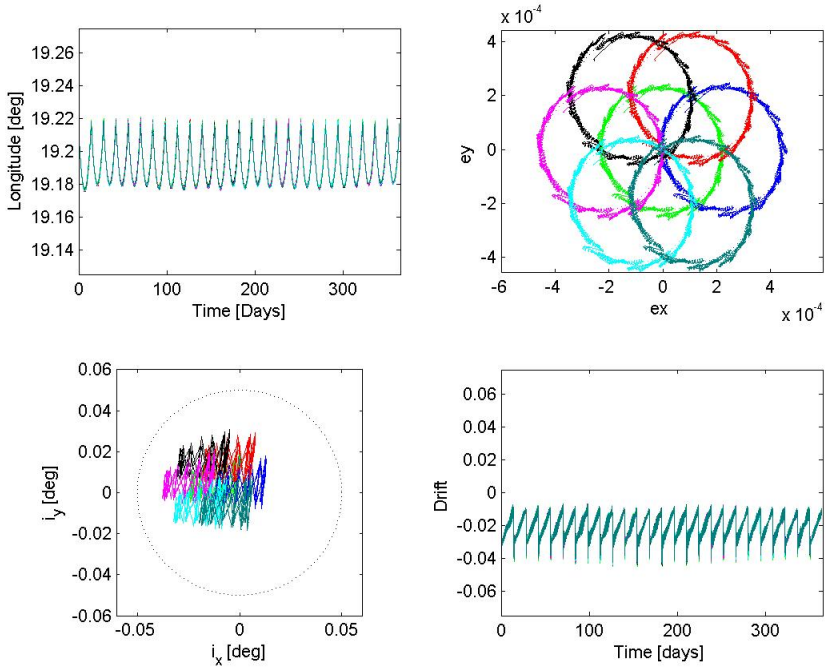

Figure 4.7. Mean Equinoctial Orbit Elements for Case 5 for One Year for an Ideal Propulsion System

The Figures in this section are again for numercial simulations of one year duration, comprised of 26 14-day stationkeeping cycles. The same color scheme as in the previous section is employed with the chief's motion represented in bright green, the first deputy in blue, the second deputy in red, the third deputy in black, the fourth deputy in purple, the fifth deputy in cyan and the sixth deputy in turquoise. The planar projections of the deputy relative orbits in the chief-centered Cartesian frame are plotted in Figure 4.8. The location of the deputies at the end of the one year simulation is illustrated with the chief at the origin. As is apparent in Figure 4.8, the relative orbit remains maintained for the duration but there is increased shifting primarily along the tangential direction. This is because the deterministic thruster cross-coupling is now taken into consideration in the computation of the deputies stationkeeping maneuvers.

Table 4.2 Total Annual Cost for E-W Corrections for both Ground-based Stationkeeping and the Relative Orbit Control Concept for an Ideal Propulsion System using Chief-centered Cartesian Coordinates Coordinates and 14 Day Stationkeeping Cycles.

Case 1:	Ground Based [m/s]	Relative Cost [m/s]	Change [%]
Chief	2.3997	2.3997	
1^{st} Deputy	2.4407	2.3945	-1.8919
2^{nd} Deputy	2.4184	2.4071	-0.4684
3^{rd} Deputy	2.4118	2.4023	-0.3951
4^{th} Deputy	2.4386	2.3982	-1.6565
Case 2:	Ground Based [m/s]	Relative Cost [m/s]	Change [%]
Chief	2.3162	2.3162	
1^{st} Deputy	2.3085	2.3051	-0.1479
2^{nd} Deputy	2.3168	2.3275	0.4618
3^{rd} Deputy	2.3258	2.2997	-1.1217
4^{th} Deputy	2.3141	2.3249	0.4666
Case 3:	Ground Based [m/s]	Relative Cost [m/s]	Change [%]
Chief	2.3162	2.3162	
1^{st} Deputy	2.3168	2.3275	0.4618
2^{nd} Deputy	2.3089	2.3251	0.7012
3^{rd} Deputy	2.3089	2.3204	0.4996
4^{th} Deputy	2.3085	2.3051	-0.1479
5^{th} Deputy	2.3262	2.2977	-1.2240
6^{th} Deputy	2.3052	2.3273	0.9593
Case 4:	Ground Based [m/s]	Relative Cost [m/s]	Change [%]
Chief	3.1790	3.1790	
1^{st} Deputy	3.1657	3.1670	0.0407
2^{nd} Deputy	3.1883	3.1874	-0.0297
3^{rd} Deputy	3.1585	3.1801	0.6848
4^{th} Deputy	3.1628	3.1725	0.3069
Case 5:	Ground Based [m/s]	Relative Cost [m/s]	Change [%]
Chief	3.1790	3.1781	
1^{st} Deputy	3.1883	3.1787	-0.0297
2^{nd} Deputy	3.1746	3.1781	0.1097
3^{rd} Deputy	3.1605	3.1683	0.2447
4^{th} Deputy	3.1657	3.1670	0.0407
5^{th} Deputy	3.1590	3.1746	0.4950
6^{th} Deputy	3.1608	3.1850	0.7655

Table 4.3 Total Annual Cost for E-W Corrections for both Ground-based Stationkeeping and the Relative Orbit Control Concept using Curvilinear Coordinates for an Ideal Propulsion System and 14 Day Stationkeeping Cycles.

Case 1:	Ground Based [m/s]	Relative Cost [m/s]	Change [%]
Chief	2.3997	2.3997	
1^{st} Deputy	2.4407	2.3913	-2.0220
2^{nd} Deputy	2.4184	2.4117	-0.2767
3^{rd} Deputy	2.4118	2.4037	-0.3350
4^{th} Deputy	2.4386	2.3986	-1.6399
Case 2:	Ground Based [m/s]	Relative Cost [m/s]	Change [%]
Chief	2.3162	2.3162	
1^{st} Deputy	2.3085	2.3119	0.1472
2^{nd} Deputy	2.3168	2.3354	0.8014
3^{rd} Deputy	2.3258	2.3129	-0.5534
4^{th} Deputy	2.3141	2.3334	0.8348
Case 3:	Ground Based [m/s]	Relative Cost [m/s]	Change [%]
Chief	2.3162	2.3162	
1^{st} Deputy	2.3168	2.3236	0.2920
2^{nd} Deputy	2.3089	2.3201	0.4826
3^{rd} Deputy	2.3089	2.3016	-0.3134
4^{th} Deputy	2.3085	2.2929	-0.6739
5^{th} Deputy	2.3262	2.3088	-0.7477
6^{th} Deputy	2.3052	2.3491	1.9044
Case 4:	Ground Based [m/s]	Relative Cost [m/s]	Change [%]
Chief	3.1790	3.1790	
1^{st} Deputy	3.1657	3.1683	0.0817
2^{nd} Deputy	3.1883	3.1947	0.2011
3^{rd} Deputy	3.1585	3.1797	0.6738
4^{th} Deputy	3.1628	3.1721	0.2963
Case 5:	Ground Based [m/s]	Relative Cost [m/s]	Change [%]
Chief	3.1790	3.1781	
1^{st} Deputy	3.1883	3.1787	-0.0297
2^{nd} Deputy	3.1746	3.1781	0.1097
3^{rd} Deputy	3.1605	3.1683	0.2447
4^{th} Deputy	3.1657	3.1670	0.0407
5^{th} Deputy	3.1590	3.1746	0.4950
6^{th} Deputy	3.1608	3.1650	0.1329

The osculating equinoctial orbit elements are plotted in Figure 4.10 and the respective mean equinoctial orbit elements are plotted in Figure 4.9. The repetitive nature of the cycles is again easily observed in the time histories corresponding to longitude and drift. The shifting motion that was apparent in Figure 4.8 is also observed in the time histories of longitude and drift, where the deputy vehicles no longer follow the chief's motion as closely as in the case of an ideal propulsion system. In the eccentricity phase space in Figure 4.9, the eccentricity control circles are represented by the dashed circles and the eccentricity vector (reflected by the coordinates e_x,e_y) corresponding to each spacecraft are seen to follow the dashed circles. In the inclination phase space, in Figure 4.9, again note that only the mean secular drift is corrected for each spacecraft; a net motion along the i_x direction is apparent. The drift of the inclination vector along the i_x direction is the result of only correcting for the mean secular drift of the inclination vector. This drift reverses every six months as seen in the year-long propagation in Figure 4.10. Osculating equinoctial orbit elements are shown in Figure 4.10. The short-term oscillations introduced from the gravitational forces of the Sun, Moon and Earth are apparent.By targeting the relative orbit differences at the end of cycle, the orbits of the deputy spacecraft are well maintained within the imposed constraints, while still using proven fuel efficient strategies.

A comparison for the total E-W stationkeeping cost over the course of one year between traditional ground-based stationkeeping and the relative orbit control for a realistic propulsion system appears in table 4.4 for chief-centered Cartesian coordinates and in table 4.5 for curvilinear coordinates. The relative control concept is seen to supply a propellant cost that is comparable to ground-based stationkeeping approach over the course of one year. The difference in out-of-plane stationkeeping cost between the two approaches and the total annual cost is again found to be negligible.

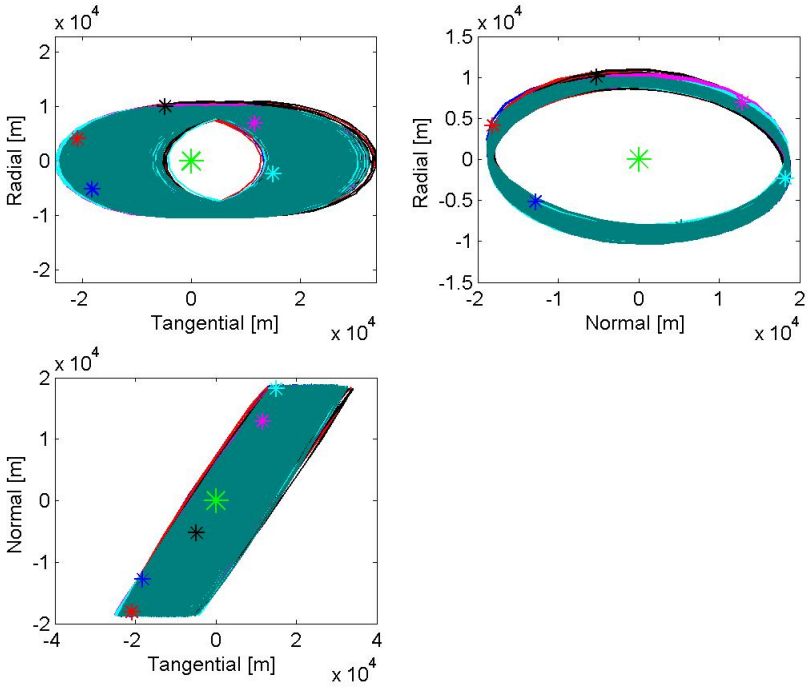

Figure 4.8. Projections of the Relative Orbit for Case 5 in the Chief Centered Cartesian Frame for a One Year Simulation for a Realistic Propulsion System

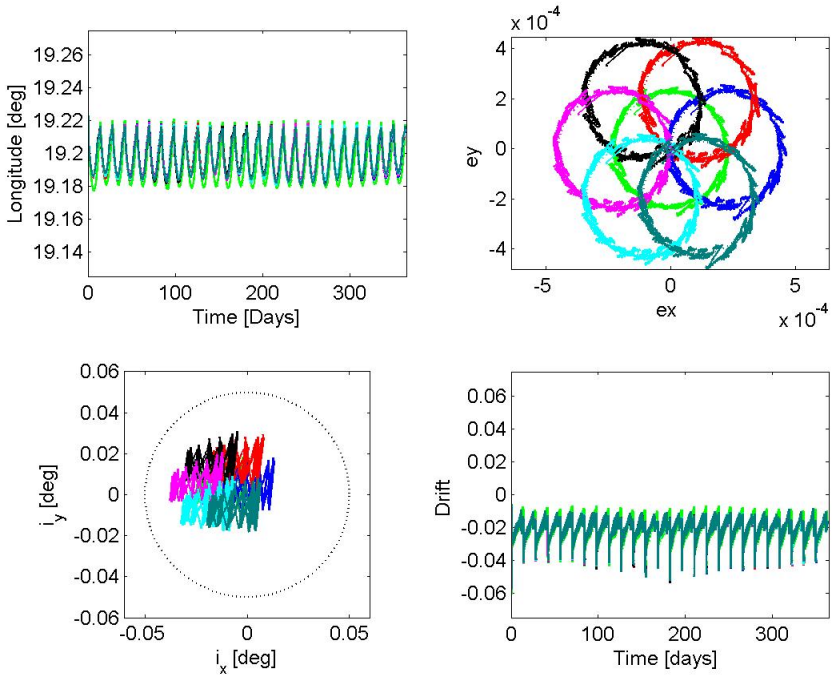

Figure 4.9. Mean Equinoctial Orbit Elements for Case 5 for One Year for a Realistic Propulsion System

4.7 Conclusion

The investigation demonstrates that the proposed relative formulation is capable at maintaining the deputy spacecraft in a pre-described relative orbit satisfying the absolute constraints. For the different constellations considered, it is shown that the propellant cost is comparable to traditional ground-based stationkeeping, hence demonstrating that currently employed fuel-efficient stationkeeping strategies are followed. This observation is also made from the observed motion in the eccentricity and inclination phase spaces. Further, it is found that the use of chief-centered Cartesian and curvilinear coordinates to use for the measurement vector results in comparable stationkeeping cost and for the consellations considered. Given these results, the advantages of curvilinear coordinates over chief-centered Cartesian coordinates likely

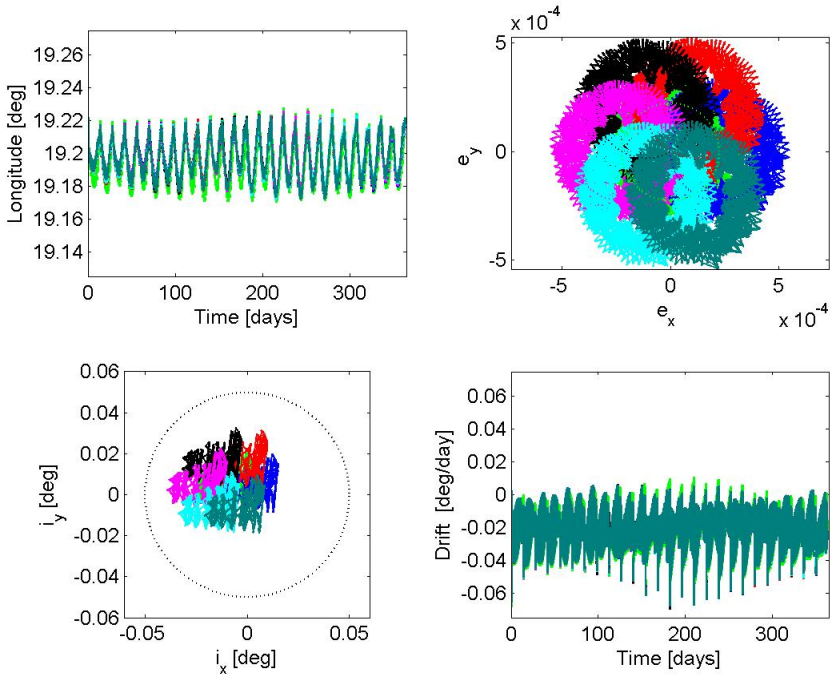

Figure 4.10. Osculating Equinoctial Orbit Elements for Case 5 for One Year for a Realistic Propulsion System

appear insignificant since both chief and deputy spacecraft share the same nominal longitude. It is demonstrated that the proposed framework is capable of handling the thruster cross-coupling present in a realistic propulsion system, while still maintaining safe seperation between the spacecraft. Increased autonomy is, inherently, obtained since the deputy spacecraft are controlled from on-board the chief limiting the required interaction by ground-based satellite controllers.

Table 4.4 Total Annual Cost for E-W Corrections for both Ground-based Stationkeeping and the Relative Orbit Control Concept for a Realistic Propulsion System using Chief-centered Cartesian Coordinates Coordinates and 14 Day Stationkeeping Cycles.

Case 1:	Ground Based [m/s]	Relative Cost [m/s]	Change [%]
Chief	2.4428	2.4428	
1^{st} Deputy	2.4660	2.4813	-0.6212
2^{nd} Deputy	2.4599	2.5039	-1.7864
3^{rd} Deputy	2.4709	2.5141	-1.7508
4^{th} Deputy	2.4645	2.4776	-0.5337
Case 2:	Ground Based [m/s]	Relative Cost [m/s]	Change [%]
Chief	2.2992	2.2993	
1^{st} Deputy	2.3435	2.3377	-0.2465
2^{nd} Deputy	2.3607	2.3737	0.5527
3^{rd} Deputy	2.3599	2.3409	-0.8091
4^{th} Deputy	2.3455	2.3423	-0.1359
Case 3:	Ground Based [m/s]	Relative Cost [m/s]	Change [%]
Chief	2.2992	2.2993	
1^{st} Deputy	2.3607	2.3737	0.5527
2^{nd} Deputy	2.3478	2.3503	0.1037
3^{rd} Deputy	2.3485	2.3299	-0.7927
4^{th} Deputy	2.3435	2.3377	-0.2465
5^{th} Deputy	2.3505	2.3656	0.6410
6^{th} Deputy	2.3522	2.3448	-0.3105
Case 4:	Ground Based [m/s]	Relative Cost [m/s]	Change [%]
Chief	3.1645	3.1646	
1^{st} Deputy	3.1935	3.1976	0.1273
2^{nd} Deputy	3.1974	3.2220	0.7695
3^{rd} Deputy	3.2059	3.2150	0.2848
4^{th} Deputy	3.1862	3.2071	0.6554
Case 5:	Ground Based [m/s]	Relative Cost [m/s]	Change [%]
Chief	3.1645	3.1646	
1^{st} Deputy	3.1974	3.2220	0.7695
2^{nd} Deputy	3.1896	3.2198	0.9474
3^{rd} Deputy	3.1904	3.2025	0.3778
4^{th} Deputy	3.1935	3.1976	0.1273
5^{th} Deputy	3.2017	3.2062	0.1408
6^{th} Deputy	3.2013	3.2188	0.5479

Table 4.5 Total Annual Cost for E-W Corrections for both Ground-based Stationkeeping and the Relative Orbit Control Concept for a Realistic Propulsion System using Curvilinear Coordinates Coordinates and 14 Day Stationkeeping Cycles.

Case 1:	Ground Based [m/s]	Relative Cost [m/s]	Change [%]
Chief	2.4428	2.4428	
1^{st} Deputy	2.4813	2.4804	0.5858
2^{nd} Deputy	2.5039	2.5031	1.7561
3^{rd} Deputy	2.5141	2.5130	1.7031
4^{th} Deputy	2.4776	2.4893	1.0066
Case 2:	Ground Based [m/s]	Relative Cost [m/s]	Change [%]
Chief	2.2992	2.2993	
1^{st} Deputy	2.3435	2.3273	-0.6903
2^{nd} Deputy	2.3607	2.3519	-0.3717
3^{rd} Deputy	2.3599	2.3471	-0.5447
4^{th} Deputy	2.3455	2.3579	-0.5262
Case 3:	Ground Based [m/s]	Relative Cost [m/s]	Change [%]
Chief	2.2992	2.2993	
1^{st} Deputy	2.3607	2.3519	-0.3717
2^{nd} Deputy	2.3478	2.3520	0.1760
3^{rd} Deputy	2.3485	2.3341	-0.6137
4^{th} Deputy	2.3435	2.3273	-0.6903
5^{th} Deputy	2.3505	2.3344	-0.6868
6^{th} Deputy	2.3522	2.3606	0.3578
Case 4:	Ground Based [m/s]	Relative Cost [m/s]	Change [%]
Chief	3.1645	3.1646	
1^{st} Deputy	3.1935	3.1957	0.0683
2^{nd} Deputy	3.1974	3.2225	0.7859
3^{rd} Deputy	3.2059	3.2129	0.2202
4^{th} Deputy	3.1862	3.2069	0.6497
Case 5:	Ground Based [m/s]	Relative Cost [m/s]	Change [%]
Chief	3.1645	3.1646	
1^{st} Deputy	3.1974	3.2225	0.7859
2^{nd} Deputy	3.1896	3.2176	0.8791
3^{rd} Deputy	3.1904	3.1988	0.2625
4^{th} Deputy	3.1935	3.1957	0.0683
5^{th} Deputy	3.2017	3.2043	0.0821
6^{th} Deputy	3.2013	3.2168	0.4855

5. RELATIVE LINE OF SIGHT CONSTRAINT ENFORCEMENT

Future proposed communications platforms such as ESA SkyKit and SkyLAN concepts require Inter-Satellite communications Links (ISL) [5, 6]. Thus, these concepts envision smaller, more specialized spacecraft that can share data on-orbit via high bandwidth inter-satellite communications links to provide increased flexibility in response to customer needs and for optimal use of the bandwidth that is available within the assigned Earth-to-spacecraft frequency spectrum. Such concepts likely employ a nominal constellation design that meets the required line-of-sight constraint. For contingency operation, it is however necessary to understand how to effectively and efficiently reestablish the line-of-sight constraint once violated. Reestablishing a relative line-of-sight constraint efficiently and quickly, with corrections limited to the tangential and normal directions, is examined.

5.1 Concept Overview

Such concepts likely employ a nominal constellation design that meets the required line-of-sight constraint requiring a longitude offset between spacecraft for optical ISL. A schematic illustration of a constellation with the chief and deputy spacecraft offset in adjacent longitudinal control boxes appears in Figure 5.1. Maneuver execution errors in a regular stationkeeping maneuver, such as an over- or undershoot, or a delay in executing the maneuver, could however result in a line-of-sight violation. Reestablishing a relative line-of-sight constraint efficiently and quickly, with corrections limited to the tangential and normal directions, is a challenging problem. From examining Eckstein's maneuver planning equations or GVE (3.34), it is clear that the optimal burn sequence to reestablish the desired configuration only occurs twice

per orbital revolution. A robust approach is required that delivers possible burn sequences reestablishing the line-of-sight in minimal time as well as minimal propellant consumption. A systematic procedure is developed that explores alternative burn sequences to reestablish the line-of-sight and yields safe separation with other spacecraft in the constellation.

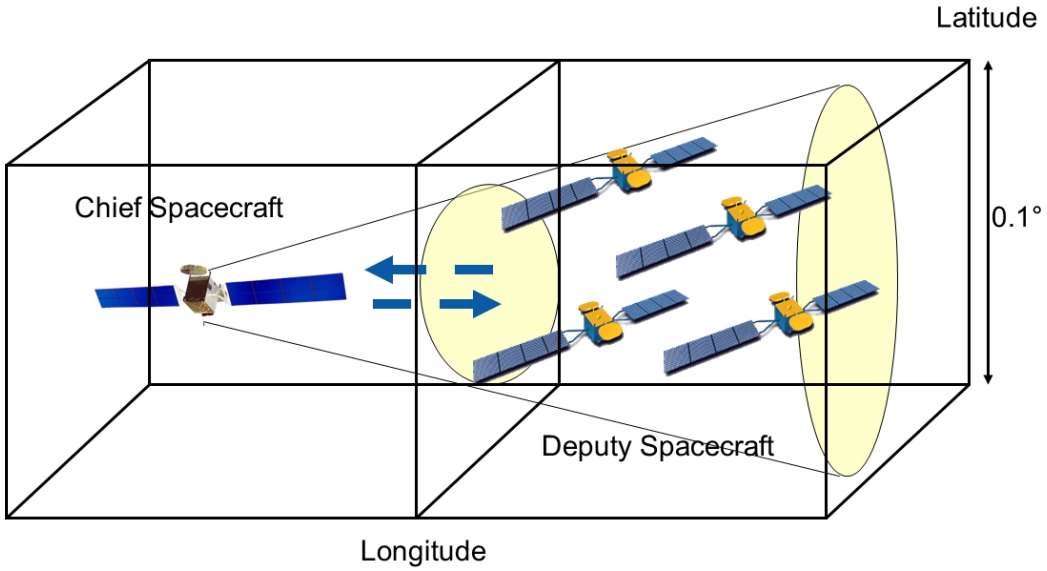

Figure 5.1. Schematic illustration of a constellation with the chief and deputy spacecraft in adjacent longitudinal boxes to allow for a line-of-sight constraint.

A constraint enforcement algorithm for a line-of-sight constraint is proposed in terms of orbit element differences. The feasible region within the line-of-sight is modeled by a circular cone originating on the chief spacecraft as is apparent in Figure 5.1. To first order, the planar and out-of-plane motions are decoupled. Hence, for an out-of-plane coning constraint violation, only the differential inclination vector is significant, whereas, an in-plane violation requires examination of the eccentricity vector as well as the differential longitude and drift.

The methods proposed in this chapter allow a spacecraft operator to select a burn sequence best balancing propellant consumption with minimizing the time of the constraint violation.

5.2 Out-of-plane Line-of-Sight Enforcement

For an out-of-plane coning constraint violation, only the differential inclination vector is significant. The proposed algorithm utilizes insight obtained from the inclination vector phase space to obtain options that re-establishes the line-of-sight constraint using limited control directions. The two relevant equations from the linearized Gauss' variational equations are

$$\Delta i_x = \frac{1}{2V_{Geo}} \Delta V^{NS} \cos\alpha, \tag{5.1}$$

$$\Delta i_y = \frac{1}{2V_{Geo}} \Delta V^{NS} \sin\alpha. \tag{5.2}$$

One can deduce that both the nominal i_x and i_y components of the inclination vector can be reestablished with a single burn performed at the proper right ascension as in

$$\alpha = \arctan\left(\frac{\Delta i_y}{\Delta i_x}\right), \tag{5.3}$$

with magnitude of the Δv computed by

$$\Delta V_{fuel}^{inc} = 2V_{Geo}\Delta i, \tag{5.4}$$

where

$$\Delta i = \sqrt{\Delta i_x^2 + \Delta i_y^2}. \tag{5.5}$$

A 'line-of-sight' constraint violation hence can be reestablished with one burn executed at the proper right ascension or time. This 'one-burn' solution is refered to as the 'fuel-optimal' burn, since it has the lowest possible cost to reestablish the nominal inclination. Since the period of the geostationary orbit is 24 hours, however it could take up to 12 hours for the spacecraft to reach the required right ascenscion. Depending on the mission specifics, such a delay may be unacceptable for operational reasons, and a higher cost two burn correction sequence, reestablishing the 'line-of-sight' faster may be preferable. Examing the relevant first order Gauss variational equations (5.1, 5.2) and the geometry of the line-of-sight cone from Figure 5.2 and

how the relative orbit relates to magnitude of the inclination vector difference as illustrated in Figure 3.4, it is apparent that to first order the feasible region in the inclination phase space can be approximated by

$$|\Delta i| \approx \delta\gamma \tan \beta_{\max}. \tag{5.6}$$

It implies that the feasible region inside the line-of-sight can be approximated by a circle in the inclination phase space. From equation (5.3), it is apparent that the right ascension is related to the direction of the Δi change in the phase space and this direction evolves with time, as is demonstrated in Figure 5.3. Analyzing the possible burn directions and their evolution over time, an algorithm is developed that determines feasible burn sequences capable of reestablishing the constraint faster than the ideal burn. After a maneuver execution error occurs, a time lapse is assumed to occur until either the constraint violation is detected or the earliest time a correction burn can be implemented. During this duration no corrective maneuver is allowed. First, it is determined if it is possible to reestablish the line-of-sight constraint with a single correction before reestablishing the nominal inclination with a second correction. If it is possible, the time to reestablish the line-of-sight and the cost of such a burn sequence is determined. Then alternative two burn sequences reestablishing the nominal relative orbit are computed. Performing the first correction burn as soon as possible after the constraint violation is detected as well as later times for the first burn are explored. The magnitude Δv_1 and time, respectively right ascension α_1 of the first maneuver are hence selected but the magnitude Δv_2 and right ascension α_2 of the second maneuver will be strictly determined to meet the nominal target states. The developed procedure allows either a spacecraft operator or an algorithm to select a burn sequence best balancing propellant consumption with minimizing the time of the constraint violation.

To demonstrate the proposed enforcement scheme an arbitrary violation is chosen. A constellation similar to case 1 in table 4.6 but with the chief offset in an adjacent longitudinal box is selected. The first deputy spacecraft will perform a 35% overshoot of the N-S stationkeeping meuver. It is then further assumed that it takes three

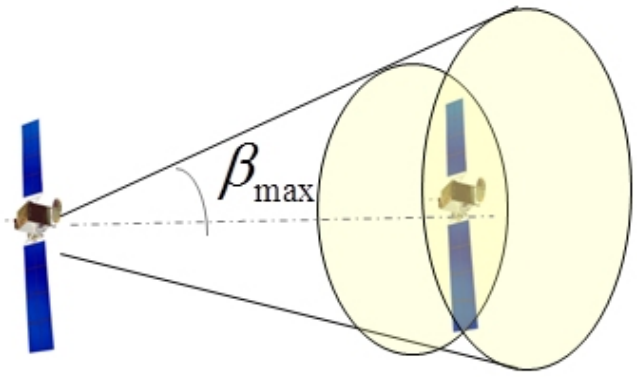

Figure 5.2. Line-of-Sight Cone between a chief and deputy spacecraft separated in longitude

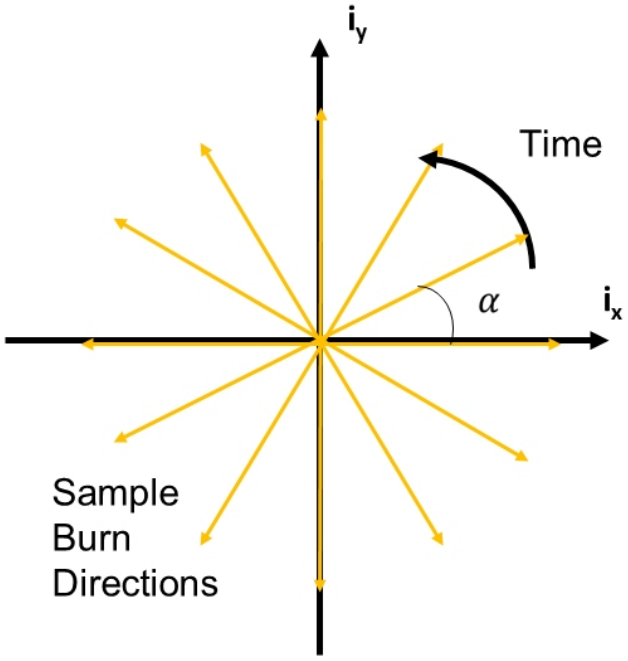

Figure 5.3. Sample Burn Directions in the Inclination Phase Space for Normal Corrections as Time (Right Ascension) Varies

hours until the violation is first observed or can be reestablished. At that time a line-of-sight violation will have occured. In Figure 5.4, the feasible region in the

inclination phase space for the first deputy is identified. For this particular case, the deputy is not allowed within the region $ix > 0$ to ensure collision avoidance. The dashed orange lines indicate a sample two burn sequence that could reestablish the nominal relative orbit and hence line-of-sight constraint in a shorter time than the ideal burn. In Figure 5.5, the dashed orange lines indicate a sample two burn sequence that could reestablish the line-of-sight constraint with the first correction and then reestablish the nominal orbit with a second correction. Figure 5.6a, shows 'pseudo-pareto' fronts for four different 'families' of correction sequences. Each point corresponds to the total cost to return to the nominal location versus the time until the line-of-sight constraint is reestablished. Figure 5.6b, illustrates the resulting changes in the inclination phase space for these correction sequences. In Figure 5.7, the relative trajectory is shown for a sample scenario involving a two burn scenario to reestablish the line-of-sight constraint in 8.9 hours for a total cost of 12.2 m/s compared to the ideal burn at 8.6 m/s requiring a 12 hour wait. For this particular violation, a short wait allows reconfiguration options that reestablish the constraint with the first correction burn. Sample maneuver sequences are plotted in magenta in Figure 5.6 and a sample relative trajectory appears in Figure 5.8. The proposed algorithm is hence capable at identifying possible burn sequences and reestablishing a line-of-sight faster than the fuel-optimal correction would.

5.3 In-plane Line-of-Sight Enforcement

For an in-plane 'line-of-sight' constraint violation, it is necessary to reestablish the nominal differences in the eccentricity vector, semi-major axis and longitude. This requires three correction maneuvers to be performed. Since geostationary spacecraft typically are not equipped with radial thrusters, only tangential correction burns are considered. The goal is to reestablish the line-of-sight constraint by the time the third correction is performed. The relevant equations from equations 3.34 then reduce to

$$\Delta a = 2\frac{a_C}{V_{Geo}}\left(\Delta v_1 + \Delta v_2 + \Delta v_3\right), \tag{5.7}$$

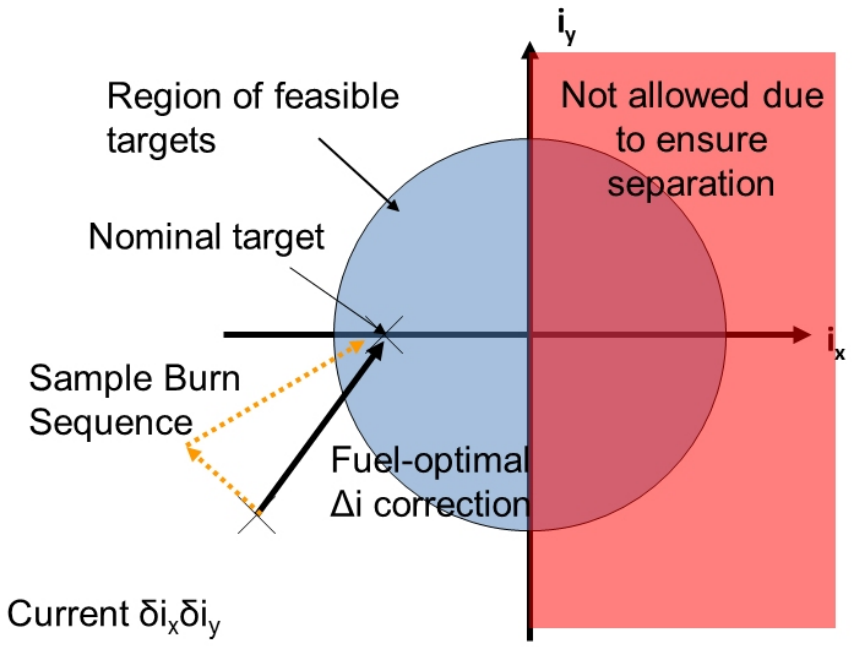

Figure 5.4. The Feasible Region for a Line-of-Sight Constraint to Be Met by the 1st Deputy Vehicle in a Constellation Similar to Case 1 from Table 4.6; The Fuel-optimal Burn Correction is Illustrated in Black and a Sample Two-burn sequence is Illustrated in Orange.

$$\Delta\gamma = -3\frac{n}{V_{Geo}}\left(\tau_1\Delta v_1 + \tau_2\Delta v_2\right), \tag{5.8}$$

$$\Delta e_x = \frac{2}{V_{Geo}}\left(\cos\alpha_1\Delta v_1 + \cos\alpha_2\Delta v_2 + \cos\alpha_3\Delta v_3\right), \tag{5.9}$$

$$\Delta e_y = \frac{2}{V_{Geo}}\left(sin\alpha_1\Delta v_1 + sin\alpha_2\Delta v_2 + sin\alpha_3\Delta v_3\right), \tag{5.10}$$

where τ_1 and τ_2 is the time between the first and second correction burn to the third correction burn. From the above equations, it is clear that a tangential correction maneuver will immeadiately affect the semi-major axis and eccentricity vector but the longitude if only affected over time. The deviations Δa, $\Delta\gamma$, Δe_x, Δe_y are the difference between the nominal orbit element differences and the measured orbit element difference at the time the violation is detected, propagated to the time the third correction burn is performed as in

$$\Delta\overline{oe} = \delta\overline{oe}_{\text{Nominal}} - \delta\overline{oe}_{\text{Propag}}. \tag{5.11}$$

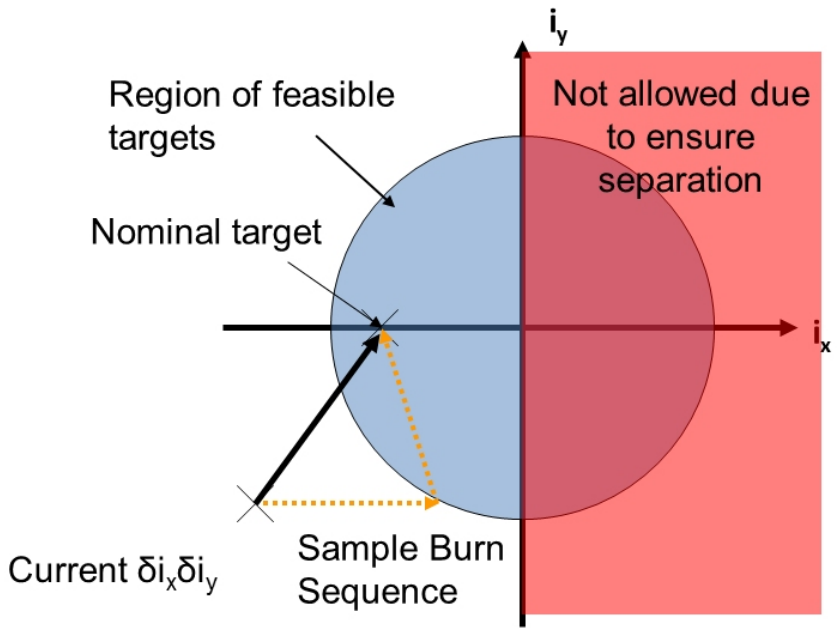

Figure 5.5. The Feasible Region for a Line-of-Sight Constraint to Be Met by the 1st Deputy Vehicle in a Constellation Similar to Case 1 from Table 4.6; The Fuel-optimal Burn Correction is Illustrated in Black and a Sample Two-burn sequence Reestablishing the Line-of-Sight with the First Correction Burn is Illustrated in Orange.

Assuming two-body relative dynamics as in equation (3.31), the semi-major axis and eccentricity vector differences remain invariant and only the change in the longitude difference needs to be computed. The fuel-optimal solution is identical to equations (4.18-4.20)with τ_3 equal to zero. It assumes that the right ascension of the first correction burn α_1 is given by the necessary Δe correction, α_2 and α_3 are then offset by half a period each to achieve fuel optimality. The fuel optimal solution assumes that the change in the eccentricity vector for each correction burn is in in the same direction and therefore requires the correction burns to be seperated by half an orbital revolution resulting in up to a 36 hour wait until the line-of-sight constraint is reestablished. For operational reason, it may be more important to reestablish the line-of-sight constraint faster than the fuel-optimal solution allows. Finding a solution that satisfies all four equations (5.7-5.10) and allows re-establishing the line of sight

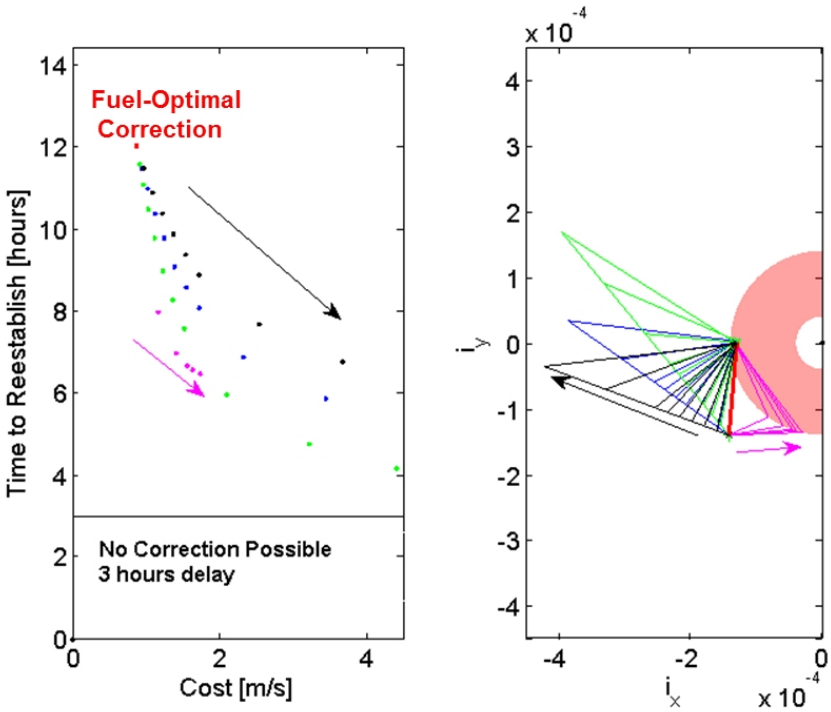

Figure 5.6. (a) Total Cost of Correction Sequences versus time to reestablish a line-of-sight constraint. (b) Movement in phase space for correction sequences is illustrated.

constraint faster than the 'fuel-optimal' solution, is very challenging. The approach proposed in this investigation is to solve equations by eliminating the Δv dependency and then solving for the burn right ascensions, which is equivalent to the burn times, that satisfies all four equations in less time. Solving equation(5.8) for Δv_2

$$\Delta v_1 = \frac{\alpha_3 - \alpha_2}{\alpha_1 - \alpha_2}\left[\frac{2\pi V_{Geo}}{3n\left(\alpha_3 - \alpha_2\right)}\Delta\gamma + \frac{V_{Geo}}{2a}\delta a - \Delta v_3\right] \tag{5.12}$$

and subsituting into equation(5.7) yields

$$\Delta v_2 = -\frac{2\pi\frac{V_{Geo}}{3n}\Delta\gamma + \left(\alpha_3 - \alpha_1\right)\Delta v_1}{\left(\alpha_3 - \alpha_2\right)}. \tag{5.13}$$

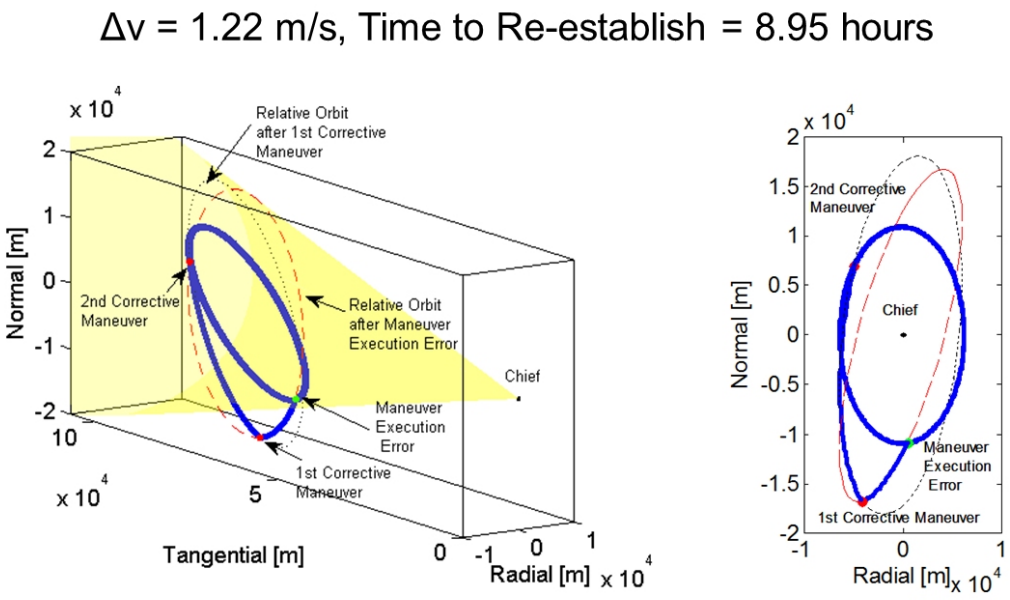

Figure 5.7. (a) The relative trajectory of the deputy spacecraft encountering a line-of-sight constraint violation. (b) The relative trajectory of the deputy spacecraft encountering a line-of-sight constraint violation is viewed in the meridian plane from the chief spacecraft.

Substituing both equation(5.12) and equation(5.13) into equation(5.9) and equation(5.10) yields

$$\Delta v_3^x = \left[-\frac{\alpha_3-\alpha_2}{\alpha_1-\alpha_2}\cos\alpha_1 + \frac{\alpha_3-\alpha_1}{\alpha_1-\alpha_2} cos\alpha_2 + cos\alpha_3\right]^{-1} \left[\frac{V_{Geo}}{2}\delta e_x - \Delta\gamma\frac{V_{Geo}2\pi}{3n\left(\alpha_3-\alpha_2\right)}\left(cos\alpha_1\frac{\alpha_3-\alpha_2}{\alpha_1-\alpha_2} - cos\alpha_2\left(1+\frac{\alpha_3-\alpha_1}{\alpha_1-\alpha_2}\right)\right) + \delta a\frac{V_{Geo}}{2a\left(\alpha_1-\alpha_2\right)}\left(cos\alpha_2\left(\alpha_3-\alpha_1\right) - cos\alpha_1\left(\alpha_3-\alpha_2\right)\right)\right], \quad (5.14)$$

$$\Delta v_3^y = \left[-\frac{\alpha_3-\alpha_2}{\alpha_1-\alpha_2}\sin\alpha_1 + \frac{\alpha_3-\alpha_1}{\alpha_1-\alpha_2}\sin\alpha_2 + \sin\alpha_3\right]^{-1} \left[\frac{V_{Geo}}{2}\delta e_y - \Delta\gamma\frac{V_{Geo}2\pi}{3n\left(\alpha_3-\alpha_2\right)}\left(\sin\alpha_1\frac{\alpha_3-\alpha_2}{\alpha_1-\alpha_2} - \sin\alpha_2\left(1+\frac{\alpha_3-\alpha_1}{\alpha_1-\alpha_2}\right)\right) + \delta a\frac{V_{Geo}}{2a\left(\alpha_1-\alpha_2\right)}\left(\sin\alpha_2\left(\alpha_3-\alpha_1\right) - \sin\alpha_1\left(\alpha_3-\alpha_2\right)\right)\right]. \quad (5.15)$$

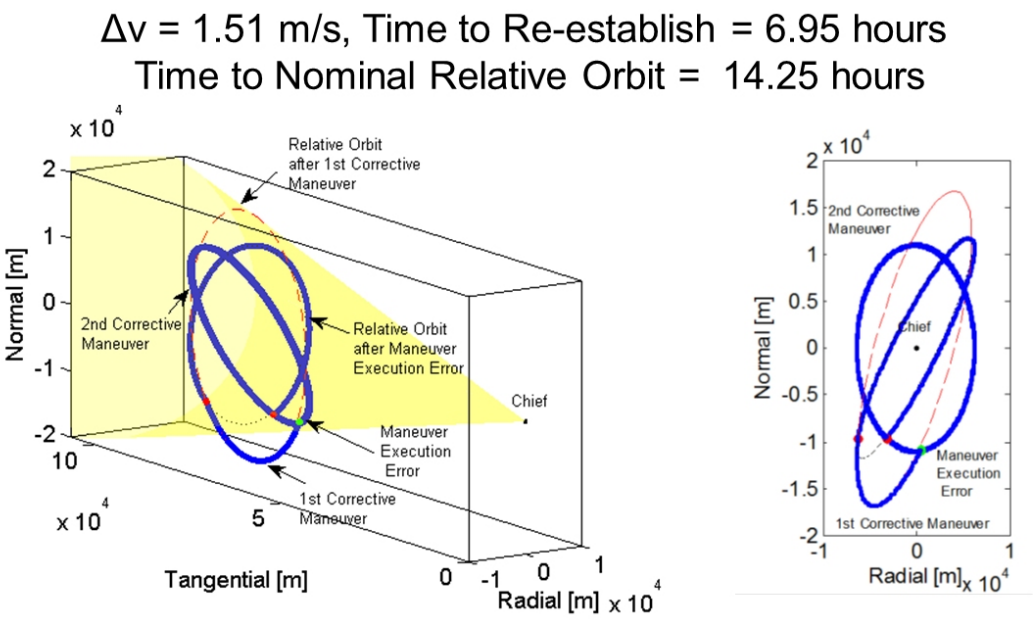

Figure 5.8. (a) The relative trajectory of the deputy spacecraft encountering a line-of-sight constraint violation. The line-of-sight constraint is reestablished with the first corrective maneuver and the second maneuver reestablishes the nominal relative orbit. (b) The relative trajectory of the deputy spacecraft encountering a line-of-sight constraint violation is viewed in the meridian plane from the chief spacecraft.

Note that Δv_3^x and Δv_3^y must match, hence the equations can be set equal yielding

$$\begin{aligned}
&\left[-\frac{\alpha_3-\alpha_2}{\alpha_1-\alpha_2}\cos\alpha_1+\frac{\alpha_3-\alpha_1}{\alpha_1-\alpha_2}cos\alpha_2+cos\alpha_3\right] \\
&\quad\left[\frac{V_{Geo}}{2}\delta e_y-\Delta\gamma\frac{V_{Geo}2\pi}{3n\left(\alpha_3-\alpha_2\right)}\left(\sin\alpha_1\frac{\alpha_3-\alpha_2}{\alpha_1-\alpha_2}-\sin\alpha_2\left(1+\frac{\alpha_3-\alpha_1}{\alpha_1-\alpha_2}\right)\right)\right. \\
&\qquad\left.+\delta a\frac{V_{Geo}}{2a\left(\alpha_1-\alpha_2\right)}\left(\sin\alpha_2\left(\alpha_3-\alpha_1\right)-\sin\alpha_1\left(\alpha_3-\alpha_2\right)\right)\right] \\
&\qquad-\left[-\frac{\alpha_3-\alpha_2}{\alpha_1-\alpha_2}\sin\alpha_1+\frac{\alpha_3-\alpha_1}{\alpha_1-\alpha_2}\sin\alpha_2+\sin\alpha_3\right] \\
&\quad\left[\frac{V_{Geo}}{2}\delta e_x-\Delta\gamma\frac{V_{Geo}2\pi}{3n\left(\alpha_3-\alpha_2\right)}\left(cos\alpha_1\frac{\alpha_3-\alpha_2}{\alpha_1-\alpha_2}-cos\alpha_2\left(1+\frac{\alpha_3-\alpha_1}{\alpha_1-\alpha_2}\right)\right)\right. \\
&\qquad\left.+\delta a\frac{V_{Geo}}{2a\left(\alpha_1-\alpha_2\right)}\left(cos\alpha_2\left(\alpha_3-\alpha_1\right)-cos\alpha_1\left(\alpha_3-\alpha_2\right)\right)\right]=0. \quad (5.16)
\end{aligned}$$

Since solving equation(5.16) analytically would be very challenging if not impossible, it is solved numerically in this investigation. However many different formulations are possible to solve equation(5.16) numerically. In this investigation, the right ascensions α_1 is selected to be the time the maneuver execution error is first detected and α_2 and α_3 are then solved for numerically. This approach was selected as it appears to be most robust in terms of converging onto a solution and provided the shortest overall time to reestablish the nominal relative orbit for cases examined. However numerically solving for the right ascension of the third correction maneuver also means that it will not be known ahead of times to propagate the longitude difference forward in time, hence an iterative process requiring a few iterations is required.

To demonstrate the proposed enforcement scheme an arbitrary violation is chosen. Again a constellation similar to case 1 in table 4.6 with the chief offset in an adjacent longitudinal box is selected. The first deputy spacecraft will perform a 350% overshoot of the second E-W stationkeeping meuver. It is then further assumed that it takes seven hours until the violation is first observed or can be reestablished. Note that this is a very large maneuver execution error and also a fairly long time to detect the violation. This particular case is selected to lead to likely a fairly fast line-of-sight violation and to demonstrate that the proposed algorithm is capable at reestablishing the nomincal relative orbit faster than the fuel-optimal burn sequence. In Figures 5.9 and 5.10 the deputy vehicle's motion is shown with no relative control corrections performed to illustrate how a line-of-sight violation would likely quickly occur. In Figure 5.9 the osculating equinoctial orbit elements for both the chief and the deputy are displayed. The chief is plotted in green and the deputy is displayed in blue and this coloring is used for all future figures. As is apparent from the longitude vs time subfigure, the longitudinal seperation between the chief and deputy vehicles quickly increases if no correction are performed. In Figure 5.10 projections of the chief-centered Cartesian coordinates are plotted. From the subfigure displaying the radial vs tangential motion, the fast increasing longitudinal seperation is very apparent. Such a motion would likely quickly result in a line-of-sight violation. In Figures

5.11 through 5.13, the deputy vehicle's motion is displayed with relative correction maneuvers performed and their location shown by black dots. In Figure 5.11, the osculating equinoctical orbit elements for both chief and deputy vehicles are plotted. Figure 5.13 shows the equinoctial orbit element differences. From the subfigures displaying longitude vs time and drift vs time, it becomes apparent how the relative correction burns quickly reestablish the nominal differential longitude and differential drift. The same can be observed in Figure 5.12, which shows the relative motion of the deputy vehicle in the chief-centered Cartesian frame. The fuel-optimal burn sequence with the maneuvers seperated by half an orbit would cost 0.0428 m/s and would require 36.02 hours after the maneuver is detected to reestablish the nominal orbit. The maneuver sequence computed using the proposed algorithm costs 0.1026 m/s and reestablishes the nominal orbit in just about 27 hours. Furthermore, for this particular case, it was possible to completely avoid a line-of-sight violation by using the computed burn sequence. Clearly, the 59.8% increase in propellant consumption is significant but also ensured that no line-of-sight violation took place. From the example scenario illustrated in this section, it is clear that the proposed approach is capable at reestablishing the nominal relative orbit faster than the fuel-optimal solution and is suitable to avoid planar line-of-sight violations.

5.4 Conclusion

This preliminary investigation is a proof of concept to illustrate how a relative line-of-sight constraint can be enforced using different non-fuel-optimal maneuver sequences in less time than the fuel-optimal maneuver sequence would require. The methods proposed in this chapter can serve as basic framework or starting point for future investigations into this problem. For the planar problem, for example different formulations could be explored both in solving equation(5.16). It may also be possible that insight from the longitude-eccentricity phase space may be gained aiding in the selection of the burn times.

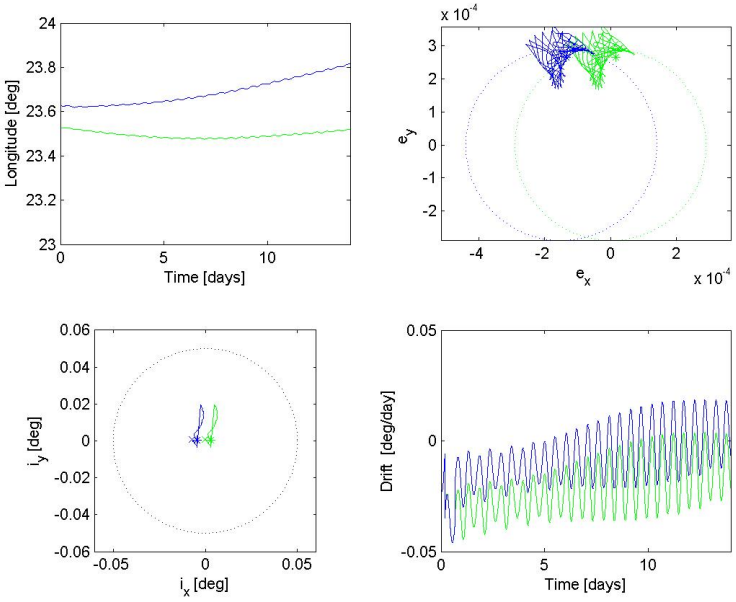

Figure 5.9. Osculating Equinoctial Orbit Elements with Maneuver Execution Error Occuring and No Line-of-Sight Enforcement

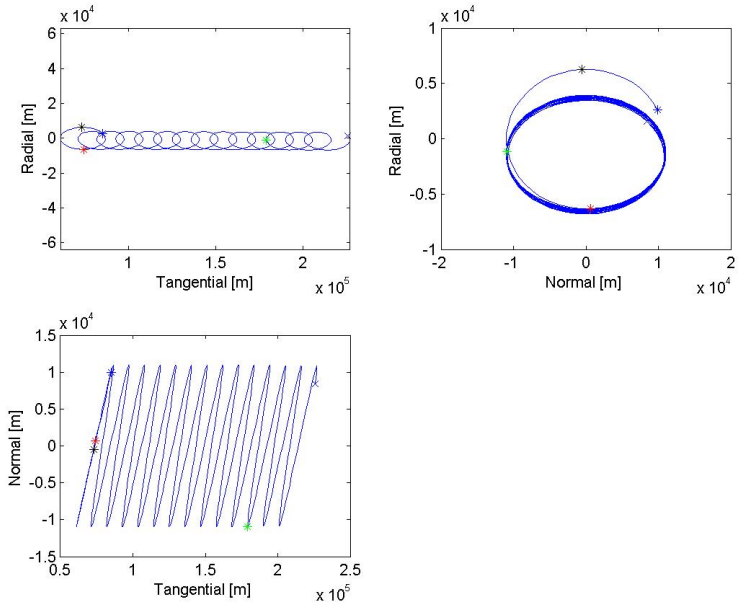

Figure 5.10. Projections of the Chief-Centered Cartesian Coordinates with Maneuver Execution Error Occuring and No Line-of-Sight Enforcement

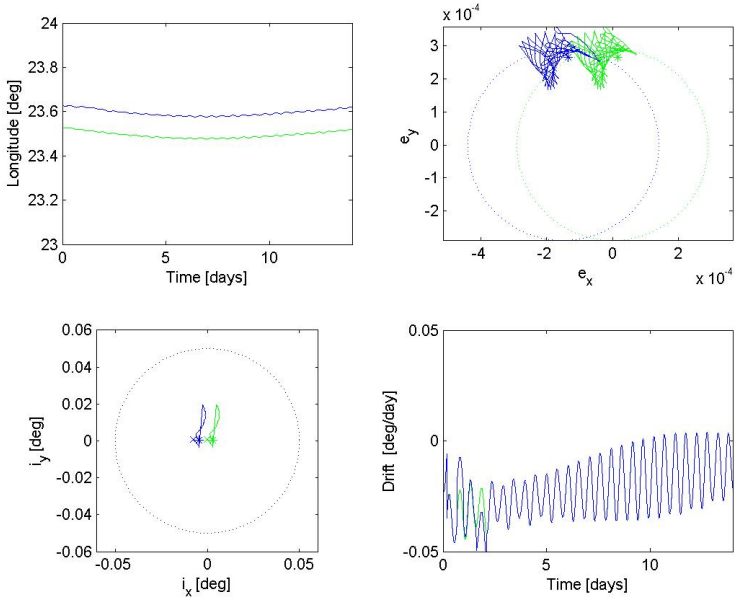

Figure 5.11. Osculating Equinoctial Orbit Elements with Maneuver Execution Error Occuring with Line-of-Sight Enforcement

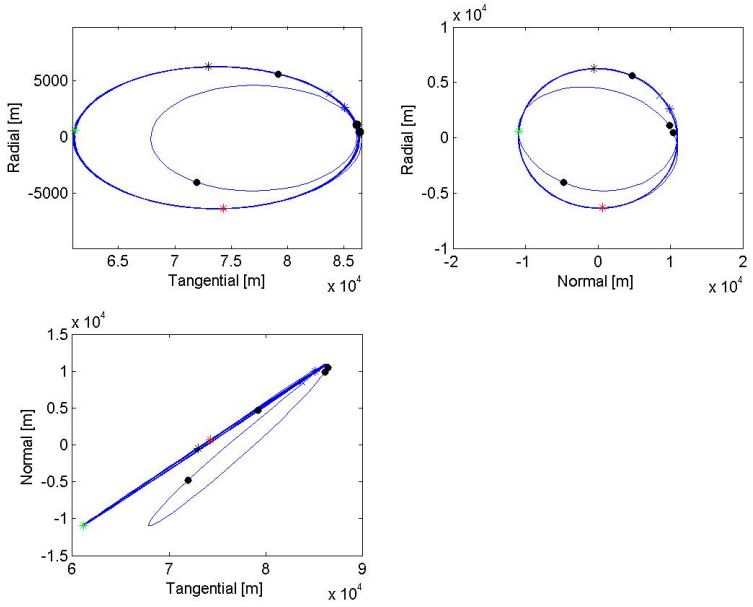

Figure 5.12. Projections of the Chief-Centered Cartesian Coordinates with Maneuver Execution Error Occuring with Line-of-Sight Enforcement

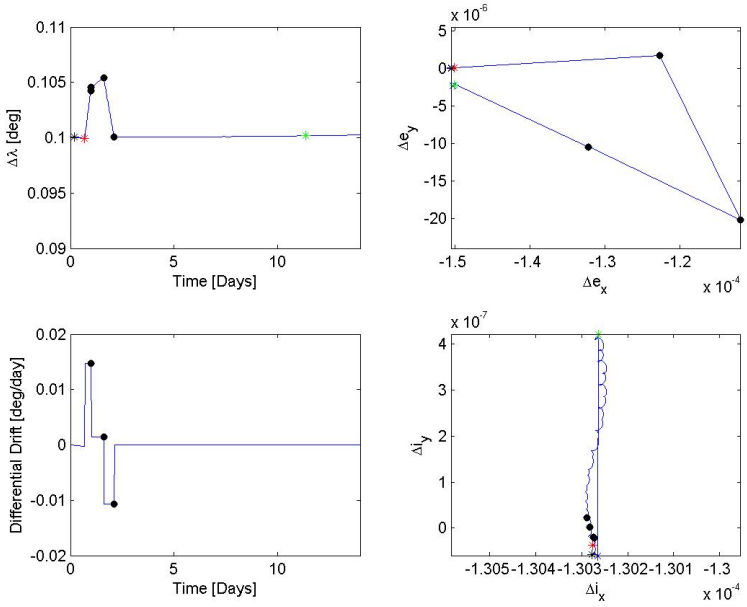

Figure 5.13. Projections of the Chief-Centered Cartesian Coordinates with Maneuver Execution Error Occuring with Line-of-Sight Enforcement

6. SUMMARY AND RECOMMENDATIONS

6.1 Summary

The primary goal of this study is a relative orbit control framework suitable for collocated geostationary spacecraft providing increased autonomy in the orbital maintenance over traditional ground-based stationkeeping. The work is decomposed into three separate problems. First, the relative orbit guidance and control framework is considered. Second, the proposed relative framework is applied to the orbital maintenance, or stationkeeping, problem for a constellation of collocated geostationary spacecraft. And finally, a relative 'line-of-sight' enforcement scheme is presented allowing the enforcement between a chief and deputy spacecraft separated in longitude. The goals of this study are accomplished by limiting the required ground-based control to one spacecraft and maintaining the remaining spacecraft from on-board that spacecraft.

In the first part of the investigation, a relative orbit determination and control concept is developed in terms of mean equinoctial orbit elements. A linear mapping mapping is presented to quickly and efficiently relate relative orbit measurements to mean equinoctial orbit element differences. The nominal relative orbit is defined and a simplified relative dynamic model is presented. Finally, the relative orbit control framework taking deterministic thruster cross-coupling into account is presented. The relative framework provided is utilized in the later portions of this work.

The second part of this study, demonstrates that the proposed relative formulation is capabable at maintaining the deputy spacecraft in a pre-described relative orbit satisfying the absolute constraints. A number of different constellations and deterministic thruster cross-coupling are considered. It is shown that the propellant cost is comparable to traditional ground-based stationkeeping. Hence demonstrating

that currently employed fuel-efficient stationkeeping strategies are followed. Increased autonomy is, inherently, obtained since the deputy spacecraft are controlled from on-board the chief.

The last part of this analysis, focuses on the enforcement of a relative line-of-sight 'coning' constraint between a chief separated in longitude from a deputy spacecraft. An enforcement scheme for both in-plane and out-of-plane violations is developed. The proposed approach utilizes insight gained from the orbit element difference formulation and the relative orbit control concept to provide burn sequences for reconfiguration. A satellite operator is provided a tool to select burn sequences to reestablish a line-of-sight based on the missions requirements and avilable propellant budget.

In conclusions, a relative orbit control concept is presented that: i) is capable at maintaining the deputy spacecraft in a pre-described relative orbit satisfying the absolute constraints; ii) allows the continued use of fuel efficient stationkeeping strategies; iii) allows for easy consideration of potential relative constraints between spacecraft, difficult to visualize and enforce using traditional ground-based approaches; and iv) provides increased autonomy over traditional ground based stationkeeping. This research validates that a relative orbit control concept could provide an alternative to traditional ground-based stationkeeping for collocated geostationary spacecraft by offering increased autonomy through on-board relative orbit control of the deputies relative orbits.

6.2 Recommendations and Future Work

Many challenges remain in the development of a relative orbit control concept for collocated geostationary spacecraft suitable for onboard use in an operational environment. The work presented here is of a preliminary nature and serves as the basis for more comprehensive investigations taking specific hardware or operational requirements into accounts. Future work is likely a combination of increasing the

fidelity of the relative guidance concept and developing a relative navigation concept suitable for on-board use on the chief spacecraft.

Potential improvements in the relative guidance concept include increasing the accuracy of the linear mapping, considering differential perturbations and extending it to different constellation desgns. It is desirable to decrease the linearization errors introduced by the mapping. Of specific interest are improvements in the estimation of the differential semi-major axis. One method could be, obtaining an approximation of the linearization error and then using it in combination with the linear mapping to improve the accuracy of the approximation. To make the proposed framework better suited for a spacecraft of varying built, differential perturbations can be incorporated into the relative dynamic model. Most important to consider is differential solar radiation pressure since the area-to-mass ratio between spacecraft in the constellation can vary substantially. For constellations involving a longitude offset, the difference in the gravitational drift due to Earth tesseral terms could also be considered.

In an operational environment, measurement errors and uncertainties need to be considered. The current investigation assumes precise relative orbit determination and is not take any orbit determination uncertianties or uncertainties in the maneuver performance or execution into account. Relative orbit measurement errors therefore should be considered and a relative orbit determination process taking these uncertainties into accountdeveloped. The sensitity of the proposed relative control formulation to such errors should also be evaluated. Such a relative orbit estimation scheme could likely be based on some sort of an iterative Kalman filtering approach. A relative orbit dermination and navigation concept is required to operate in a 'real-world' environment.

A comprehensive investigation of the benefits and limitations of the proposed phase space approach for the line-of-sight constraint enforcement is desirable. Improvements in the implementation and optimization of the enforcement schemes could be achieved by exploiting the insight from the proposed phased space approach with additional formulations such as a Lovell type multi-burn algorithm, based on

Clohessy-Wiltshire dynamics [35]. A systematic trade-off study comparing planar control options limited to tangential burns with both radial-tangential, as well as only radial control is of interest. Finally, improvements in characterizing the feasible region in the phase space could possibly be achieved.

6.3 Concluding Remarks

Spacecraft formation flying and relative orbit control formulations are an enabling tool for many future space applications. Much effort has been dedicated to study it for applications ranging from Earth observation in LEO to space space telescope in libration point orbits. However, few studies have investigated a relative orbit control formulation for collocated geostationary spacecraft. One such formulation, based on an orbit element difference approach is proposed and investigated in this work. It is demonstrated that it provides the potential for increased autonomy in the station-keeping of constellations of collocated spacecraft. The enforcement of a line-of-sight constraint using the same formalism is also considered. The proposed relative framework may serve as a foundation for future constellations of collocated geostationary controlled from on-board one vehicle. Although, the feasibility is demonstrated, many improvements are needed to take operational constraints, measurement errors and uncertainties into account before it can employed on-board a vehicle.

LIST OF REFERENCES

LIST OF REFERENCES

[1] C. Chao, *Applied Orbit Perturbation and Maintenance*. El Segundo, California: The Aerospace Press, 1st ed., 2005.

[2] P. Wauthier, P. Francken, and H. Laroche, "The ASTRA Co-Location Strategy for Three to Six Satellites." Journal of the Braz. Soc. Mechanical Sciences, Vol. XVI, 1994.

[3] L. Pattinson, "EUTELSAT Satellite Collocation, Proceedings of the International Communications Satellite Conference and Exhibit." AIAA Paper No. 96-1187-CP, 1996.

[4] M.Eckstein, *Maneuver Schedule and Target Orbits for the 4 Colocated Satellites TDF-1, Olympus, TVSAT2,TDF2*. Oberpfaffenhofen: DFVLR-GSOC, 1989.

[5] P. Wauthier, "SkyKit Pre-Phase A, TN1400."

[6] J. Geyrard, T. Zein-Alabedeen, A. Cotellessa, G. Gallinaro, B. Perrot, and E. Bertenyi, "SkyLAN: A Cluster of Geostationary Satellites for Broadband Communications." AIAA, Monterey, CA, 2004.

[7] S. D'Amico, *Autonomous Formation Flying in Low Earth Orbit*. PhD thesis, Technical University of Delft, 2010.

[8] A. C. Clarke, "Extra-Terrestrial Relays." ESA Journal, Vol 9, P65, 1985.

[9] S. Shrivastava, "Orbital Perturbations and Stationkeeping of Communication Satellites." Journal of Spacecraft and Rockets Vol.15 (2), 1978.

[10] A. Kamel, I. Ekman, and R. Tibbitts, "East-West Stationkeeping Requirements of Nearly Synchronous Satellites due to Earths Triaxiality and Luni-Solar Effects." Celestial Mechanics, Vol. 8, 1973.

[11] J. Kechichian, "A Split-DV Technique for Drift Control of Geosynchronous Control of Geosynchronous Spacecraft." AIAA 21st Aerospace Sciences Meeting, Reno, Nevada, 1983.

[12] J. Kechichian, "One Impulse Targeting Strategy for Longitudinal Drift Control of Geosynchronous Spacecraft Subject to Tesseral Harmonics and Luni-Solar Gravity Perturbations." AIAA/AAS, Astrodynamica Conference, Seattle, Washington, August 1984.

[13] C. F. Gartrell, "Simultaneous Eccentricity and Drift Rate Control." Journal of Guidance, Control, and Dynamics, Vol. 4, No. 3.

[14] A. Kamel and C. Wagner, "On the Orbital Eccentricity Control of Synchronous Ssatellites." Journal of Astronautical Sciences, Vol. 30, Pages 61 - 73, 1982.

[15] C. Chao and J. Baker, "On the Propagation and Control of Geosynchronous Orbits." Journal Astronautical Sciences, Vol. XXXI (1), pp. 99-115, 1983.

[16] T. Kelly, L. White, and D. Gamble, "Stationkeeping of Geostationary Satellites with Simultaneous Eccentricity and Longitude Control." Journal of Guidance, Control and Dynamics, Vol. 17, No.4, May-June, 2003.

[17] P. Romero and J. Gambi, "Optimal Control in the East/West Station-keeping Manoeuvres for Geostationary Satellites." Aerospace Science and Technology, Vol. 8, pages 729-734, 2004.

[18] B. Emma and H. Pernicka, "Algorithm for Autonomous Longitude and Eccentricity Control for Geostationary Spacecraft." Journal of Guidance, Control and Dynamics, Vol. 26, No. 3, May-June, 2003.

[19] D. Slavinskas, H. Dabbaghi, and W. Benden, "EfficientInclination Control for Geostationary Satellites." Journal of Guidance, Control and Dynamics, Vol. 11, No. 6.

[20] E. Soop, *Handbook of Geostationary Orbits*. Kluwer Academic Publishers, 1994.

[21] M. Sidi, *Spacecraft Dynamics and Control*. Cambridge University Press, 1997.

[22] A. Hartling, M. Eckstein, A. Leibold, and K. Murthy, "On the Collision Hazard of Colocated Geostationary Satellites, publisher = DLR Technical Report, DFVLR-FB 88-02,

[23] J.-P. Carrou, *Spaceflight Dynamics Part 2*. Toulouse, France: Cepadues, 1995.

[24] V. J. Slabinski, "Colocation Sation Keeping of Geostationary Satellites." 3rd Deep Space Sensor and Surveillance Workshop, MIT Lincoln Lab, Lexington, Ma., 1985.

[25] J. Murdoch, G. Swinerd, M. Chabrol, and J. Marie, *Satcom International Review of Synchronised Attitude and Orbit Control of Satellites operating in clusters*. ESTEC Contract 5817/84/NL/BI(SC), 1984.

[26] B. K. Park, M. J. Tahk, H. C. Bang, and S. B. Choi, "Station Collocation Design Algorithm for Multiple Geostationary Satellites Operation." Journal of Spacecraft and Rockets, Nov.-Dec. 2003.

[27] C. Kluever and G. Tanck, "A Feedback Control Law for Stationkeeping with on-off Thrusters." Advances in the Astronautical Sciences, pages 387-399, 1997.

[28] C. Chao and G. Peterson, "A Coordinated Stationkeeping Strategy for Collocated Geosynchronous Satellites." AAS 05-196, 1995.

[29] B. K. Park, M. J. Tahk, H. C. Bang, C. S. Park, and J. H. Jin, "A New Approach to On-board Stationkeeping of Geo-satellites." Aerospace Science and Technology, Vol. 9, 2005.

[30] C. Chao and H. Bernstein, "Onboard Stationkeeping of Geosynchronous Satellites Using a Global Positioning System Receiver." Journal of Guidance, Navigation and Control, Vol.17 No. 4, July-Aug. 1994.

[31] G. W. Hill, "Researches in the Lunar Theory." American Journal of Mathematics, Vol. 1, No. 1, 1878.

[32] W. H. Clohessy and R. S. Wiltshire, "Terminal Guidance System for Satellite Rendezvous." Journal of the Astronautical Sciences, Vol.27, No. 9, 1960.

[33] R. Burns, C. McLaughlin, J. Leitner, and M. Martin, "TechSat 21: Formation Design, Control, and Simulation." ARFL.

[34] S. Vaddi, S. Vadali, and K. Alfriend, "Formation Flying: Accommodating Nonlinearity and Eccentricity Perturbations." Journal of Guidance, Navigation and Control, Vol. 26, No. 2, March-April 2003.

[35] T. Lovell, K. Horneman, S. Tragesser, and M. Tollefson, "A Guidance Algorithm for Formation Reconfiguration and Maintenance Based on the Perturbed Clohessy-Wiltshire Equations." AAS 03-649, 2003.

[36] K. Alfriend, H. Schaub, and D. Gim, "Gravitational Perturbations, Nonlinearity and Circular Orbit Assumption Effects on Formation Flying Control Strategies."

[37] D. Gim and K. Alfriend, "State Transition Matrix of Relative Motion for the Perturbed Noncircular Reference Orbit." Journal of Guidance, Navigation and Control, Vol. 26, No. 6, Nov.-Dec. 2003.

[38] D. W. Gim and K. Alfriend, "Satellite Relative Motion Using Differential Equinoctial Elements." Celestial Mechanics and Dynamical Astronomy, Vol. 92, 2005.

[39] H. Schaub and K. Alfriend, "Impulsive Feedback Control to Establish Specific Mean Orbit Elements of Spacecraft Formations." Journal of Guidance, Navigation and Control, Vol. 24, No.4, Aug 2004.

[40] H. Schaub and K. Alfriend, "Hybrid Cartesian and Orbit Element Feedback Law for Formation Flying Spacecraft." Journal of Guidance, Navigation and Control, Vol. 25, No. 2, March-April 2002.

[41] L. Breger, *Model Predictive Control for Formation Flying Spacecraft.* MIT Master of Science Thesis, 2004.

[42] L. Breger and J. How, "Gauss Variational Equation-Based Dynamics and Control for Formation Flying Spacecraft." Journal of Guidance, Control and Dynamics, Vol. 30, No.2, March-April 2007.

[43] K. Alfriend and H. Yan, "Evaluation and Comparison of Relative Motion Theories." Journal of Guidance, Control and Dynamics, Vol. 28, No. 2, Pages 295 - 336, March-April 2005.

[44] O. Montenbruck, M. Kirschner, and S. D'Amico, *E-I-Vector Separation for Grace Proximity Operations.* Space Flight Technology, German Space Operation Center, TN 04 - 08, 2008.

[45] S. D'Amico and O. Montenbruck, "Proximity Operations of Formation-Flying Spacecraft Using an Eccentricity/Inclination Vector Separation." Journal of Guidance, Control and Dynamics, Vol. 29, No. 3, May-June 2006.

[46] R. Vassar and R. Sherwood, "Formationkeeping for a Pair of Satellites in a Circular Orbit." Journal Guidance, Vol. 8, NO.2, March-April 1985.

[47] V. Kapila, "Spacecraft Formation Flying: A Survey, Final Report: Summer Faculty Research Program, Wright Site." Air Force Office of Scientific Research.

[48] A. Sparks, "Linear Control of Spacecraft Formation Flying." AIAA Guidance, Navigation, and Control Conference, AIAA2000-4438, 14-17 August 2000.

[49] P. Blumer, "A Future Concept of Coordinated Orbit Control of Colocated Geostationary Satellites." AIAA and AAS, Astrodynamics, Hilton Head Island, August 1992.

[50] P. Blumer, "Ein bordunterstztes Verfahren zur koordinierten Bahnreglung kopositionierter geostationarer Satelliten." DLR Technical Report, DLR-FB 93-41, 1993.

[51] H. Quan and H. Chao, "Dynamics and Control of Satellite Formation Flying Based on Relative Orbit Elements." AIAA Guidance, Navigation and Control Conference and Exhibit AIAA2008-6470, Honolulu, Hawaii.

[52] D. A. Vallado, *Fundamentals of Astrodynamics and Applications.* McGraw-Hill, 1997.

[53] O. Montenbruck, *Ephemeridenrechnung und Bahnbestimmung geostationarer Satelliten mit Hilfe von Taylorreihenintegration.* Munchen: Deutsche Geodatische Kommission, 1994.

[54] W. Kaula, *Theory of Satellite Geodesy.* Massachusetts: Blarsdell Waltham, 1966.

[55] K. Alfriend, S. Vadali, P. Gurfil, J. How, and L. Breger, *Spacecraft Formation Flying: Dynamics, Control and Navigation.* Oxford, United Kingdom: Elsevier Astrodynamics Series, 2010.

VITA

VITA

Raoul Rick Rausch was born in Luxembourg, Grand Duchy of Luxembourg. He attended the Lycée Technique Michel Lucius and graduated in 1999 with a Diplome de Fin D'Étude Secondaires Technique with mention Trés Bien. From 1999-2002 he attended Miami University in Oxford Ohio, and graduated with a Bachelor of Science in Physics with honors and minors in Aeronautics and Mathematics in 2002. In August 2002, he started his graduate education at Purdue Universtiy and graduated with a Master of Science degree in Aeronautics and Astronautics in August 2005. Following completion of his master's, Raoul enrolled in the PhD program in Aeronautics and Astronautics at Purdue. Throughout his graduate eduction, he completed internships with the Flight Dynamics group at SES-Astra, worked two years part-time as an Industrial Doctor Student in the Flight Dynamics group at SES-Engineering and participated in the Air Force Research Laboratory's Space Scholar's program at Kirtland AFB, NM in the summers of 2010 and 2011. He currently resides in West Lafayette, Indiana, with plans to relocate to Beavercreek, Ohio to begin his career as a Space Systems Analyst with the United States Air Force at Wright-Patterson AFB.